Reflectivity analysis from the low symmetric anisotropic media

By

Mohammadreza Malehmir

A thesis submitted in partial fulfillment of the requirements for the degree of

Doctoral of Philosophy

in

Geophysics

Department of Physics

University of Alberta

Abstract

The earth's crust and mantle is known to be anisotropic to the propagation of seismic waves. Despite this knowledge, the analysis and processing of seismic data still primarily assumes isotropy, an assumption that, in the context of active source seismic imaging, is an over-simplification that can result in flawed interpretations. Most work on seismic anisotropy has focused on improving seismic imaging by more properly accounting wave propagation paths. The incidence and azimuthal angle variations in reflectivity from anisotropic formations, however, remain poorly understood. Most analyses using structurally-constrained approximations for transversely isotropic half-spaces that are not always representative of real geological formations in the earth's crust. The work in this thesis seeks to contribute further by both analytic and physical modelling of the reflectivity from the contact between anisotropic half-spaces. This is primarily accomplished by carrying out laboratory measurements of the acoustic reflectivity from variously tilted blocks of a weakly-orthotropic composite phenolic grade CE. This material has characteristics reminiscent of fractured and layered formations in the earth. Following the lead of earlier researchers, we repeated measurements of reflectivity with respect to the angle of incidence at four azimuths from each of the four blocks studied. As expected, the reflectivity varied with both incidence and azimuth, but it could not be explained using plane-wave, Zoeppritz-type, solutions. Interpreting the results required, first, development of the appropriate understanding of the expected plane-wave reflectivity and, second, tools to account for the propagation and reflectivity of finite beams in the geometry of the laboratory. The first issue was overcome by solving the general problem for the reflections originating from the welded-contact between two half-spaces of any symmetry and arbitrary orientation with respect to one another. This solution was then developed into an open-source and readily available algorithm entitled Anisotropic

Reflectivity and Transmissivity calculator (ARTc). The second issue was addressed by the development of a second algorithm that, following earlier work of others, models the propagation and reflection of a spatially and temporally 'bounded' ultrasonic pulse within a water column overlying a flat interface. The program propagates the launched bounded pulse through the water to the interface and modulates in the 2-D Fourier domain the amplitude and phase of each of the pulse's component plane waves, before returning the pulse to the point of observation. This algorithm successfully reproduced the complicated features of the post-critical angle reflectivity from isotropic test samples in the laboratory. More importantly, however, we were able to reproduce the reflectivities observed from the anisotropic block's in the laboratory; this strong match between observation and modelling points validates the theory within ARTc. Further, the peak of the observed reflectivity curves does not coincide with that for the plane-wave solution which occurs at the critical angle. There are two implications of this work with respect to field investigations of azimuthal and incidence angle dependent seismic reflectivity. First, the azimuthal variations were not strong and this may suggest caution when attempting to deconvolve such variations out of more complicated and noisy field seismic data. Second, since all real seismic sources may deviate strongly from the plane wave assumptions normally employed, in field studies of seismic reflectivity workers may need to take account of this departure more fully.

Preface

This dissertation is submitted for the degree of Doctor of Philosophy in Geophysics at the University of Alberta. The research described herein is original and neither this nor any substantially similar dissertation was or is being submitted for any other degree or other qualification at any other university.

A version of Chapter 2, has been published as Malehmir, R., and Schmitt, D. R., 2016, ARTc: Anisotropic Reflectivity and Transmissivity Calculator, Computer and Geoscience, 93, 114-126, doi:10.1016/j.cageo.2016.05.008. I was responsible for code development, data analysis, figure preparation and writing this manuscript. Dr. Schmitt was the supervisory author and help with the concept, and assisted with the manuscript preparation.

A version of Chapter 3, has been published as Malehmir, R., and Kazemi, N., and Schmitt, D. R., 2017, Quantitative Modeling of Reflected Ultrasonic Bounded Beam with Experimental Verification, Ultrasonics, 80, 15-21, doi:10.1016/j.ultras.2017.04.013. I was the main author of this article and was responsible for writing the manuscript, algorithm, ultrasonic laboratory measurements and calibrations, figure preparation, and helped in code developments. Dr. Kazemi was the co-author and help with the code development and Dr. Schmitt was the supervisory author and assisted in the manuscript preparation and concept formation.

A version of Chapter 4, has been submitted and it is at this writing in revision, Malehmir, R., and Schmitt, D. R., 2017, Acoustic Reflectivity from Variously Oriented Orthorhombic Media: Analogies to Seismic Responses from a Fractured Anisotropic Crust, Journal of Geophysical Research-Solid Earth. I was responsible for laboratory measurements and calibration, code development, figure preparations, and writing the manuscript. A peer-reviewed data repository has been published on PANGAEA server as Malehmir, R., and Schmitt, D. R., 2016, Ultrasonic measurement of anisotropic reflectivity from Water-Phenolic CE Interface, PANGAEA, doi:10.1594/PANGAEA.864794. Dr. Schmitt was the supervisory author and involved in the manuscript preparation and concept formation.

To my family

Acknowledgments

First, I would like to express my sincere gratitude to my Ph.D. advisor Dr. Douglas Schmitt for his motivation, guidance, his patience, and continuous support during the time of research and writing this thesis. I could not have imagined having this thesis finished without his great supervision.

I also would like to thank the members of the committee: Prof. Jeffrey Gu, Prof. Lindsay LeBlanc, Prof. Peichun Amy Tsai and Prof. Edward S. Krebes for their insightful recommendations to improve the quality of this thesis. I would also like to thank the external candidacy exam members Dr. Chun Il Kim and Prof. Douglas Gingrich for their extremely constructive recommendations. Special thanks to my colleagues and friends Dr. Ramin Dokht, Dr. Nasser Kazemi, Dr. Yoones Vaezi and Tariq, and Randy for their productive discussions and valuable comments. I would also like to thank Cheryl Schmitt, Doug's wife, for their lovely hospitality and inviting my wife and I to their house to celebrate different events and having a fun night.

I would also like to thank the Helmholtz Alberta Initiative (HAI), Canada Research Chair (CRC) and National Science and Engineering Research Council (NSERC) for their financial support. Also would like to thank CSEG, EAGE, IGR-Dr.Hibbs, and FGSR travel awards for partially supporting the expenses to attend and present at conferences and workshops.

For the Chapter 2, I would like to thank Dr. James Wookey and the anonymous reviewer for their valuable comments and suggestions in the process of publishing Chapter 2.

For the Chapter 3. I would like to thank Dr. Faranak Mahmoudian for her valuable comments and suggestions in publishing Chapter 3.

For the Chapter 4, I would like to thank the Editor-in-Chief and the two anonymous reviewers for their guidance and valuable suggestions, in the publishing of Chapter 4.

Finally, I would like to thank my dear parents, sisters, and brothers for their unconditional love and support. Finally and the most importantly, my beloved wife, Sahba Kashiha, has made so many sacrifices and was extremely supportive throughout this process. I could not imagine presenting this thesis without her indefinite supports and unwavering love.

Contents

List of Tables

List of Figures

Chapter 1
Introduction

1.1 Background

It is now well known that much of the Earth's crust, its mantle, and even its inner core displays elastic anisotropy, which could have fundamental effects on seismic data interpretation, [e.g., *Backus*, 1965; *Savage*, 1999; *Belonoshko et al.*, 2008; *Schijns et al.*, 2012a; *Walker and Wookey*, 2012a]. Henceforth, the study of elastic wave propagation and the elastic wave properties in anisotropic media is crucial to global and exploration seismologists. First, identifying elastic anisotropy can hold the key to inferring rock fabrics whether they are controlled by fractures [e.g., *Gray et al.*, 2002; *Ekanem et al.*, 2013], layering, or mineralogical textures [e.g., *Boness and Zoback*, 2004]. Second, understanding the state of elastic anisotropy of the Earth increases the fidelity of seismic images of subsurface and the location of earthquakes and microseisms.

Despite the fact that the importance of anisotropy is widely recognized, there are few tools to properly investigate and incorporate it in seismic analysis; and usually rely on numerous simplifying assumptions and approximations to account for it in wave propagation and reflectivity. Such approaches have promoted a more general acceptance of seismic anisotropy into analyses, but suffer to provide suitable answers for more complicated or realistic geological structures such as would be encountered for cases of tilted media with low anisotropic symmetry. This is becoming increasingly true in the application techniques that use the variations in seismic reflectivity with

incidence angle and azimuth to reveal information about stress, fracture sets, or deposition alignments, after [*Chen et al.*, 2001; *Zheng and Ding*, 2014].

Elastic wave propagation in anisotropic media has been studied extensively over the last century as it is of fundamental concern to condensed matter physicists and of practical consequence to geophysicists and material engineers. There are numerous discussions of the sources of anisotropy in the literature which show that it can result from preferred orientations of the constituent minerals [e.g., *Wenk*, 1999], from layering [e.g., *Backus*, 1962], or from aligned fractures and cracks [e.g., *Stewart et al.*, 2013]. To review briefly, in any given propagation direction through an anisotropic material there will be three distinct and orthogonal wave modes: one quasi-longitudinal mode (qP) and two quasi-transverse modes (qS1 and qS2) with respective polarizations nearly parallel or perpendicular to the propagation direction. Generally, the wave speeds of quasi-P wave (V_{qP}) is greater than shear waves velocities (V_{qS1} and V_{qS2}) in following order $V_{qP}>V_{qS1}\geq V_{qS2}$, where the speeds of the two shear modes usually only matching along the material's symmetry direction where they are degenerate. One further point to emphasize is that for a given direction of propagation the phase speed (i.e. mono-frequency plane wave) must be distinguished from its corresponding group (i.e., ray) speed [see *Gassmann*, 1964].

A number of textbooks [e.g., *Musgrave*, 1970a; *Auld*, 1973], were developed by the pioneers of elastic anisotropy analysis in the middle of the last century, which mostly discuss the theory of elastic wave propagation in anisotropic media, and how the polarization and slowness of each wave mode is defined. Because of the mathematical complexity and lack of powerful computers at the time, various authors decided to simplify these systems of nonlinear equations to more affordable linear sets of equations. The mathematical complexity to find wave properties in anisotropic media

was computationally expensive for the processing of real seismic data. Consequently, researchers developed approximations in simpler anisotropic media. Weak elastic anisotropy was first introduced by [*Thomsen*, 1986a] to minimize amount of calculation required to solve for wave speeds in transversely isotropic media. Similar approaches were later applied to orthorhombic materials [*Tsvankin*, 1997].

The study of seismology, however, relies often on more than knowledge of the wave speeds in materials. The reflectivity and transmissivity of the interface, taken to be a welded contact, between two materials is an important problem for study. For two elastic but isotropic media a focus has been on the study of the variations in the reflected wave amplitudes from such intefaces, and within the applied geophysics community this has come to be known as Amplitude variation versus offset (AVO). The character of reflectivity with angle of incidence (or in the parlance of applied reflection seismology 'offset') provides invaluable information about the differences in the elastic parameters of the isotropic media on either side of the interface. Closed form solutions to this problem were provided by [*Knott*, 1899] for energy fluxes and by [*Zoeppritz*, 1919] who gave expressions for the amplitudes of 14 different possible reflections and transmissions from the interface (remembering that the out of the plane shear wave, SH mode, is decoupled from P-SV). This was provided to the community as a program by [*Young and Braile*, 1976], and developed into a more convenient scattering matrix form by [*Aki and Richards*, 1980]. Simplified, but incomplete, forms of these Zoeppritz equations have been provided by numerous authors [e.g., *Bortfeld*, 1961; *McCamy et al.*, 1962; *Aki and Richards*, 1980; *Shuey*, 1985] for use in the analysis of real data.

Linearized forms of these approximations for the PP reflections have been pivotal to the development of quantitative seismic assessments that employ variations of the reflected amplitudes with the angle of incidence to infer changes in elastic properties across a geological contact [e.g., *Ostrander*, 1984]). These techniques are alternately referred to as amplitude versus offset (AVO) or amplitude versus angle (AVA) analysis [e.g., *Castagna and Backus*, 1993; *Dvorkin et al.*, 2014; *Shadlow*, 2014].

More recently, there is interest in using reflectivity to predict subsurface anisotropy particularly in the search for reservoirs containing preferential joint or fracture sets. These techniques are often called amplitude variation versus azimuth (AVAZ) because they must look for changes in the reflectivity with both offset and azimuth. The introduction of anisotropy increases the level of complexity significantly over the isotropic case of Zoeppritz, and because of this, algebraic solutions for reflectivity have only been developed for a few special situations. [*Gassmann*, 1964] examined the complexities of the reflected wavefront. [*Musgrave*, 1970a] reviewed the complexities associated with reflectivity between anisotropic media and sketched the direction towards a general solution. He also calculated the amplitudes of internal waves reflected from the free surface of transversely isotropic medium revealing unexpected behaviors [*Musgrave*, 1970a; *Auld*, 1973] obtained the solutions for reflectivity within the symmetry planes of various cases. [*Daley and Hron*, 1977a; *Daley*, 1979] derived all 24 possible reflection and transmission coefficients (including the free surface condition) from the interface between transversely isotropic layers the axes of symmetry of which are oriented perpendicular to the interface. Today the two half-spaces of their solution are said to be vertical transversely isotropic (VTI). [*Graebner*, 1992] revisited the problem of reflectivity in transversely isotropic media and provided an analytic solution for P-wave reflectivity. [*Hood and Schoenberg*, 1992] reformulated the problem into one that employed a series of impedance matrices. [*Liang et al.*, 2009] developed exact and approximate expressions for reflectivity in tilted transversely isotropic media (TTI).

As just noted, solution of the general problem of reflectivity is complicated by the often unexpected aspects of wave propagation in anisotropic media and this has led to a variety of simplifications. [*Thomsen*, 1986a] linearized [*Daley and Hron*, 1977a] solutions using a 'weak boundary contrast' assumption. Various researchers extended this approach for PP (P-wave incident and reflected) approximations in weak elastic anisotropy and weak boundary contrast in transverse isotropy and orthorhombic media, which are also employed by many others [e.g., *Ursin and Haugen*, 1996; *Ruger*, 1997; *Ruger*, 1998; *Vavrycuk and Pšenčík*, 1998; *Zillmer et al.*, 1998; *Vavrycuk*, 1999; *Klimes*, 2003; *Behura and Tsvankin*, 2006; *Farra and Pšenčík*, 2010; *Golikov and Stovas*, 2010].

Along with theoretical advances in seismic anisotropy, general anisotropic media were physically modeled by numerous researchers [e.g., *Arts et al.*, 1991; *Cheadle*, 1991; *Jech*, 1991; *Vestrum*, 1994; *Mah and Schmitt*, 2001a; *Mahmoudian et al.*, 2015]. In these studies, velocity and amplitude of reflected and transmitted waves from laser or ultrasonic sources and samples with different anisotropic symmetry were monitored. These techniques are able to calculate elastic coefficients in any anisotropic material by sampling phase or group velocities of all three wave modes in wide acquisition angles. There have also been attempts to physically model the reflectivity from anisotropic media in the laboratory. Techniques developed by [*Bouzidi and Schmitt*, 2006, 2008b] carried out measurements of reflectivity from anisotropic phenolic blocks with various tilted symmetries. [*Mahmoudian et al.*, 2015] measured the azimuthal variations of reflectivity from the interface between isotropic Plexiglas and anisotropic phenolic, which she then inverted to obtain estimates of the material's properties. The work presented here was motivated by the need to better understand these laboratory observations without having to be rely solely on the existing approximate relations.

1.2 Motivation and Contributions

In this thesis, we started by introducing an algorithm that calculates the plane-wave reflectivity from the contact separating any two anisotropic media. This algorithm is not limited by the symmetry or orientation of the anisotropy on either side of the interface. Our reasons for developing this program are to provide a robust toolbox to research more realistic cases that are not limited by any approximations. The algorithm is able to solve for wave polarization, slowness and amplitude ratios of all wave modes generated from a welded interface bounding two homogenous anisotropic slabs of arbitrary symmetry and orientation.

Also, we noticed that the plane-wave theory is unable to explain the laboratory measured acoustic reflectivity from water-solid interfaces. We worked on a hybrid approach to model the reflected wavefield using the phase-advanced wave equation migration and the analytic reflectivity algorithm by ARTc. This algorithm can successfully explain the null reflection at the far off-set Rayleigh angle and the critical reflection at the acoustic critical angle.

The key question is to understand more about the elastic properties of the low-symmetric media from its reflectivity response. We examine this idea by measuring and analyzing the complete reflectivity dataset from four tilted Phenolic grade CE blocks and analyzing the reflectivity's variation with incident angle and azimuthal direction. From the reflection amplitude variation with azimuth and incident angle data we are able to understand the fracture orientations based on critical angle.

The main contributions of this thesis are summarized as:

- Introducing an algorithm to calculate reflectivity and transmissivity from general elastic anisotropic media.
- Collecting and releasing complete a reflectivity dataset from water-solid interfaces isotropic (aluminum, copper alloy) and anisotropic (phenolic CE, Quartz crystal) material.
- Proposed a new hybrid forward modeling algorithm to predict reflected wavefield from a pseudo –planar bounded pulse.
- Investigating and analyzing the reflected wavefield from water-phenolic CE with orthotropic anisotropic symmetry.

1.3 Thesis outline

It is crucial that we be able to properly account for wave propagation and reflectivity to carry out the final work in analyzing our laboratory reflectivity studies. In Chapter 2 we develop an algorithm that provides, first, the anisotropic wave slowness and corresponding particle polarizations for any propagation direction and, second, the solutions for the reflection and transmission coefficients of a welded interface bounding two homogeneous anisotropic slabs of arbitrary symmetry and orientation. Chapter 2 begins with a brief review of seismic anisotropy followed by the theory of plane-wave propagation; and a number of supporting programs are created to do this. This algorithm provides the full solution to velocity, polarization and amplitude ratios of all wave modes. The key and novel part of this Chapter, however, is the creation of code that allows for the calculation of both reflectivity and transmissivity of the interface between two

anisotropic half-spaces of both arbitrary symmetry and relative orientation. This program essentially provides the plane wave reflectivities to this problem. To illustrate the capabilities of the developed algorithm, we presented a variety of challenging tests and show the calculated reflectivity results and their application to seismic data processing and interpretations.

Plane waves do not exist in the real world of seismic observations and, most particularly, in laboratory experiments of finite dimensions. As such, the plane wave solution by itself from Chapter 2 cannot be used to properly study reflectivity in the laboratory. This is because the ultrasonic energy in the laboratory is in the form of a 'bounded pulse' that can only be described by a distribution of plane waves; and consequently this strongly influences the observed reflections. In order to account for this experimental limitation, in Chapter 3, we investigate the effect of source with bounded pulse on the reflected wavefield from water-solid interface. This hybrid technique, implements the numerical reflectivity calculator described in Chapter 2 and phase advanced wave propagation technique, and calculates the reflected wavefield. We compared numerical results with acoustic reflectivity measurements from water-aluminum and copper interface. The bounded pulse reflectivity modeling enables us to explain the null reflection at the Rayleigh angle known as the Schoch shift. That we were able to faithfully reproduce our complicated observed reflections, proved the validity of this approach to studying ultrasonic reflectivity.

The goals of the thesis, however, were to better understand reflectivity from real anisotropic media. In Chapter 4, we investigated reflectivity from a series of physical models that are representative of densely oriented fracture sets that might be found in the earth. Phenolic grade CE blocks, a manmade layered composite with weak orthorhombic symmetry, with four different tilting angles were used for laboratory measurements. The observed reflectivity variations of acoustic reflectivity with both incidence angles and azimuthal directions show distinct patterns. Using the reflection variation with azimuth and tilting angle, we show how to use critical reflection coefficients to understand the fracture orientations and estimate phase velocity in the phenolic sample. We also investigated the acoustical reflectivity variation in vicinity of critical angle using the approach described in chapter 3. We show that the properties of the bounded pulse determine the shape of acoustical reflectivity around qP-wave critical angle.

In Chapter 5, we summarize the key results from the thesis and propose potential future research directions.

Chapter 2

ARTc: Anisotropic Reflectivity and Transmissivity Calculator

2.1 Introduction

The evidence that the Earth's crust (e.g., [*Lin et al.*, 2011],[*Ozacar and Zandt*, 2009]), mantle (e.g., [*Di Leo et al.*, 2014; *Bao et al.*, 2016]), and inner core (e.g., [*Belonoshko et al.*, 2008]) are anisotropic to seismic waves has grown significantly in the last half-century. Despite this, seismic observations are still largely interpreted assuming that the media through which seismic waves pass are isotropic or, occasionally, transversely isotropic (e.g., [*Ozacar and Zandt*, 2004; *Schijns et al.*, 2012b]).

Incorporating elastic anisotropy into seismic data analysis will have two significant advantages. First, elastic anisotropy exists once the structural symmetry at any scale is broken; and generally less symmetry implies higher degrees of anisotropy. Examples of anisotropic structures at various scales that illustrate these different sources of anisotropy are shown in Figure 2-1. The character and degree of anisotropy are apparent in traditionally varying wave speeds and anomalous polarization. Consequently such observations can tell us about *i*) mineralogical textures (e.g., [*Kaarsberg*, 1959; *Gassmann*, 1964; *Mainprice and Nicolas*, 1989]; *ii*) layering (e.g., Helbig 1994; Backus 1962), and *iii*) fracturing and stress regimes of the region (e.g. Sayers et al. 2015; Crampin 1985; Stewart et al. 2013), or *iv*) combination of them (e.g., Far et al. 2013; Schijns et al. 2012).

Second, the transit times and travel paths of seismic rays moving through anisotropic layers can differ significantly from those through isotropic structures, (e.g., [*Merkulov*, 1963; *Kendall and Thomson*, 1989; *Ben-Menahem and Sena*, 1990; *Behura and Tsvankin*, 2009]. Ignoring this deviation in the patterns of reflection and refraction introduces error in seismic imaging (e.g., [*Isaac and Lawton*, 1999]); considering it in the processing scheme results in improvements in the veracity of seismic imaging. There is no need to emphasize the potential use of this algorithm in addition to

the applications in exploration seismology including but not limited to the computation of the synthetic receiver function in global and local seismology, to its use as a key component of a ray tracer for general anisotropic layered media and the construction of the synthetic seismic data as implemented by (e.g., Kendall & Thomson 1989; Guest et al. 1993).

The Chapter begins with a review of studies of reflectivity, continues through the essential mathematical background, provides a description of the programs provided, and ends with some examples of the application of the program to cases of increasing complexity.

2.1.1 *Background of elastic anisotropy*

There are many sources, which are linked to elastic anisotropy, which can be categorized as mineralogical or structural. Figure 2-1 *a*, *b* show how the preferred orientation of minerals in the rock, as well as very finely deposited layers of rocks which are very common in the Earth, reflects elastic anisotropy in seismic data. Satellite picture from Utah, United States, which shows two sets of fractures occuring in large-scale also could represent two different elastic anisotropic media in the very close proximity, after [*Far et al.*, 2013].

Elastic wave propagation in anisotropic media has been studied extensively over the last century as it is of fundamental concern to condensed matter physicists and of practical consequence to geophysicists and material engineers. A number of textbooks exist that cover the mathematics in details (e.g., Auld 1973; Helbig 1994; Musgrave 1970). Despite the fact that the importance of anisotropy is widely recognized, there are rather few tools to properly deal with it in seismology; and usually, we rely on numerous simplifying assumptions and approximations that have made including anisotropy more palatable, such as the weak anisotropy formulations introduced by [Thomsen, 1986a] for transversely isotropic (TI) and later for orthorhombic materials by [Ruger, 1997; Tsvankin, 1997; Rüger, 1998] as well as many others. Such approaches have promoted the more general acceptance of seismic anisotropy, but they usually cannot provide suitable answers for more realistic geological structures that may be less symmetric. This is becoming increasingly vital in the techniques, which use the variations in seismic properties with respect to the direction of propagation to understand how the stress regime, fracture orientation, spacing, or deposition alignments are around the point of interest deep underground.

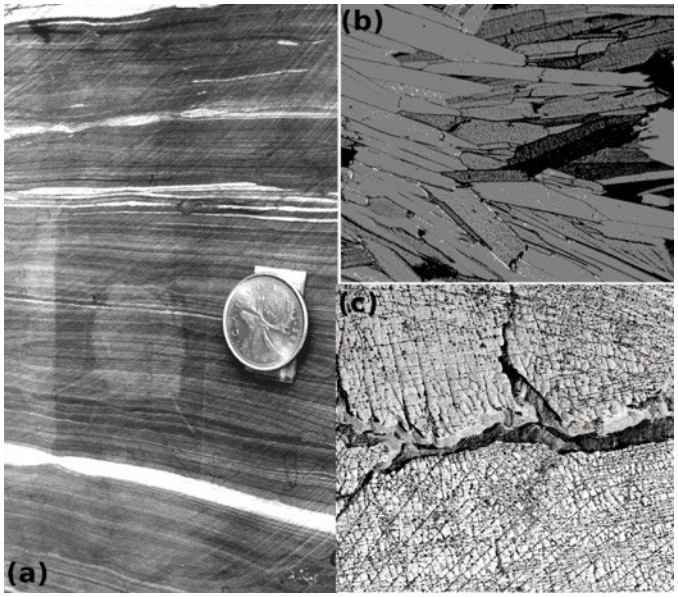

Figure 2.1. Structural deformation or crystallographic orientation of minerals are two main sources of elastic anisotropy in the hard rock environment. a) and b) depict two media with microscopic scale preferred orientation of minerals and deposition of the minerals, respectively; which would create elastic anisotropy. c) Displays two sets of large-scale fractures on the surface with different orientation on North from South of the Freshwater Spring River in Utah. In the North part fractures are almost orthogonal which could create orthorhombic anisotropy, however in the Southern part of the river non-orthogonal fractures may represent monoclinic or triclinic elastic anisotropy, Malehmir and Schmitt [2016] after [Far et al., 2013].

Our primary objective in this thesis is to provide to the community a program that provides the general solution for the reflection and transmission from all wave-modes and welded interface bonding two homogeneous anisotropic slabs with arbitrary symmetry and orientation. Our motivation stems from our need to properly interpret laboratory reflectivity tests first described in [Ortiz-osornio and Schmitt, 2011b]. The program calculates the plane-wave reflection and transmission coefficients for the welded interface between two arbitrarily oriented anisotropic half spaces A number of requisite subsidiary programs that determine directionally dependent wave speeds, ray paths, and particle motion polarizations are also included.

2.1.2 Early modeling of seismic anisotropy

To briefly review, for any given propagation direction through an anisotropic material there are three distinct and orthogonal wave-modes. Of these, one is a quasi-longitudinal mode (qP) and two are quasi-transverse modes (qS1 and qS2), where 'quasi' indicates that the particle polarizations are no longer perfectly parallel or perpendicular to the propagation direction, respectively. One further point to emphasize is that for a given direction of propagation the phase velocity (i.e. mono-frequency plane wave) must be distinguished from its corresponding group (i.e. ray) velocity (refer to (Auld 1973; Musgrave 1970; Gassmann 1964) for more details). The mathematical complexity to calculate wave properties in general anisotropic media makes it computationally expensive for the processing of real seismic data. Consequently, researchers developed approximate solutions in simpler anisotropic symmetries since the 1980's. Weak elastic anisotropy was first introduced by [*Thomsen*, 1986a] to linearize the calculations that are required to solve for wave speeds in transversely isotropic media. Similar approaches were later introduced for orthorhombic materials by [*Tsvankin*, 1997].

The variation in seismic reflectivity from the interface between two differing materials with both angle and azimuth is a second important problem. Amplitude variation versus offset (AVO) provides invaluable information about elastic parameters of isotropic media. The classic solutions for the reflectivity problem between two elastically isotropic layers was provided nearly a century ago by [*Knott*, 1899] for energy fluxes and by [*Zoeppritz*, 1919] for the amplitudes of fourteen possible reflections and transmissions from the interface. Within the geophysical community, these are commonly referred to as the Zoeppritz's equations. [*Young and Braile*, 1976] provided a Fortran-based code in this journal to carry out this calculation and [*Aki and Richards*, 1980] solved it using a convenient scattering matrix form.

Numerous authors have developed approximate solutions to Zoeppritz's equations, [*Bortfeld*, 1961; *McCamy et al.*, 1962; *Aki and Richards*, 1980; *Shuey*, 1985]. Linear forms of these approximations for the PP (P-wave incident, and P-wave reflected) reflections have been pivotal to the development of quantitative seismic assessments leading from [*Ostrander*, 1984] suggestion, that the variation of the reflected amplitudes with angle of incidence could be used to indicate changes in the elastic properties across a geological contact. Today the practice of amplitude versus offset

(AVO) or amplitude versus angle of incident (AVA) is a well-developed tool (e.g., Castagna & Backus 1993; Dvorkin et al. 2014; Shadlow 2014).

More recently, there is an interest to further extend the use of reflectivity to predict subsurface anisotropy particularly in the search for petroleum reservoirs with preferential joints or fracture sets. These techniques are often called amplitude variation versus azimuth (AVAz) or velocity variation versus azimuth (VVAz) because they must look for changes in the reflectivity with both offset and azimuth. The introduction of anisotropy increases the level of mathematical complexity significantly, over the isotropic case, and because of this algebraic solution for reflectivity have only been developed for a few special situations particularly for vertical (VTI) and horizontal (HTI) transversely isotropic media. (Musgrave 1970) reviewed these complexities in anisotropic media and sketched the direction towards a general solution. He also calculated the amplitudes of internal waves reflected from the free surface of arbitrarily tilted transversely isotropic medium revealing unexpected behaviors. [*Auld*, 1973] obtain the solutions for reflectivity within the symmetry planes of various cases of elastic anisotropy.

[*Daley and Hron*, 1977b; *Daley*, 1979] derived all twenty-four possible reflection and transmission coefficients (including the free surface condition) from the boundary between two VTI layers the axes of symmetry of which are oriented perpendicular to the interface.[*Mallick and Frazer*, 1991] modeled the azimuthal variations in seismic reflectivity from a fractured seabed that required them to solve the problem for a liquid over a HTI elastic solid [*Guest and Thomson*, 1992] calculated synthetic seismograms to extract anomalous converted SH-mode reflections from the interface between an isotropic layer and a HTI half-space. [*Hood and Schoenberg*, 1992] revisited the problem of reflectivity in transversely isotropic media and provided an analytic solution for P-wave reflectivity which is calculated from series of impedance matrices. Motivated by the need to explain the generation of shear waves observed within deep crustal seismic surveys that employed air gun sources, [*Guest et al.*, 1993] developed a ray-based approach that estimated the anisotropic reflection and transmission coefficients. [*Carcione*, 1997] developed anelastic formulae for the reflectivity and transmissivity for two VTI half-spaces. [*Li*, 2008] provided corrected solutions for the scattering between an isotropic and a triclinic medium. [*Liang et al.*, 2009] developed exact and approximate expressions for reflectivity in tilted

transversely isotropic media (TTI).

Solution of the general problem of reflectivity is complicated by the unexpected aspects of wave propagation that occurs in anisotropic media, which has led to a variety of simplifications. [*Thomsen*, 1986b] linearized [*Daley and Hron*, 1987] solutions using a weak boundary contrast assumption. Various authors extended this approach for PP approximations in weak elastic anisotropy and weak boundary contrast in transverse isotropic and orthorhombic media were also employed by other researchers (e.g., [*Ursin and Haugen*, 1996; *Ruger*, 1997; *Rüger*, 1998; *Vavrycuk and Pšenčík*, 1998; *Zillmer et al.*, 1998; *Vavrycuk*, 1999; *Klimeš*, 2003; *Behura and Tsvankin*, 2006; *Farra and Pšenčík*, 2010; *Golikov and Stovas*, 2010].

More general problems have also been considered. [*Keith and Crampin*, 1977] developed a methodology for determining the energy reflection coefficients for the interface between two generally anisotropic media and carried out calculations within symmetry planes for TI and orthorhombic cases. [*Rokhlin*, 1986] provide the full solution for the scattering between two arbitrary anisotropic half-spaces the algorithm developed here builds on this work. [*Chattopadhyay et al.*, 2015] describe calculations made using the general solution.

Along with theoretical advances in seismic anisotropy, general anisotropic media were physically modeled by numerous researchers in lab to better understand wave propagation inside the anisotropic medium with known elastic coefficients (e.g., [*Arts et al.*, 1991; *Cheadle*, 1991; *Jech*, 1991; *Vestrum and Brown*, 1994; *Mah and Schmitt*, 2001b]). In these studies, the velocity and amplitude of a reflected and transmitted wave from ultrasonic sources and the samples with different anisotropic symmetry are monitored. These techniques are able to calculate elastic coefficients in any anisotropic material by sampling phase or group velocities of all three wave-modes in wide acquisition angles. Also, there have been attempts to physically model the reflectivity from anisotropic media in the laboratory. Following techniques developed for the precise study of reflectivity in the laboratory (e.g., [*Bouzidi and Schmitt*, 2006, 2012; *Ortiz-osornio and Schmitt*, 2011b]), we carried out measurements of reflectivity from anisotropic phenolic blocks with various tilted symmetries and a large single quartz crystal sheet. [*Mahmoudian*, 2013; *Innanen and Mahmoudian*, 2015] also physically modeled the azimuthal variations of reflectivity from the interface between isotropic Plexiglas and anisotropic phenolic.

The algorithm presented in this Chapter was motivated by the need to better understand these laboratory observations without having to rely solely on the existing approximate relations. In the next section, mathematical insights behind a general solution to wave properties in anisotropic media are explained in detail.

2.2 Theory

The theoretical basis upon which the program relies is given in this section. Before beginning, however, it is useful to review the salient characteristics of wave propagation in anisotropic media so that it is clear what needs to be input and what is calculated. There are essentially two sets of algorithms, i) subroutines to first determine propagation dependent velocities and particle polarizations given material properties and geometries of the layers, and with this information ii) subroutines to determine angles, speeds, polarizations, and amplitudes of the waves upon reflection and refraction from the interface between the two materials.

The orthogonal *x1-x2-x3* co-ordinate system (Figure 2-2) with the *x1-x2* plane co-incident with the planar interface between the two materials is employed. For any given propagation direction through the material $\boldsymbol{n}$ there will, in general, be three independent wave-modes. The first set of subroutines describes the propagation of a single plane wave-mode. The polarizations $\boldsymbol{\xi}$ of these three modes are mutually orthogonal to one another with, one longitudinal mode qP and two transverse modes qS1 and qS2. The *q* prefix indicates that these are quasi-longitudinal or shear modes because their individual polarization $\boldsymbol{\xi}$ will not necessarily be parallel or perpendicular to the wave propagation direction described by the unit vector **n**. The speed of these three modes also depends on the elastic properties and density of the material; which must be specified. Hence, with the inputs of the elastic coefficients Cij (with up to 21 independent components) the density ρ, and the propagation direction **n**, the first component of the program calculates the three phase velocities ($\boldsymbol{v}$) and their corresponding polarizations $\boldsymbol{\xi}$. It must be noted that stiffness matrix of the anisotropic media which we use for this algorithm are rotated from crystallographic principle to the coordinate system, for more information readers can refer to [*Guest and Kendall*, 1993; *Walker and Wookey*, 2012a] for more details.

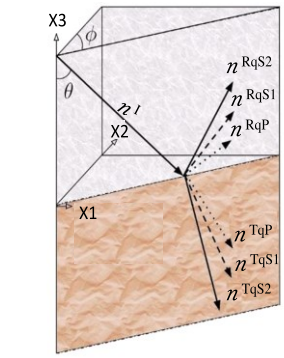

a)

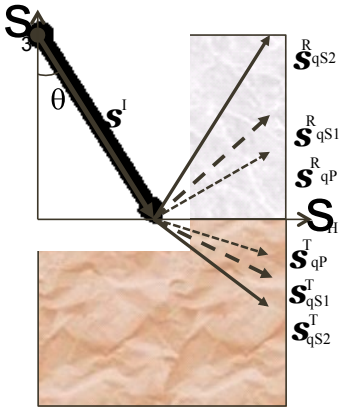

b)

Figure 2.2. Schematic wave-mode generation from a welded boundary separating two anisotropic media. θ and φ represent inclination and azimuthal direction of incident wave. b) Shows sagittal plane, which includes incident wave and all generated wave-modes from the horizontal welded boundary.

The second component describes the reflection and transmission of a given incident wave-mode to the welded interface between two elastically anisotropic half-spaces. This requires a number of different inputs provided by the first set of subroutines that includes the incident wave's mode, propagation direction **n**, phase velocity ***v*,** and particle polarization ***ξ*.** The densities and the stiffnesses C*ij* appropriately rotated into the co-ordinate axis of Figure 2-2 the incident and refracted half-spaces define the problem. Generally, the incident wave energy is partitioned into three reflected and three refracted waves. The algorithm determines the propagation directions,

polarizations, amplitude ratios of all six scattered wave-modes.

2.2.1 *General anisotropic elastic wave equation*

There are now numerous texts in which the solution to the wave equation through anisotropic media is described in details; here we only cover the components that are essential to the understanding of the algorithm. First, we assume that the problem is fully elastic and that the generalized Hooke's law constitutive relation between stress and strain holds as described in Equation 2-1.

$$\sigma_{ij} = \mathbf{C}_{ijkl}\, \varepsilon_{kl} \qquad (2\text{-}1),$$

where $\mathbf{C}_{ijkl}$ is fourth order stiffness matrix of the medium with up to twenty-one independent elastic modulus that is properly rotated into the co-ordinate axis, and, $\boldsymbol{\sigma}$, $\boldsymbol{\varepsilon}$ are tensors of stress and strain, respectively. The elastic stiffness matrix in Equation 2-1 is symmetric and stationary. As is well-known, the requisite number of independent elastic coefficients decreases as the symmetry of the medium increases ranging from only two elastic coefficients for the isotropic case to as many as twenty-one for the least symmetric triclinic medium (see recent discussion in [*Schmitt*, 2015]). With this form of Hooke's law, we recall the full elastic wave Equation 2-2.

$$\rho \ddot{u}_i = C_{ijkl}\ \partial / \partial x_l \left(\partial u_k / \partial x_l + \partial u_l / \partial x_k\right) \qquad (2\text{-}2)$$

where *u* and *x are* displacement vector and co-ordinate frame reference. For simplicity and better understanding, the [*Voigt*, 1887] conversion form of elastic coefficients will be used for the rest of the thesis.

2.2.2 Christoffel's solution for velocity and polarization

It is important to review the process by which the directionally dependent wave speeds and polarizations are determined. In order to find slowness and polarization of a wave mode in given direction, a plane-wave solution is assumed of the form Equation 2-3.

$$\mathbf{u} = A\, \xi\, e^{-i\mathrm{k}(\mathbf{n}.\mathbf{r} - \mathrm{v}t)} \qquad (2\text{-}3)$$

where, **u** is displacement, *A* is amplitude of incident wave, ξ is particle polarization vector, k wave number, **n** normal to the wave-front, **r** position vector and v phase velocity. The Eikonal Equation 2-4, more often referred to as Christoffel's equation [*Christoffel*, 1877] is then used to

find the velocity and particle polarization of all wave-modes using

$$[\Lambda_{ik} - \rho v^2 \delta_{ik}]\, \xi_k = 0 \tag{2-4}$$

where δ is Kronecker operator and $\mathbf{\Lambda}$ is calculated directly from Equation 2-5 (Musgrave 1970). We solve this problem as an eigenvector and eigenvalue system of equations, for more details about this technique, please refer to [*Aki and Richards*, 1980].

$$\begin{pmatrix} \Lambda_{11} \\ \Lambda_{22} \\ \Lambda_{33} \\ \Lambda_{23} \\ \Lambda_{31} \\ \Lambda_{12} \end{pmatrix} = \begin{pmatrix} C_{11} & C_{66} & C_{55} & 2C_{56} & 2C_{15} & 2C_{16} \\ C_{66} & C_{22} & C_{44} & 2C_{24} & 2C_{46} & 2C_{26} \\ C_{55} & C_{44} & C_{33} & 2C_{34} & 2C_{35} & 2C_{45} \\ C_{56} & C_{24} & C_{34} & C_{23}+C_{44} & C_{36}+C_{45} & C_{25}+C_{46} \\ C_{15} & C_{46} & C_{35} & C_{36}+C_{45} & C_{13}+C_{55} & C_{14}+C_{56} \\ C_{16} & C_{26} & C_{45} & C_{25}+C_{46} & C_{14}+C_{56} & C_{12}+C_{66} \end{pmatrix} \begin{pmatrix} n_1^2 \\ n_2^2 \\ n_3^2 \\ n_2 n_3 \\ n_3 n_1 \\ n_1 n_2 \end{pmatrix}, \tag{2-5}$$

By solving Equation 2-4, which includes general case of anisotropy (up to triclinic), we get the phase velocities of all three wave-modes, each associated with their corresponding polarization**.** So far, we were able to calculate **v** and **ξ** of all three orthogonal wave-modes, (qP, qS1, qS2). The polarization of the qP wave is sub-parallel to **n**. The polarizations of the two shear wave-modes are sub-perpendicular to **n** and we are categorizing qS1 and qS2 based which is faster and slower, respectively.

2.2.3 Reflectivity and Transmissivity

In this section, the general problem of determining the reflectivity and transmissivity is developed. To avoid confusion and maintain consistency, we assume that incident wave propagating in the direction **n** impinges the boundary from upper medium. Consider a *qP*, *qS1* or *qS2* plane-wave travelling obliquely downward through an arbitrary elastic anisotropic half-space (Figure 2-2). Upon incidence with the boundary six wave-modes are considered, where half will reflect back to the top upper medium and the other half will transmit into the lower medium. In order to calculate amplitude ratio of each generated wave-mode, we first need to know their propagation direction and then satisfy the welded boundary conditions. The subroutine "*ChrisKel*" is defined to calculate velocity and polarization for all generated waveforms, the main body of subroutine "*ChrisKels* is as follows.

```
function [vel,pol]=chrisKel(n1,n2,n3,c,ro)
% c is the stiffness matrix
% rho is the density of the medium
% n1, n2, n3 are the direction of the wave-mod

L11 = n1^2*c(1,1) + n2^2*c(6,6) + n3^2*c(5,5) + 2*n2*n3*c(5,6) +
2*n3*n1*c(1,5) + 2*n1*n2*c(1,6);

L22 = n1^2*c(6,6) + n2^2*c(2,2) + n3^2*c(4,4) + 2*n2*n3*c(2,4) +
2*n3*n1*c(4,6) + 2*n1*n2*c(2,6);

L33 = n1^2*c(5,5) + n2^2*c(4,4) + n3^2*c(3,3) + 2*n2*n3*c(3,4) +
2*n3*n1*c(3,5) + 2*n1*n2*c(4,5);

L23 = n1^2*c(5,6) + n2^2*c(2,4) + n3^2*c(3,4) + n2*n3*(c(2,3)+c(4,4)) +
n3*n1*(c(3,6)+c(4,5)) + n1*n2*(c(2,5)+c(4,6));

L13 = n1^2*c(1,5) + n2^2*c(4,6) + n3^2*c(3,5) + n2*n3*(c(3,6)+c(4,5)) +
n3*n1*(c(1,3)+c(5,5)) + n1*n2*(c(1,4)+c(5,6));

L12 = n1^2*c(1,6) + n2^2*c(2,6) + n3^2*c(4,5) + n2*n3*(c(2,5)+c(4,6)) +
n3*n1*(c(1,4)+c(5,6)) + n1*n2*(c(1,2)+c(6,6));

L = [L11 L12 L13;
     L12 L22 L23;
     L13 L23 L33];

[pol,ev] = eigs(L);
vel = sqrt(diag(ev)/ro);
```

2.2.4 Direction of generated waves

We quantify the direction of propagation of generated wave modes by their corresponding slowness vector $\mathbf{n}^{\alpha} = \mathbf{s}^{\alpha}/|\mathbf{s}^{\alpha}|$, which we assign superscripts α for the reflected waves of 1 (qPR), 2 (qS1R), and 3 (qS2R) and for the transmitted waves 4 (qPT), 5 (qS1T), and 6 (qS2T). The subscript 'I' and α=0, are assigned to the incoming wave regardless of its mode. According to the generalized Snell's law the horizontal slowness component s_h^{α} (i.e. parallel to the interface) of all of these seven modes are equal and lie in the sagittal plane that includes **n** and the interface normal (Musgrave 1970; Rokhlin 1986). Since all the horizontal slownesses ($\mathbf{s}_h^{\alpha}$) are equal,

$$s_h^{\alpha} = s_h^{0} \mid \alpha = 1{:}6. \tag{2-6}$$

the problem is now being reduced to finding the vertical slowness of the reflected and refracted wave-modes. Following [*Rokhlin*, 1986] we first define a shorthand Ω_{ik} in Equation 2-7,

$$\Omega_{ik} = \frac{C_{ijkl}\, s_j\, s_l}{\rho}\ , \tag{2-7}$$

which allows Equation 2-4 to be recast in terms of the slowness vector with unknown vertical slowness (s_3),

$$[\Omega ik - \delta ik]\, \xi_k = 0, \tag{2-8}$$

To find vertical slowness of both reflected and transmitted wave-modes, the algorithm needs to solve the Equation 2-8. [*Rokhlin*, 1986] suggested to zero the determinant of the matrix in Equation 2-8, to find vertical slowness of all wave-modes. The subroutine "*ChrsKel_RT*", is implemented to find vertical slowness of each medium. The code, initially calculate the coefficients of the quadratic form of $\mathbf{\Omega}$ in the vector format, $\Omega_{ik} = [a_{ik},\ b_{ik},\ c_{ik}\ ] \times [s_3^2,\ s_3^1,\ s_3^0]^T$; where *a, b, c* are calculated from Equation 2-5. The algorithm, forms polynomial equation based on determinant of the matrix in Equation 2-8 and quadratic format of $\mathbf{\Omega}$. We reach two sixth-degree polynomial equations for reflected and refracted waves, in which vertical s_3 is the only unknown. Only three of six roots are physically possible, which we select them based on the geometry of the boundary. We implemented convolutional theorem to form sixth-order polynomial equation of s_3 with faster speed. The main body of the MATLAB® subroutine "*ChrsKel_RT*" is as follows.

```
function s3 = ChrstKel RT(c,s1,s2,rho)
% c is the stiffness matrix
% rho is the density of the medium
% s1 & s2 are horizontal slowness values
c=c./rho; % density normalizing the stiffness matrix
% s1 & s2 are horizontal slowness values
%Omega11:
O11=[c(5,5),2*s1*c(1,5)+2*s2*c(5,6),s1^2*c(1,1)+s2^2*c(6,6)+...
2*s1*s2*c(1,6)-1];
%Omega22:
O22=[c(4,4),2*s1*c(4,6)+2*s2*c(2,4),s1^2*c(6,6)+s2^2*c(2,2)+...
2*s1*s2*c(2,6)-1];
%Omega33:
O33=[c(3,3),2*s1*c(3,5)+2*s2*c(3,4),s1^2*c(5,5)+s2^2*c(4,4)+...
2*s1*s2*c(4,5)-1];
%Omega23:
O23=[c(3,4),s1*(c(3,6)+c(4,5))+s2*(c(2,3)+c(4,4)),s1^2*c(5,6)+...
s2^2*c(2,4)+s1*s2*(c(2,5)+c(4,6))];
%Omega13:
O13=[c(3,5),s1*(c(1,3)+c(5,5))+s2*(c(3,6)+c(4,5)),s1^2*c(1,5)+...
s2^2*c(4,6)+s1*s2*(c(1,4)+c(5,6))];
%Omega12:
O12=[c(4,5),s1*(c(1,4)+c(5,6))+s2*(c(2,5)+c(4,6)),s1^2*c(1,6)+...
s2^2*c(2,6)+s1*s2*(c(1,2)+c(6,6))];
% Creating 6th-degree polynomial equation:
% p=a0 s3^0 +a1 s3^1 +a2 s3^2 +a3 s3^3 +a4 s3^4 +a5 s3^5 +a6 s3^6
p=conv(O11,(conv(O22,O33)-conv(O23,O23)))-conv(O12,(conv(O12,O33)-...
conv(O13,O23)))+conv(O13,(conv(O12,O23)-conv(O13,O22)));
% Solution to polynomial equation is calculation by roots.m function.
s3 = roots(p);
```

After determining vertical slowness of all wave-modes from the previous step, we calculate the direction $\boldsymbol{n}^{\alpha}$ of each wave mode is calculated by

$$\mathbf{n}^{\alpha} = \mathbf{s}^{\alpha}/|\mathbf{s}^{\alpha}| \tag{2-9}$$

Now that we know the direction of all generated wave-mode, ARTc uses $\mathbf{n}^{\alpha}$ in subroutine "*chrisKel*" to calculate velocity and polarization of each wave-mode.

2.2.5 *Welded boundary conditions*

At this step, we have all the required information about the incident and generated wave-modes, we can calculate amplitude ratios of generated wave-modes. To solve for reflectivity and transmissivity, two main boundary conditions must be satisfied; first, continuity of displacements on the interface, Equation 2-10, where **u** is calculated from $u^{\alpha} = \xi^{\alpha} A^{\alpha}$.

$$\sum_{\alpha=1}^{3}(\mathbf{u}^{\alpha}) + \sum_{\alpha=4}^{6}(\mathbf{u}^{\alpha}) = \mathbf{u}^{0}, \tag{2-10}$$

Second welded boundary condition which has to be satisfied is continuity of traction force ($\boldsymbol{\tau}$) formulated as

$$\sum_{\alpha=1}^{3}(\boldsymbol{\tau}^{\alpha}) + \sum_{\alpha=4}^{6}(\boldsymbol{\tau}^{\alpha}) = \boldsymbol{\tau}^{0}, \tag{2-11}$$

where for the convenience we introduced $\tau^{\alpha} = C_{ij}\ \eta_j\ s^{\alpha}\ \xi^{\alpha}\ A^{\alpha}$, $\boldsymbol{\eta}$ *is the normal to the boundary.* The only unknown in the system of Equations of 2-10 and 2-11, is amplitude of the generated wave-modes (A^{α}) and the amplitude of the incident wave (A^{0}), but we rearrange them to find the amplitude ratios (A^{α}/A^{0}).

The subroutines "*boundary_condition*" and "*traction*" uses Equation 2-10 and Equation 2-11 to form and solve the system of linear equations with the kernel matrix of **G** and vector of displacement and traction force from incident wave **I**, and the vector **X**, with unknown amplitude ratios. The matrix representation of this system of equations is

$$\mathbf{G}\,\mathbf{X} = \mathbf{I}. \tag{2-12}$$

We reach amplitude ratio by inverting the boundary condition kernel matrix Equation 2-13.

$$\mathbf{X} = \mathbf{G}^{-1}\,\mathbf{I}, \tag{2-13}$$

The code block of the subroutines "boundary_condition" and "traction" are followed.

```
%% function traction3.m
function T3j= traction3 (C,p,s)
% Calculate normal traction force to the boundary given:
% C, stiffness tensor, p: polarization vector and S, slowness vector
p1 = p(1); p2 = p(2); p3 = p(3);
k1 = s(1); k2 = s(2); k3 = s(3);
ps33 = [p1*k1 ; p2*k2  ;  p3*k3 ; (p2*k3 + p3*k2) ; (p3*k1 + p1*k3) ;
(p1*k2 + p2*k1)];
T3j = C(3:5,:) * ps33;
end
```

```
function R = boundary_condition(cu,cl,pi,si,pr,sr,pt,st)
% pr, sr polarization & slowness matrix of reflected wave-modes
% pt,st polarization & slowness matrix of transmitted wave-modes
% pi,si polarization & slowness vector of incident wave
DIS = [-pr(1,1) -pr(1,2) -pr(1,3) pt(1,1) pt(1,2) pt(1,3);
       -pr(2,1) -pr(2,2) -pr(2,3) pt(2,1) pt(2,2) pt(2,3);
       -pr(3,1) -pr(3,2) -pr(3,3) pt(3,1) pt(3,2) pt(3,3)];
% incident wave
 DIS0 = pi;
%% conservation of traction force on the surface

for i=1:3 % for reflected waves
    T3_R(:,i) = traction3(cu,pr(:,i),sr(:,i));% for reflected waves
    T3_T(:,i) = traction3(cl,pt(:,i),st(:,i));% for transmitted waves
end
% incident wave
T3_0 = traction3(cu,pi,si);

%% forming the G matrix form equations 10 , 11

G = [  DIS; -T3_R T3_T];
I = [ DIS0;  T3_0];
R = inv(G)*I;
```

The mathematical and programing implementation of (Rokhlin 1986; Musgrave 1970) in defining the polynomial equation for vertical slowness and extending the [*Rokhlin*, 1986] to the general case of anisotropy with up to twenty-one elastic modules in addition to rotation is one of the advantages of the mathematical and physical novelties in ARTc package. The ARTc solves the amplitude ratios problem by least square inversion to avoid numerical error caused beyond post critical angles, which makes it easier for the users to get reliable results from all possible direction.

2.2.6 *Testing the algorithm*

The programs are tested for a number of different cases. The first example consists of an imaginary virtual interface existing within a whole space filled with water, a liquid with no shear modulus. By construction, there are no differences in the physical properties of the water on either side of the imaginary interface and no reflections or refractions should be generated. Application of the programs to this trivial example showed that no reflected waves were generated at the interface at any angle of incidence. Numerical errors did exist at the level of 10^{-15}. In the first example the incident P-wave travels through the virtual boundary and is fully transmitted without generating any shear wave-mode, reflection or refraction.

In the second trivial test, an imaginary interface was defined within a complex triclinic medium. Here too, no new converted waves were generated by qP, qS1, or qS2 modes incident to

this virtual surface again to the same level. These trivial tests confirmed that the program created no ghost.

In the third test, we compared the results of our algorithm directly to Zoepprit's equations (using [*Aki and Richards*, 1980] scattering matrix approach) to the interface between water and Copper metal. We used this high contrast water-Copper model to test the accuracy of the program to the Zoeppritz's direct analytic solution for PP^R, reflection and PS^T, PP^T transmission in all possible scattering directions. The numerical implementation matched the analytic solution within the numerical machine error of the calculations (10^{-15}), (Figure 2-3). The reader will find explanations on how to use the programs in the Appendix 2-A.

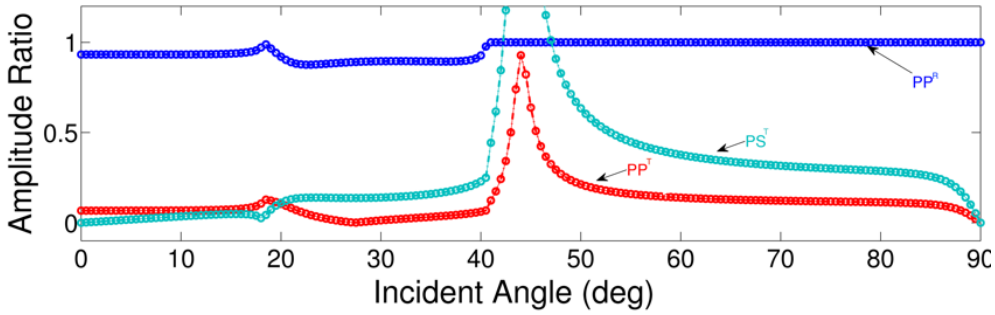

Figure 2.3. Amplitude ratios of reflected PP and transmitted PP and PS waves are calculated from high contrast water-Copper alloy boundary from a P-wave incident angle in all scattering angles ($\theta = 0^\circ$ to 90°). Results are showed from the ARTc (circles) and Zoeppritz (solid lines) solution, which matches perfectly within the computers precision.

2.3 Case Examples

A number of example calculations are presented in this section to illustrate the capabilities. First, the variations of slownesses and polarizations within a single anisotropic medium are calculated. Next, the reflectivity and transmissivity programs are used to replicate some existing solutions. Finally, the reflectivities from example boundaries from progressively complex cases are presented. In these calculations we use the stiffnesses and densities for single mineral crystals of

differing symmetries (Table 1-1) as extracted from [*Bass*, 1995; *Schmitt*, 2015] compilation.

Table 2.1. Elastic coefficients of anisotropic media used for modeling, ISO, VTI, HTI, ORT, MON, TRI stand for isotropic, vertical transverse isotropic, horizontal transverse isotropy, orthorhombic, monoclinic and triclinic anisotropic symmetry in GPa, and their respective density in (*gr/cc*), after [*Bass*, 1995; *Schmitt*, 2015].

	Water	ISO	VTI	HTI	ORT	MON	TRI
ρ	1.0	2.7	2.0	2.2	2.1	3.5	4
C_{11}	2.19	5.12	10.0	7.56	20.56	18.58	41.42
C_{12}	2.19	1.49	2.00	4.53	1.34	6.85	7.41
C_{13}	2.19	1.49	2.00	4.53	1.78	7.07	7.98
C_{14}	0.00	0.00	0.00	0.00	0.00	0.00	0.11
C_{15}	0.00	0.00	0.00	0.00	0.00	0.98	-0.30
C_{16}	0.00	0.00	0.00	0.00	0.00	0.00	1.92
C_{22}	2.19	5.12	10.0	9.00	9.72	18.1	37.23
C_{23}	2.19	1.49	6.00	3.22	1.39	6.26	7.45
C_{24}	0.00	0.00	0.00	0.00	0.00	0.00	0.24
C_{25}	0.00	0.00	0.00	0.00	0.00	0.94	0.19
C_{26}	0.00	0.00	0.00	0.00	0.00	0.00	1.57
C_{33}	2.19	5.12	15.0	9.00	12.7	23.44	41.27
C_{34}	0.00	0.00	0.00	0.00	0.00	0.00	0.00
C_{35}	0.00	0.00	0.00	0.00	0.00	2.14	-1.10
C_{36}	0.00	0.00	0.00	0.00	0.00	0.00	0.34
C_{44}	0.00	1.81	2.50	2.89	4.66	6.29	14.97
C_{45}	0.00	0.00	0.00	0.00	0.00	0.00	0.63
C_{46}	0.00	0.00	0.00	0.00	0.00	0.77	0.47
C_{55}	0.00	1.81	2.50	2.65	4.92	5.10	15.82
C_{56}	0.00	0.00	0.00	0.00	0.00	0.00	0.20
C_{66}	0.00	1.81	2.00	2.65	4.33	4.74	15.24

2.3.1 *Velocity and Polarizarion*

The ARTc is able to calculate slownesses of the modes propagating at all possible azimuths ($\varphi = 0^\circ$ to 360°) and incidence angles ($\theta = 0^\circ$ to 90°) for different degrees of anisotropy from isotropic to triclinic are shown in Figure 2-4. Further, as mentioned in general the polarization and propagation directions are not perfectly parallel or perpendicular for longitudinal and transverse modes, respectively. This is illustrated in Figure 2-5 where the deviation of the qP particle polarization $\boldsymbol{\xi}$ from the normal to the wave-front $\boldsymbol{n}$ is imaged over all possible incidence and azimuths. As expected for the isotropic case the polarization and the wave-front normal are always parallel and no derivations appear at any angle. However as the symmetry decreases through transversely isotropic to monoclinic $\boldsymbol{\xi}$ can deviate quite substantially from $\boldsymbol{n}$ and appears with increasingly complex patterns.

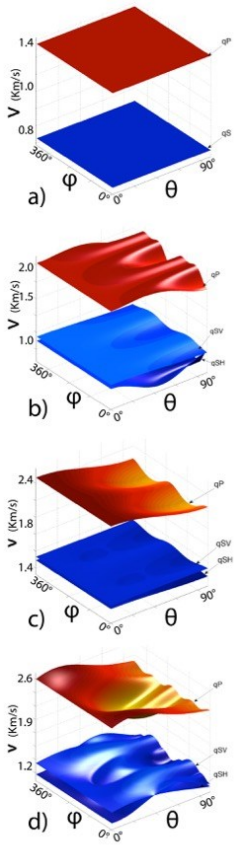

Figure 2.4. This figures depicts slowness variation inside four major anisotropic media in all possible azimuthal and scattering angles directions. a) Inside an isotropic medium, P-wave, and

other two shear waves have constant slowness in all directions. b) With transverse isotropic (TI) medium, all three the wave-modes travel faster in the plane of symmetry and become slower up to the perpendicular direction. Inside the c) orthorhombic and d) monoclinic anisotropic media, the slowness variation with direction shows more complex pattern.

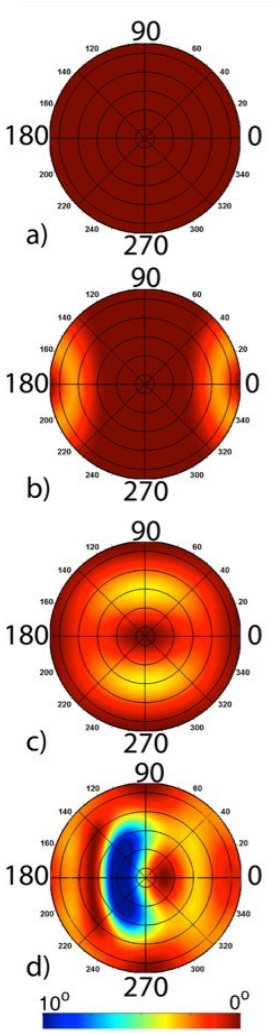

Figure 2.5. This figure shows the deviation of P-wave particle polarization from normal to the wave-front. This angular variation is calculated for cases of a) isotropic b) horizontal transverse isotropy (TI) c) orthorhombic d) monoclinic media. By looking into the patterns, we could see strong correlation between angular deviation pattern and symmetry of the anisotropic medium, by decreasing symmetry of the medium; the deviation pattern also shows less symmetry.

2.3.2 *Reflectivity variation with direction*

ARTc is applied to calculate the PP reflectivity for a variety of different cases. It must be noted that the following figures required iterative application of the ARTc to cover both azimuthal and incidental direction with high resolution.

The first case considers the contact between a topmost TI medium over an orthorhombic half-space. The TI medium is variously tilted in the three examples with VTI at 0° (Figure 2-6a), at 30° (Figure 2-6b), and at 60° (Figure 2-6c). One clear feature of all of these panels is the locus of the PP critical angles indicated by the warm red color ribbon. For the VTI case the pattern is controlled primarily by the symmetry of the underlying orthorhombic medium. This is because the VTI medium is rotationally symmetric and does not change with azimuth. The reflectivity for the second case with a 30° tilt displays asymmetry as would be expected as the rotational symmetry is broken. The final 60° case is again more symmetric. This is somewhat unexpected as we might expect to see the greatest difference as the HTI case is approached. One should note that the critical angles are largely indicative of the generally higher wave speeds in the tilted TI medium but the apparent increase in symmetry for this case is probably somewhat co-incidental and dependent on the choice of the elastic constants.

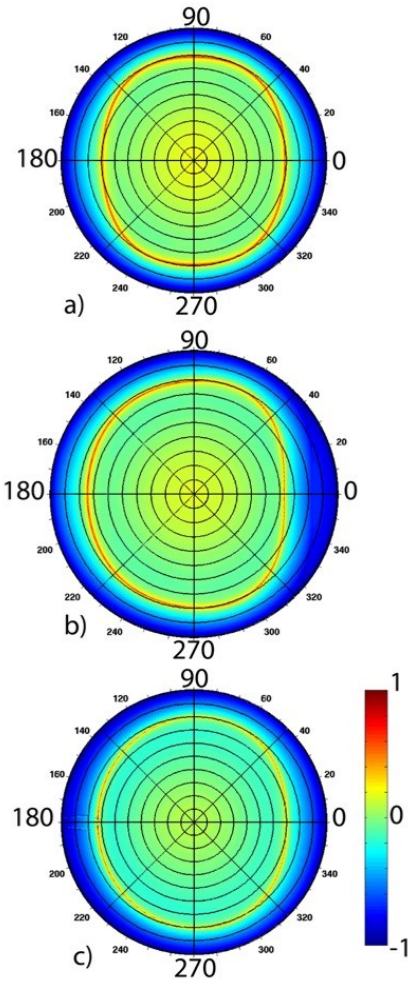

Figure 2.6. This figure depicts calculated PP reflectivity from TI-ORT boundary in all possible directions. Location of warm color ribbon, which represents critical angle for P-wave reflection, varies with azimuth. The pattern for $\psi = 0°$ shows two planes of symmetries where located at azimuthal direction $\varphi = 0°$ and 90° degrees. However, planes of symmetry of the TI medium is rotated to (b) $\psi = 30°$ and c) $\psi = 60°$ degrees about the x1 axis.

The second, more challenging, case places stacks monoclinic over triclinic materials. This requires knowledge of 34 original elastic coefficients. Here the one symmetry axis of the monoclinic material is aligned parallel to *x3* and it is rotated around this axis through angles of 0° (Figure 2-7a), 45° (Figure 2-7b), and 60° (Figure 2-7c). The reflectivity pattern for this case is oddly shaped as might be expected from the lack of symmetry in both of the materials. The rotation of the pattern, however is apparent.

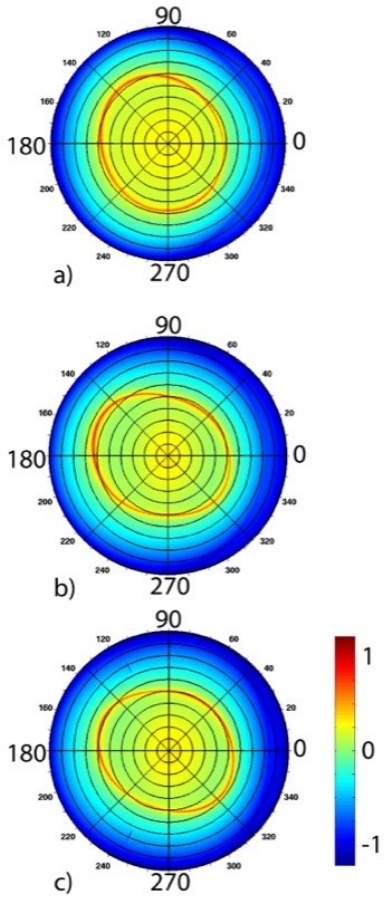

Figure 2.7. This figure shows how calculated PP amplitude ratio from monoclinic (top layer) and triclinic anisotropy (base layer) varies with direction. Warm color ribbon indicates PP critical angle reflection, changes with azimuthal direction, as we would have imagined, but the pattern is highly non-symmetric. To emphasize the effect of medium orientation on reflectivity, it is also calculated for angular orientation about x1 axis with b) $\psi = 45^\circ$ and c) $\psi = 60^\circ$ degrees rotations about the x1 axis. Patterns show significant difference in amplitude variation with the non-rotated model (a).

2.4 Discussion and Conclusion

In this Chapter, we describe an algorithm, which is able to calculate velocity, particle polarization and amplitude variations with direction in all anisotropic media up to triclinic symmetry. We have carried out some basic tests to ensure that it does not produce spurious errors,

and that it can reproduce some previous results. We can see how the velocity varies with direction inside an elastic anisotropic media which shows a very complex behavior when propagates within the least symmetric ones as illustrated in Figure. 2-4. Accurate calculation of the velocity of all wave-modes is important in being able to extract additional information from seismic data sets via inversion and to understand possible complex behavior by forward modeling.

The deviations of the particle polarizations (Figure 2-5) reveal complex patterns. Observations of particle motions are key to investigations of earthquake focal mechanisms and shear wave splitting. Such studies are mostly carried out under the presumption that the observed particle motions follow those expected through an isotropic medium. However, these deviations from the isotropic case may carry additional useful information about the subsurface textures and structures.

The most important implication of this program is that it will allow workers to more readily investigate seismic reflectivity in complex cases. As noted in the literature review, most studies have studied special cases (e.g. two stacked VTI media) or have relied on approximations that often remain valid only at small angles of incidence. The program here is not restricted in this way and will allow workers to more readily test more sophisticated hypotheses with regards to the Earth's structure.

It is now well-known that seismic anisotropy is often more the rule than the exception at all scales from the laboratory to the Earth's mantle. The tools available to the research community to study seismic reflectivity, particularly for cases of lower symmetry, are limited. The algorithm presented in this Chapter should be considered an advanced tool for the quantitative analysis of plane-wave propagation in elastic anisotropic media. We expect it will find particular use in studies seeking to better understand seismic reflectivity in complex geological geometries.

2.5 Appendix 2-A. Guide to use the software

The set of subroutines which ARTc are written using MATLAB®. Figure 2-A1, shows the flowchart of the ARTC packager and how and when the subroutines are called. All subroutines can be used as a stand-alone functions to solved related parameters, e.i. ChrisKel is used to create

velocity and polarization figures 2-4 and 2-5. We also designed a MATLAB® GUI (intentionally similar to conventional calculators) that solves for wave properties (velocity and polarization) in a general anisotropic medium, and, more importantly solves for amplitude ratio of generated wave-modes from two slabs of anisotropic medium with arbitrary orientation. ARTc has a great potential for developers to extended it to multi-layered scenario. The following list, shows the table of subroutines and their corresponding application in the calculations.

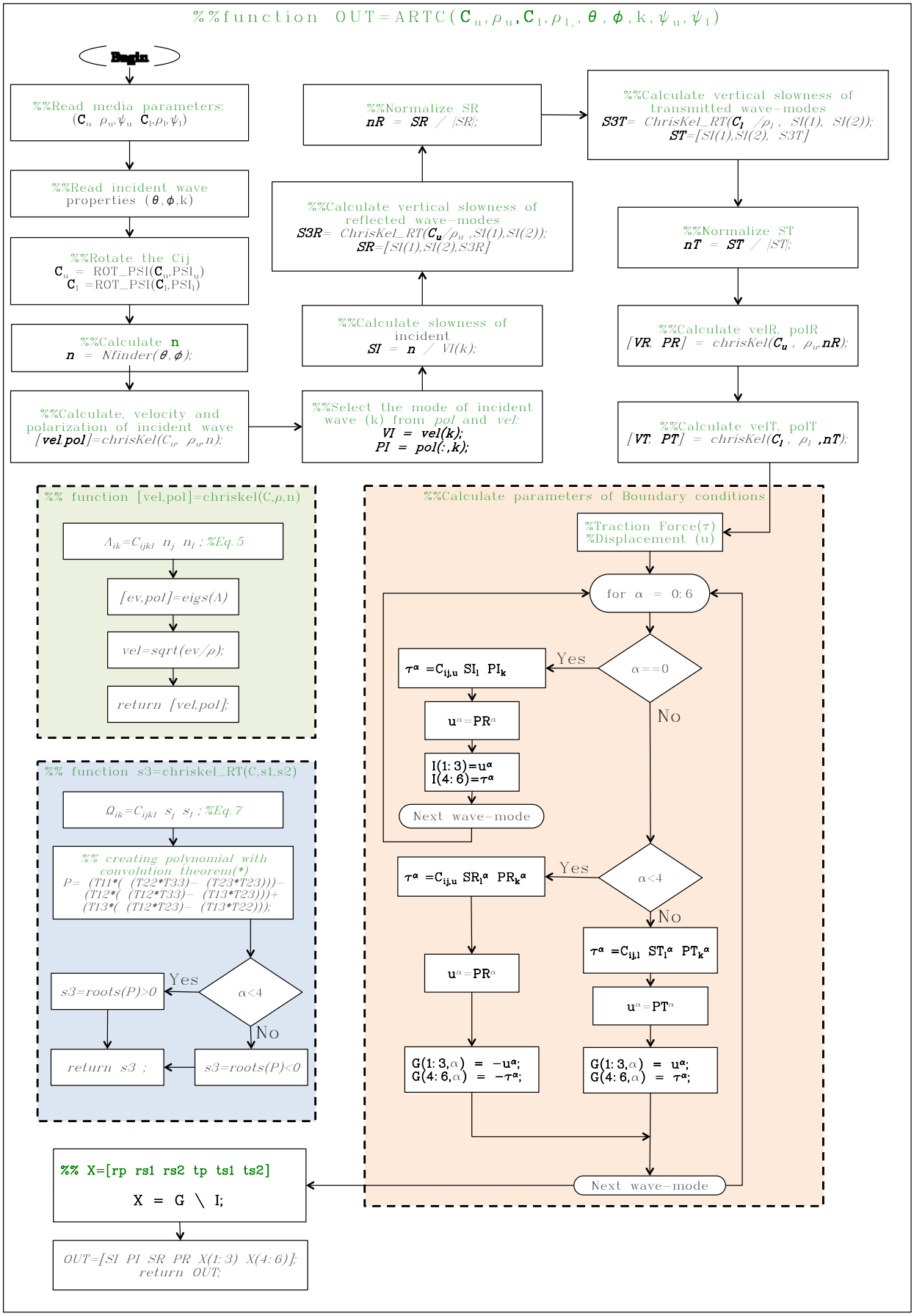
%%function OUT=ARTC(C_u, ρ_u, C_l, ρ_l, θ, ϕ, k, ψ_u, ψ_l)
Begin
%%Read media parameters: (C_u ρ_u,ψ_u C_l,ρ_l,ψ_l)
%%Read incident wave properties (θ,ϕ,k)
%%Rotate the Cij C_u = ROT_PSI(C_u,PSI_u) C_l =ROT_PSI(C_l,PSI_l)
%%Calculate n n = Nfinder(θ,ϕ);
%%Calculate, velocity and polarization of incident wave [vel,pol]=chriskel(C_u, ρ_u,n);
%%Select the mode of incident wave (k) from pol and vel: VI = vel(k); PI = pol(:,k);
%%Calculate slowness of incident SI = n / VI(k);
%%Calculate slowness of reflected wave-modes S3R= ChrisKel_RT(C_u/ρ_u ,SI(1),SI(2)); SR=[SI(1),SI(2),S3R]
%%Normalize SR nR = SR / |SR|;
%%Calculate vertical slowness of transmitted wave-modes S3T= ChrisKel_RT(C_l /ρ_l , SI(1), SI(2)); ST=[SI(1),SI(2), S3T]
%%Normalize ST nT = ST / |ST|;
%%Calculate velR, polR [VR, PR] = chriskel(C_u , ρ_u,nR);
%%Calculate velT, polT [VT, PT] = chriskel(C_l , ρ_l ,nT);
%% function [vel,pol]=chriskel(C,ρ,n)
Λ_ik=C_ijkl n_j n_l ; %Eq. 5
[ev,pol]=eigs(Λ)
vel=sqrt(ev/ρ);
return [vel,pol];
%% function s3=chriskel_RT(C,s1,s2)
Ω_ik=C_ijkl s_j s_l ; %Eq. 7
%% creating polynomial with convolution theorem(*)
P= (T11*((T22*T33)- (T23*T23)))- (T12*((T12*T33)- (T13*T23)))+ (T13*((T12*T23)- (T13*T22)));
s3=roots(P)>0
Yes
α<4
No
return s3 ;
s3=roots(P)<0
%%Calculate parameters of Boundary conditions
%Traction Force(τ) %Displacement (u)
for α = 0:6
α==0
Yes
τ^α =C_ij,u SI_l PI_k
No
u^α=PR^α
I(1:3)=u^α I(4:6)=τ^α
Next wave-mode
α<4
Yes
τ^α =C_ij,u SR_l^α PR_k^α
No
τ^α =C_ij,l ST_l^α PT_k^α
u^α=PR^α
u^α=PT^α
G(1:3,α) = −u^α; G(4:6,α) = −τ^α;
G(1:3,α) = u^α; G(4:6,α) = τ^α;
Next wave-mode
%% X=[rp rs1 rs2 tp ts1 ts2]
X = G \ I;
OUT=[SI PI SR PR X(1:3) X(4:6)]; return OUT;

Figure 2.A1. Displays the flowchart of the ARTC main function. Dashed block diagram illustrate subroutines '*ChrisKel'*, '*ChrisKel_RT'*, and '*Boundary_Condition'* and their corresponding role in the ARTc algorithm.

Subroutine	Application
ARTc.m	Main function
Nfinder.m	Converts angular direction to vector direction
ChrisKel.m	Solves for velocity and polarization. (Eqn. 2-4 & 2-5)
ChrisKel_RT.m	Find vertical Slowness of reflected and refracted waves (Eqn.2-8)
Boundary_condition.m	Form boundary condition system of Eqn. (2-10,2-13)
ph2gr.m	Calculate group velocity from phase velocity
stiff.m	Preset elastic coefficients of popular anisotropic symmetries
run_artc.m	run ARTC calculator with given parameters
traction3.m	Calculate traction force at the boundary, Eqn.(2-11)
REFLECTIVITY.fig	GUI designed to easily calculate wave properties
input.i	input file to run run_artc.
Output.mat, .ascii	Includes $\mathbf{v}$, $\boldsymbol{\xi}$, amplitude ratios and direction of all generated waves

The structure of *input.i* files dictates the model parameters of the media on top and base of the boundary, '*t', 'b'* suffix indicate top and base medium, respectively.

```
% 't' and 'b' suffix stands for properties of top and base layers.
% Cij is stifness of the medium
% rho: density
% psi: represents angular rotation about x1 axis.
wavetype % mode of the incident wave; 1=qP, 2=qS1, 3=qS2
theta phi % direction of propagation
c11t c12t c13t c14t c15t c16t % top layer elastic coefficients
c22t c23t c24t c25t c26t
c33t c34t c35t c36t
c44t c45t c46t
c55t c56t
c66t
rhot % density of the top layer
psit % orientation of the top layer
c11b c12b c13b c14b c15b c16b % base layer elastic coefficients
c22b c23b c24b c25b c26b
c33b c34b c35b c36b
c44b c45b c46b
c55b c56b
c66b
rhob % density of the base layer
psib % orientaiton of the base layer
```

The subroutine "*stiff*" has several sample cases of anisotropy which could be used to in the "*run_artc*" to quickly run the algorithm. The structure of the *output* of the ARTC includes Reflectivity; Slowness; polarization, angle of generated waves from the boundary; that could be easily saved in *".mat"* or "*.ascii"* format via MATLAB built in functions.

There are three ways that user can work with the ARTc. Directly running ARTc.m file in MATLAB®, is imperative, in addition we have developed a bash file which reads the input file(s) and performs the calculation on the parallel computers. To run the ARTc with the input file, one need to run the bash file, *runARTc.sh*. Where the structure of the *runARTc.sh* is:

```
#!/bin/bash
matlab -nojvm -r run_artc.m &
```

We also designed a GUI in MATLAB ® to run and monitor the algorithm visually as displayed in Figure 2-A2 The user has options to modify the elastic stiffnesses and densities in

Panels 1 and 2. Information about the incident wave's mode and incidence inclination and azimuth angles are in Panel 3. Execution buttons are contained in Panel 4 and the final results displayed in Panel 5. You might take the advantage of MATLAB ® built in *parfor* loop to use *run_artc.m* in a parallel form on multiprocessor machine.

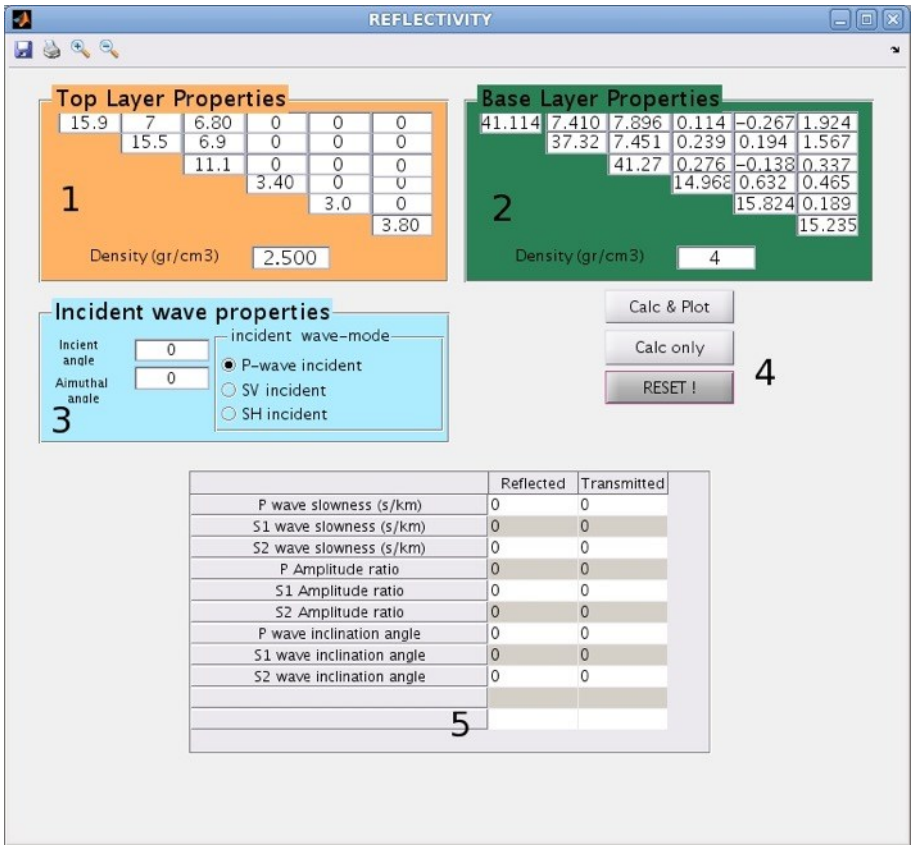

Figure 2.A2. We designed the GUI to easily calculate and monitor wave properties in two-layered anisotropic model. Panels 1 and 2 describes elastic coefficients and densities of the top and base layer, panel 3 describes the input wave-mode properties. Panel 4 includes executive buttons and panel 5 displays the results. Defaults in the GUI represents orthorhombic (top) triclinic (base) layer model with P-wave incident wave-mode.

Index

ρ	Bulk density
$\boldsymbol{v}$	Phase velocity
V	Group velocity
$\boldsymbol{\xi}$	Particle polarization
θ	Inclination angle from x3 axis
φ	Azimuthal angle from x1 axis
ψ	Rotational angle from about x1 axis
u	Particle displacement vector
C	Rotated fourth order stiffness tensor,
$\boldsymbol{\Lambda}$	Elastic coefficients multiplied by $\boldsymbol{n}$
$\boldsymbol{\Omega}$	Density-normalized elastic coefficients multiplied by $\boldsymbol{n}$
τ	Stress tensor
ε	Strain tensor
$\boldsymbol{s}$	Slowness vector
η	Normal vector to the boundary
$\mathbf{n}$	Normal to the wave-front vector
δ	Kronecker operator
A	Amplitude of the plane-wave

Reference

Aki, K., and P. G. Richards (1980), *Quantitative seismology: Theory and methods, v.1*, W.H. Freeman and Co, San Francisco.

Aleardi, M., and A. Mazzotti (2014), A feasibility study on the expected seismic AVA signatures of deep fractured geothermal reservoirs in an intrusive basement, *J. Geophys. Eng.*, *11*(6), 65008, doi:10.1088/1742-2132/11/6/065008.

Alhussain, M. (2007), Spherical Wave AVO Response of Isotropic and Anisotropic Media : Laboratory Experiment versus Numerical Simulations Mohammed Abdullah K Alhussain, University of Curtin.

Alhussain, M., E. Liu, B. Gurevich, M. Urosevic, and S. U. Rehman (2007), AVOaz response of a fractured medium: Laboratory measurements versus numerical simulations, *SEG Tech. Progr. Expand. Abstr.*, *26*(1), 254–258, doi:10.1190/1.2792421.

Alhussain, M., B. Gurevich, and M. Urosevic (2008), Experimental verification of spherical-wave effect on the AVO response and implications for three-term inversion, *Geophysics*, *73*(2), C7–C12, doi:10.1190/1.2837641.

Almqvist, B. S. G., L. Burlini, D. Mainprice, and A. M. Hirt (2010), Elastic properties of anisotropic synthetic calcite-muscovite aggregates, *J. Geophys. Res. Solid Earth*, *115*(8), 1–15, doi:10.1029/2009JB006523.

Arts, R., P. Rasolofosaon, and B. Zinszner (1991), Complete inversion of the anisotropic elastic tensor in rocks: Experiment versus theory, *1991 SEG Annu. Meet.*, 1538–1541.

Auld, B. A. (1973), *Acoustic fields and waves in solids- Vol 2*, John Wiley & Sons, Inc.

Backus, G. E. (1962), Long-wave elastic anisotropy produced by horizontal layering, *J. Geophys. Res.*, *67*(11), 4427, doi:10.1029/JZ067i011p04427.

Backus, G. E. (1965), Possible forms of seismic anisotropy of the uppermost mantle under oceans, *J. Geophys. Res.*, *70*(14), 3429, doi:10.1029/JZ070i014p03429.

Bakulin, A., V. Grechka, and I. Tsvankin (2000), Estimation of fracture parameters from reflection seismic data—Part II: Fractured models with orthorhombic symmetry, *Geophysics*, *65*(6).

Bao, X., D. W. Eaton, and Y. J. Gu (2016), Rayleigh-wave azimuthally anisotropic phase-

velocity maps beneath western Canada, *J. Geophys. Res. Solid Earth*, n/a-n/a, doi:10.1002/2015JB012453.

Bass, J. D. (1995), Elasticity of minerals, glasses, and melts, in *Mineral Physics and Crystallography: A Handbook*, pp. 45–63.

Behura, J., and I. Tsvankin (2006), Small-angle AVO response of PS-waves in tilted transversely isotropic media, *Geophysics*, *71*(5), C69, doi:10.1190/1.2329865.

Behura, J., and I. Tsvankin (2009), Reflection coefficients in attenuative anisotropic media, *Geophysics*, *74*(5), WB193, doi:10.1190/1.3142874.

Belonoshko, A. B., N. V Skorodumova, A. Rosengren, and B. Johansson (2008), Elastic anisotropy of Earth's inner core., *Science*, *319*(5864), 797–800, doi:10.1126/science.1150302.

Ben-Menahem, A., and A. G. Sena (1990), Seismic source theory in stratified anisotropic media, *J. Geophys. Res.*, *95*(B10), 15395, doi:10.1029/JB095iB10p15395.

Bertoni, H. L., and T. Tamir (1973), Unified theory of Rayleigh-angle phenomena for acoustic beams at liquid-solid interfaces, *Appl. Phys.*, *2*(4), 157–172, doi:10.1007/BF00884205.

Boness, N. L., and M. D. Zoback (2004), Stress-induced seismic velocity anisotropy and physical properties in the SAFOD Pilot Hole in Parkfield, CA, *Geophys. Res. Lett.*, *31*(15), L15S17, doi:10.1029/2003GL019020.

Bortfeld, R. (1961), APPROXIMATIONS TO THE REFLECTION AND TRANSMISSION COEFFICIENTS OF PLANE LONGITUDINAL AND TRANSVERSE WAVES*, *Geophys. Prospect.*, *9*(4), 485–502, doi:10.1111/j.1365-2478.1961.tb01670.x.

Bouzidi, Y., and D. R. Schmitt (2006), A large ultrasonic bounded acoustic pulse transducer for acoustic transmission goniometry: Modeling and calibration, *J. Acoust. Soc. Am.*, *119*(1), 54, doi:10.1121/1.2133683.

Bouzidi, Y., and D. R. Schmitt (2008a), Acoustic reflectivity goniometry of bounded ultrasonic pulses: Experimental verification of numerical models, *J. Appl. Phys.*, *104*(6), doi:10.1063/1.2982094.

Bouzidi, Y., and D. R. Schmitt (2008b), Quantitative modeling of refected ultrasonic bounded beams and a new estimate of the schoch shift, *IEEE Trans. Ultrason. Ferroelectr. Freq.*

Control, *55*(12), 2661–2673, doi:10.1109/TUFFC.2008.981.

Bouzidi, Y., and D. R. Schmitt (2012), Incidence-angle-dependent acoustic reflections from liquid-saturated porous solids, *Geophys. J. Int.*, *191*(3), 1427–1440, doi:10.1111/j.1365-246X.2012.05695.x.

Breazeale, M. A., L. Adler, and G. W. Scott (1977), Interaction of ultrasonic waves incident at the Rayleigh angle onto a liquid-solid interface, *J. Appl. Phys.*, *48*(2), 530–537, doi:10.1063/1.323677.

Brekhovskikh, L. M. (1960), *Waves in layered media.*, Academic Press, New York,.

Brown, R. J., D. C. Lawton, and S. P. Cheadle (1991), Scaled physical modelling of anisotropic wave propagation: multioffset profiles over an orthorhombic medium, *Geophys. J. Int.*, *107*(3), 693–702, doi:10.1111/j.1365-246X.1991.tb01428.x.

Carcione, J. M. (1997), Reflection and transmission of qP-qS plane waves at a plane boundary between viscoelastic transversely isotropic media, *Geophys. J. Int.*, *129*, 669–680.

Castagna, J., and M. Backus (1993), *Offset-dependent refletivity-theory and practice of AVO analysis*, Society of Exploration Geophysicist.

Chattopadhyay, A., P. Kumari, and V. K. Sharma (2015), Reflection and refraction at the interface between distinct generally anisotropic half spaces for three-dimensional plane quasi-P waves, *J. Vib. Control*, *21*, 493–508.

Cheadle, S. P. (1991), Orthorhombic anisotropy: A physical seismic modeling study, *Geophysics*, *56*(10), 1603, doi:10.1190/1.1442971.

Chen, H., J. P. Castagna, R. L. Brown, and A. C. B. Ramos (2001), Three-parameter AVO crossplotting in anisotropic media, *Geophysics*, *66*(5), 1359, doi:10.1190/1.1487081.

Christensen, N. I. (1965), Compressional wave velocities in metamorphic rocks at pressures to 10 kilobars, *J. Geophys. Res.*, *70*(24), 6147–6164, doi:10.1029/JZ070i024p06147.

Christoffel, E. B. (1877), Uber die Fortpflanzung von Stossen durch elastische fest Korper, *Ann. Mater.*, *8*, 193–243.

Claerbout, J. F. (1985), *IMAGING THE EARTH's INTERIOR*, Blackwell Scientific Publications, Oxford, London, Edinburgh, Boston, Palo Alto, Victoria.

Crampin, S. (1985), Evaluation of anisotropy by shear-wave splitting, *Geophysics*, *50*(1), 142,

doi:10.1190/1.1441824.

Daley, P. ., and F. Hron (1987), Reflection and transmission coefficients for transversely isotropic media, *Bull. Seism. Soc. Am.*, *67*(3), 661–675.

Daley, P. F. (1979), Reflection and transmission coefficients for seismic waves in ellipsoidally anisotropic media, *Geophysics*, *44*(1), 27, doi:10.1190/1.1440920.

Daley, P. F., and F. Hron (1977a), REFLECTION AND TRANSMISSION COEFFICIENTS TRANSVERSELY ISOTROPIC MEDIA, *BSSA*, *67*(3), 661–675.

Daley, P. F., and F. Hron (1977b), REFLECTION AND TRANSMISSION COEFFICIENTS TRANSVERSELY ISOTROPIC MEDIA, *BSSA*, *67*(3), 661–675.

Declercq, N. F. (2006), Fast beating null strip during the reflection of pulsed Gaussian beams incident at the Rayleigh angle, *Ultrasonics*, *44*(SUPPL.), e1447–e1451, doi:10.1016/j.ultras.2006.05.205.

Declercq, N. F., R. Briers, J. Degrieck, and O. Leroy (2005), The history and properties of ultrasonic inhomogeneous waves, *IEEE Trans. Ultrason. Ferroelectr. Freq. Control*, *52*(5), 776–791, doi:10.1109/TUFFC.2005.1503963.

Descamps, M., and B. Hosten (1991), The effects of viscoelasticity on the reflection and transmission of ultrasonic waves by an orthotropic plate, *J. Acoust. Soc. Am.*, *29*(6), 1763–1770, doi:10.1006/jsvi.1996.0374.

Diachok, O. I. (1970), Conical Reflection of Ultrasound from a Liquid-Solid Interface, *J. Acoust. Soc. Am.*, *47*(1B), 155, doi:10.1121/1.1911450.

Dvorkin, J., M. Gutierrez, and D. Grana (2014), *Seismic Reflections of Rock Properties*.

Ekanem, a. M., J. Wei, X. Y. Li, M. Chapman, and I. G. Main (2013), P-wave attenuation anisotropy in fractured media: A seismic physical modelling study, *Geophys. Prospect.*, *61*(SUPPL.1), 420–433, doi:10.1111/j.1365-2478.2012.01127.x.

Far, M. E., C. M. Sayers, L. Thomsen, D. H. Han, and J. P. Castagna (2013), Seismic characterization of naturally fractured reservoirs using amplitude versus offset and azimuth analysis, *Geophys. Prospect.*, *61*(2), 427–447, doi:10.1111/1365-2478.12011.

Farra, V., and I. Pšenčík (2010), First-order reflection/transmission coefficients for unconverted plane P waves in weakly anisotropic media, *Geophys. J. Int.*, *183*(3), 1443–1454,

doi:10.1111/j.1365-246X.2010.04794.x.

Gassmann, F. (1964), Introduction to seismic travel time methods in anisotropic media, *Pure Appl. Geophys. PAGEOPH*, *58*(1), 63–112, doi:10.1007/BF00879140.

Gazdag, J. (1978), Wave equation migration with the phase-shift method, *Geophysics*, *43*(7), 1342, doi:10.1190/1.1440899.

Godfrey, N. J., N. I. Christensen, and D. a. Okaya (2000), Anisotropy of schists: Contribution of crustal anisotropy to active source seismic experiments and shear wave splitting observations, *J. Geophys. Res.*, *105*(B12), 27991–28007, doi:10.1029/2000JB900286.

Golikov, P., and A. Stovas (2010), New weak-contrast approximation for reflection coefficients in transversely isotropic media, *J. Geophys. Eng.*, *7*(4), 343–350, doi:10.1088/1742-2132/7/4/001.

Graebner, M. (1992), Plane- wave reflection and transmission coefficients for a transversely isotropic solid, *GEOPHYSICS*, *57*(11), 1512–1519, doi:10.1190/1.1443219.

Gray, D., G. Roberts, and K. Head (2002), Recent advances in determination of fracture strike and crack density from P-wave seismic data, *Lead. Edge*, *21*(3), 280, doi:10.1190/1.1463778.

Grech, M. G. K., D. C. Lawton, and S. H. Gray (2002), A multioffset vertical seismic profiling experiment for anisotropy analysis and depth imaging, *Geophysics*, *67*(2), 348–354, doi:10.1190/1.1468595.

Grechka, V., and I. Tsvankin (2004), Characterization of dipping fractures in a transverselyisotropic background, *Geophys. Prospect.*, *52*(1), 1–10, doi:10.1046/j.1365-2478.2004.00396.x.

Guest, W. S., and J.-M. Kendall (1993), Modelling waveforms in anisotropic inhomogeneous media using ray and Maslov asymptotic theory: applications to exploration seismology, *Can. J. Expl. Geophys.*, *29*, 78–92.

Guest, W. S., and C. J. Thomson (1992), A SOURCE OF SIGNIFICANT TRANSVERSE ARRIVALS FROM AN ISOTROPIC ANISOTROPIC INTERFACE, eg THE MOHO., *Geophys. J. Int.*, *111*, 309–318.

Guest, W. S., C. J. Thomson, and C. P. Spencer (1993), Anisotropic reflection and transmission

calculations with application to a crustal seismic survey from the East Greenland Shelf, *J. Geophys. Res.*, *98*(B8), 14161, doi:10.1029/93JB01156.

Hall, S. A., and J. Kendall (2003), Fracture characterization at Valhall: Application of P-wave amplitude variation with offset and azimuth (AVOA) analysis to a 3D ocean-bottom data set, *Geophysics*, *68*(4), 1150, doi:10.1190/1.1598107.

Helbig, K. (1994), *Foundations of Anisotropy for Exploration Seismics*, Elsevier, Utrecht.

Henneke, E. G. (1972), Reflection-Refraction of a Stress Wave at a Plane Boundary between Anisotropic Media, *J. Acoust. Soc. Am.*, *51*(1B), 210, doi:10.1121/1.1912832.

Henneke, E. G., and G. L. Jones (1976), Erratum: ''Critical angle for reflection at a liquid–solid interface in single crystals'', *J. Acoust. Soc. Am.*, *60*(3), 759, doi:10.1121/1.381248.

Hood, J. A., and M. Schoenberg (1992), NDE of fracture-induced anisotropy, *Rev. Prog. Quant. Nondestruct. Eval. Vol. 11B*, *11*, 2101–2108.

Innanen, K. A., and F. Mahmoudian (2015), Characterizing the degree of amplitude-variation-with-offset nonlinearity in seismic physical modelling reflection data, *Geophys. Prospect.*, *63*(1), 133–140, doi:10.1111/1365-2478.12169.

Isaac, J. H., and D. C. Lawton (1999), Image mispositioning due to dip-ping TI Media: A physical seismic modeling study, *Geophysics*, *64*, 1230–1238.

Jech, J. (1991), Computation of elastic parameters of anisotropic medium from travel times of quasi-compressional waves, *Phys. Earth Planet. Inter.*, *66*(3–4), 153–159, doi:10.1016/0031-9201(91)90074-R.

Ji, S., T. Shao, K. Michibayashi, C. Long, Q. Wang, Y. Kondo, W. Zhao, H. Wang, and M. H. Salisbury (2013), A new calibration of seismic velocities, anisotropy, fabrics, and elastic moduli of amphibole-rich rocks, *J. Geophys. Res. E Planets*, *118*(9), 4699–4728, doi:10.1002/jgrb.50352.

Jocker, J., and D. Smeulders (2007), Minimization of finite beam effects in the determination of reflection and transmission coefficients of an elastic layer, *Ultrasonics*, *46*(1), 42–50, doi:10.1016/j.ultras.2006.10.001.

Kaarsberg, E. A. (1959), Introductory Studies of Natural and Artificial Argillaceous Aggregates by Sound-Propagation and X-ray Diffraction Methods, *J. Geol.*, *67*(4), 447–472,

doi:10.1086/626597.

Kebaili, A., and D. R. Schmitt (1997), Ultrasonic anisotropic phase velocity determination with the Radon transformation, *J. Acoust. Soc. Am.*, *101*(6), 3278, doi:10.1121/1.418344.

Keith, C. M., and S. Crampin (1977), Seismic body waves in anisotropic media: Reflection and refraction at a plane interface, *Geophys. J. Roy. Astr. Soc.*, *49*, 181–208.

Kendall, J.-M., and C. J. Thomson (1989), A comment on the form of the geometrical spreading equations, with some numerical examples of seismic ray tracing in inhomogeneous, anisotropic media, *Geophys. J. Int.*, *99*(2), 401–413, doi:10.1111/j.1365-246X.1989.tb01697.x.

Kern, H., and H. R. Wenk (1990), Fabric-related velocity anisotropy and shear wave splitting in rocks from the Santa Rosa Mylonite Zone, California, *J. Geophys. Res. Solid Earth*, *95*(B7), 11213–11223, doi:10.1029/JB095iB07p11213.

Klimes, L. (2003), Weak-contrast reflection–transmission coefficients in a generally anisotropic background, *Geophysics*, *68*(6), 2063, doi:10.1190/1.1635060.

Knott, C. G. (1899), Reflexion and Refraction of Elastic Waves with Seismological Applications, *Philos. Mag.*, *54*(5th series), 64–97.

Krail, P. M., and H. Brysk (1983), Reflection of spherical seismic waves in elastic layered media, *Geophysics*, *48*(6).

Landrø, M., and I. Tsvankin (2006), Seismic critical-angle reflectometry: A method to characterize azimuthal anisotropy?, *Geophysics*, *72*(3), 120–124, doi:10.1190/1.2437145.

Leary, P. C., S. Crampin, and T. V. McEvilly (1990), Evolution of Mid Ocean Ridges, edited by J. M. Sinton, *J. Geophys. Res.*, *95*(B7), 11105–11114, doi:10.1029/GM057.

Di Leo, J. F., A. M. Walker, Z. H. Li, J. Wookey, N. M. Ribe, J. M. Kendall, and A. Tommasi (2014), Development of texture and seismic anisotropy during the onset of subduction, *Geochemistry, Geophys. Geosystems*, *15*(1), 192–212, doi:10.1002/2013GC005032.

Leroy, O., and B. Poirèe (1988), On the Reflection Coefficient of Acoustic Beams, *Acustica*, *66*, 84–89.

Li, L. (2008), Calculation of reflection and transmission coefficients for qP waves incident on a planar interface between isotropic and triclinic media, *Acta Geophys.*, *56*, 518–528.

Liang, K., X. Yin, and G. Wu (2009), Approximate PP reflection coefficient in TTI media, in *Beijing 2009 International Geophysical Conference and Exposition, Beijing, China, 24–27 April 2009*, edited by L. Zhenwu and Y. Sun, pp. 126–126, Society of Exploration Geophysicists.

Lin, F.-C., M. H. Ritzwoller, Y. Yang, M. P. Moschetti, and M. J. Fouch (2011), Complex and variable crustal and uppermost mantle seismic anisotropy in the western United States, *Nat. Geosci.*, *4*(1), 55–61, doi:10.1038/ngeo1036.

Liu, Y., and D. R. Schmitt (2006), The transition between the scale domains of ray and effective medium theory and anisotropy: Numerical models, *Pure Appl. Geophys.*, *163*(7), 1327–1349, doi:10.1007/s00024-006-0075-5.

Mah, M., and D. R. Schmitt (2001a), Experimental determination of the elastic coefficients of an orthorhombic material, *Geophysics*, *66*(4), 1217, doi:10.1190/1.1487068.

Mah, M., and D. R. Schmitt (2001b), Experimental determination of the elastic coefficients of an orthorhombic material, *Geophysics*, *66*(4), 1217, doi:10.1190/1.1487068.

Mahmoudian, F. (2013), Physical Modeling and Analysis of Seismic Data from a Simulated Fractured Medium, University of Calgary.

Mahmoudian, F., G. Margrave, and P. Daley (2014), Estimation of elastic stiffness coefficients of an orthorhombic physical model using group velocity analysis on transmission data, *Geophysics*, *79*(1), R27–R39, doi:10.1190/geo2013-0203.1.

Mahmoudian, F., G. F. Margrave, J. Wong, and D. C. Henley (2015), Azimuthal amplitude variation with offset analysis of physical modeling data acquired over an azimuthally anisotropic medium, *GEOPHYSICS*, *80*(1), C21–C35, doi:10.1190/geo2014-0070.1.

Mainprice, D., and A. Nicolas (1989), Development of shape and lattice preferred orientations: application to the seismic anisotropy of the lower crust, *J. Struct. Geol.*, *11*(1–2), 175–189, doi:10.1016/0191-8141(89)90042-4.

Malehmir, R., and D. R. Schmitt (2016a), ARTc: Anisotropic reflectivity and transmissivity calculator, *Comput. Geosci.*, *93*, 114–126, doi:10.1016/j.cageo.2016.05.008.

Malehmir, R., and D. R. Schmitt (2016b), Ultrasonic measurement of anisotropic reflectivity from Water-Phenolic CE Interface, *PANGAEA*, doi:10.1594/PANGAEA.864794.

Malehmir, R., and D. R. Schmitt (2017), Acoustic Reflectivity from an Orthorhombic Media : Understanding the Fractured Anisotropic Crust, *J. Geophys. Res.*, Under review.

Malehmir, R., N. Kazemi, and D. R. Schmitt (2017), An Algorithm to Quantitatively Model Reflected Ultrasonic Bounded Beam with Experimental Validation, *Ultrasonics*.

Mallick, S., and L. N. Frazer (1991), REFLECTION-TRANSMISSION COEFFICIENTS AND AZIMUTHAL ANISOTROPY IN MARINE SEISMIC STUDIES, *Geophys. J. Int.*, *105*, 241–252.

Mallick, S., K. L. Craft, L. J. Meister, and R. E. Chambers (1998), Determination of the principal directions of azimuthal anisotropy from P-wave seismic data, *GEOPHYSICS*, *63*(2), 692–706, doi:10.1190/1.1444369.

Mann, R. W., G. A. Baum, and C. C. Habeger (1980), Determination of all nine orthotropic elastic constants for machine-made paper, *Tappi*, *63*(84), 163–166.

McCamy, K., R. P. Meyer, and T. J. Smith (1962), Generally applicable solutions of Zoeppritz' amplitude equations, *BSSA*, *52*, 923–955.

Merkulov, L. G. (1963), Ultrasonic waves in crystals, *Appl. Mater. Res.*, *2*(4), 231–240.

Musgrave, M. J. P. (1970a), *Crystal Acoustics: Introduction to the Study of Elastic Waves and Vibrations in Crystals*, Holden-Day.

Musgrave, M. J. P. (1970b), *Musgrave M.J.P. Crystal Acoustics 1970.djvu.pdf*, HOLDEN-DAY, San Francisco.

Nakagawa, S., K. T. Nihei, L. R. Myer, and E. L. Majer (2003), Three-dimensional elastic wave scattering by a layer containing vertical periodic fractures, *J. Acoust. Soc. Am.*, *113*(6), 3012, doi:10.1121/1.1572139.

Nayfeh, A. H. (1989), The propagation of horizontally polarized shear waves in multilayered anisotropic media, *J. Acoust. Soc. Am.*, *86*(5), 1–16, doi:10.1121/1.398580.

Ngoc, T. D. K., and W. G. Mayer (1979), Ultrasonic nonspecular reflectivity near longitudinal critical angle, *J. Appl. Phys.*, *50*(12), 7948–7951, doi:10.1063/1.325971.

Nishizawa, O., and K. Kanagawa (2010), Seismic velocity anisotropy of phyllosilicate-rich rocks: characteristics inferred from experimental and crack-model studies of biotite-rich schist, *Geophys. J. Int.*, *182*(1), no-no, doi:10.1111/j.1365-246X.2010.04614.x.

Ortiz-osornio, M., and D. R. Schmitt (2009), Measurements of the reflectivity of a liquid – anisotropic solid interface, in *8th Euro Conference of Rock Physics & Geomechanics*, p. 4pp, Ascona, Switzerland.

Ortiz-osornio, M., and D. R. Schmitt (2010a), The Reflectivity and Transmissivity of Anisotropic Materials : A Physical Modeling Study, in *American Rock Mechanics Association*, p. 5pp.

Ortiz-osornio, M., and D. R. Schmitt (2010b), The reflectivity and transmissivity of anisotropic materials: A physical model study, in *ARMA 44th U.S. Rock Mechanics Symposium*, p. 5 pp, Salt Lake City.

Ortiz-osornio, M., and D. R. Schmitt (2010c), Velocity dispersion of a heavy oil sandstone: A case study, in *Oil Sands and Heavy Oil Technologies Conference, Calgary*, pp. 20–22.

Ortiz-osornio, M., and D. R. Schmitt (2011a), Measurements of the reflectivity and transmissivity of anisotropic materials to test the effect of tilt and azimuth, in *1st Int. Workshop on Rock Physics, August 7-12,* p. 4pp, Golden, CO.

Ortiz-osornio, M., and D. R. Schmitt (2011b), Physical Modeling of the Reflectivity and Transmissivity of Anisotropic Materials, in *73rd EAGE Conference and Exhibition incorporating SPE EUROPEC 2011, Vienna*, p. 4 pp, Vienna.

Ostrander, W. J. (1984), Plane-wave reflection coefficients for gas sands at nonnormal angles of incidence - ostrander1984.pdf, *Geophysics*, *49*(10), 1637–1648.

Ozacar, A. A., and G. Zandt (2004), Crustal seismic anisotropy in central Tibet: Implications for deformational style and flow in the crust, *Geophys. Res. Lett.*, *31*(23), 1–4, doi:10.1029/2004GL021096.

Ozacar, A. A., and G. Zandt (2009), Crustal structure and seismic anisotropy near the San Andreas Fault at Parkfield, California, *Geophys. J. Int.*, *178*(2), 1098–1104, doi:10.1111/j.1365-246X.2009.04198.x.

Pedersen, H. A. (2006), Impacts of non-plane waves on two-station measurements of phase velocities, *Geophys. J. Int.*, *165*(1), 279–287, doi:10.1111/j.1365-246X.2006.02893.x.

Plona, T. J. (1976), Ultrasonic bounded beam reflection and transmission effects at a liquid/ solid-plate/liquid interface, *J. Acoust. Soc. Am.*, *59*(6), 1324, doi:10.1121/1.381011.

Rokhlin, S. I. (1986), Reflection and refraction of elastic waves on a plane interface between two

generally anisotropic media, *J. Acoust. Soc. Am.*, *79*(4), 906, doi:10.1121/1.393764.

Rokhlin, S. I., and W. Wang (1992), Double through transmission bulk wave method for ultrasonic phase velocity measurement and determination of elastic constants of composite materials, *Acoust. Soc. Am.*, *91*(6), 3303–3312.

Ruger, A. (1997), P -wave reflection coefficients for transversely isotropic models with vertical and horizontal axis of symmetry, *Geophysics*, *62*(3), 713–722.

Rüger, A. (1998), Variation of P-wave reflectivity with offset and azimuth in anisotropic media, *Geophysics*, *63*(3), 935, doi:10.1190/1.1444405.

Savage, M. K. (1999), Siesmic anisotropy and mantle deformation, *Rev. Geophys.*, (98), 65–106, doi:10.1029/98RG02075.

Sayers, C. M., and S. Dean (2001), Azimuth-dependent AVO in reservoirs containing non-orthogonal fracture sets gave an analytic expression, valid for, *Geophys. Prospect. Ikelle Ru È ger*, *49*, 100–106.

Sayers, C. M., and M. Kachanov (1995), Microcrack-induced elastic wave anisotropy of brittle rocks, *J. Geophys. Res. Solid Earth*, *100*(B3), 4149–4156, doi:10.1029/94JB03134.

Sayers, C. M., S. Guo, and J. Silva (2015), Sensitivity of the elastic anisotropy and seismic reflection amplitude of the Eagle Ford Shale to the presence of kerogen, *Geophys. Prospect.*, *63*(1), 151–165, doi:10.1111/1365-2478.12153.

Schijns, H., D. R. Schmitt, P. J. Heikkinen, and I. T. Kukkonen (2012a), Seismic anisotropy in the crystalline upper crust: Observations and modelling from the Outokumpu scientific borehole, Finland, *Geophys. J. Int.*, *189*(1), 541–553, doi:10.1111/j.1365-246X.2012.05358.x.

Schijns, H., D. R. Schmitt, P. J. Heikkinen, and I. T. Kukkonen (2012b), Seismic anisotropy in the crystalline upper crust: Observations and modelling from the Outokumpu scientific borehole, Finland, *Geophys. J. Int.*, *189*(1), 541–553, doi:10.1111/j.1365-246X.2012.05358.x.

Schmitt, D. R. (2015), *Geophysical Properties of the Near Surface Earth: Seismic Properties*, Elsevier B.V.

Schoch, A. (1950), Schallreflexion, Schallbrechung und Schallbeugung, in *Ergebnisse der*

exakten Naturwissenschaften, vol. 23, pp. 127–234.

Schoch, A. (1952a), b, Seitliche versetzung eines total reflektierten strahles bei ultraschall-wellen, *Acustica*, *2*(17).

Schoch, A. (1952b), Der schallbeugung durch platten, *Acustica*, *1*(2).

Schoenberg, M. (1997), Orthorhombic media: Modeling elastic wave behavior in a vertically fractured earth, *Geophysics*, *62*(6), 1954, doi:10.1190/1.1444297.

Shadlow, J. (2014), A description of seismic amplitude techniques, *Explor. Geophys.*, *45*(3), 154, doi:10.1071/EG13070.

Shen, F., J. Sierra, D. R. Burns, and M. N. Toksöz (2002), Azimuthal offset- dependent attributes applied to fracture detection in a carbonate reservoir, *GEOPHYSICS*, *67*(2), 355–364, doi:10.1190/1.1468596.

Shuey, R. T. (1985), A simplification of the Zoeppritz equations, *Geophysics*, *50*(4), 609, doi:10.1190/1.1441936.

Skopintseva, L., and T. Alkhalifah (2013), An analysis of AVO inversion for postcritical offsets in HTI media, *GEOPHYSICS*, *78*(3), N11–N20, doi:10.1190/geo2011-0288.1.

Stewart, R. R., N. Dyaur, B. Omoboya, J. J. S. de Figueiredo, M. Willis, and S. Sil (2013), Physical modeling of anisotropic domains: Ultrasonic imaging of laser-etched fractures in glass, *Geophysics*, *78*(1), D11–D19, doi:10.1190/geo2012-0075.1.

Swokowski, E. W. (1979), *Calculus with analytic geometry*, Prindle, Weber & Schmidt.

Tamir, T., and H. L. Bertoni (1971), Lateral Displacement of Optical Beams at Multilayered and Periodic Structures, *J. Opt. Soc. Am.*, *61*(10), 1397–1413, doi:10.1364/JOSA.61.001397.

Thomsen, L. (1986a), Weak elastic anisotropy, *Geophysics*, *51*(10), 1954, doi:10.1190/1.1442051.

Tsvankin, I. (1997), Anisotropic parameters and P-wave velocity for orthorhombic media, *Geophysics*, *62*(4), 1292, doi:10.1190/1.1444231.

Ursin, B., and G. Haugen (1996), Weak-contrast approximation of the elastic scattering matrix in anisotropic media, *Pure Appl. Geophys.*, *148*(3–4), 685–714.

Vavrycuk, V. (1999), Weak-contrast reflection / transmission coefficients in weakly anisotropic elastic media : P -wave incidence, *Geophys. J. Int.*, *138*, 553–562, doi:10.1046/j.1365-

246X.1999.00890.x.

Vavrycuk, V., and I. Pšenčík (1998), PP-reflection coefficients in weakly anisotropic elastic media, *Soc. Expl. Geophys*, *63*(6), 2129–2141.

Vestrum, R. W. (1994), Group and Phase-Velocity Inversions for the General Anisotropic Stiffness Tensor, October.

Vestrum, R. W., and R. J. Brown (1994), *From group or phase velocities stiffness tensor to the general anisotropic Robert W . Vestr um and R . Jame s B ro w n*.

Voigt, W. (1887), Theorie des Lichts für bewegte Medien, *Göttinger Nachrichten*, *7*, 41–51.

Walker, A. M., and J. Wookey (2012a), Computers & Geosciences MSAT — A new toolkit for the analysis of elastic and seismic anisotropy, *Comput. Geosci.*, *49*(October 2012), 81–90, doi:10.1016/j.cageo.2012.05.031.

Walker, A. M., and J. Wookey (2012b), MSAT-A new toolkit for the analysis of elastic and seismic anisotropy, *Comput. Geosci.*, *49*, 81–90, doi:10.1016/j.cageo.2012.05.031.

Wang, X., and I. Tsvankin (2013), Multiparameter TTI tomography of P-wave reflection and VSP data, *Geophysics*, *78*(5), WC51-WC63, doi:10.1190/geo2012-0394.1.

Wenk, H.-R. (1999), A voyage through the deformed Earth with the self-consistent model, *Model. Simul. Mater. Sci. Eng.*, *7*(5), 699–722, doi:10.1088/0965-0393/7/5/304.

Weyl, H. (1919), Ausbreitung elektromagnetischer Wellen über einem ebenen Leiter, *Ann. Phys.*, *365*(21), 481–500, doi:10.1002/andp.19193652104.

Wielandt, E. (1993), Propagation and structural interpretation of non-plane waves, *Geophys. J. Int.*, *113*(1), 45–53, doi:10.1111/j.1365-246X.1993.tb02527.x.

Young, G. B., and L. W. Braile (1976), A computer program for the application of Zoeppritz's amplitude equations and Knott's energy equations, *Bull. Seismol. Soc. Am.*, *66*(6), 1881–1885.

Yousef, B. M., and D. A. Angus (2016), *When do fractured media become seismically anisotropic? Some implications on quantifying fracture properties*.

Zheng, P., and B. Ding (2014), The Generalized Reflection and Transmission Matrix Method for Wave Propagation in Stratified Fluid-Saturated Porous Media, *Transp. Porous Media*, *102*(2), 185–206, doi:10.1007/s11242-014-0271-1.

Zheng, Y. (2006), Seismic azimuthal anisotropy and fracture analysis from PP reflection data, University of Calgary.

Zillmer, M., D. Gajewski, and B. M. Kashtan (1998), Anisotropic reflection coefficients for a weak-contrast interface, *Geophys. J. Int.*, *132*(1), 159–166.

Zoeppritz, K. (1919), Erdbebenwellen VII. VIIb. Über Reflexion und Durchgang seismischer Wellen durch Unstetigkeitsflächen. Nachrichten von der Königlichen Gesellschaft der Wissenschaften zu Göttingen, *Math. Klasse*, 66–84.

Chapter 3
An Algorithm for Quantitatively Modeling Reflected Ultrasonic Bounded Pulses and Beams

3.1 Introduction

Bounded ultrasonic pulses are used in the study of many problems in acoustics, nondestructive testing, metrology, and seismic physical modeling. A full understanding of how these bounded pulses propagate and scatter in such laboratory tests is essential for the proper interpretation of the observations. Modeling ultrasonic bounded pulse propagation remains challenging, and in many cases, analyses depend on various simplifying assumptions. The most common of these presumes that a simple plane wave sufficiently describes the observations. In reality, however, a bounded pulse is composed of a distribution of wavenumbers with differing directions and frequencies; and its behavior can be much more complicated. Such effects include beam diffraction and apparent non-specular reflectivity near the Rayleigh critical incidence angle.

Here we focus on the specific problem of the reflectivity of a bounded pulse from the flat interface between liquid and solid half-spaces in support of parallel experimental work [*Malehmir and Schmitt*, 2017]. In general homogeneous elastic media, the reflection coefficients from a plane-wave incoming wave are calculated by applying the Christoffel [1877] equation together with the boundary conditions on stresses and displacements [e.g. *Musgrave*, 1970; *Rokhlin*, 1986]. What all of these reflectivity methods have in common is the assumption that the wavefront of the incoming wave and reflected waves are planar. However, creating a physical ultrasonic source to generate or mimic a plane-wave front is quite challenging [*Jocker and Smeulders*, 2007].

Often in ultrasonic reflection goniometry, theoretical plane wave solutions do not describe the observed reflected amplitudes, particularly in the vicinity of critical angles. For example, the plane wave solutions predict a sharp, discontinuous peak at the longitudinal mode (P) critical angle.

Observed reflectivity curves are, in contrast, smooth and of lower amplitude near these critical angles (e.g., [*Alhussain*, 2007; *Bouzidi and Schmitt*, 2008b; *Mahmoudian et al.*, 2015; *Malehmir and Schmitt*, 2016b]). This is one of the consequences of the fact that a real beam is constituted of the distribution of manifold plane waves having wavenumbers some of which are oriented with incidences both larger and smaller than that of the main components of the transducer's beam. One manifestation of this is that the plane wave solution by itself fails to describe the reflectivity at the longitudinal P-wave critical angle.

Further, at larger incidence angles approaching the Rayleigh critical angle (θ_R) the amplitude of a reflected wave appears to significantly decrease, a phenomenon which cannot be replicated by the plane-wave reflectivity equations [*Zoeppritz*, 1919]. This phenomenon contributes to the apparent non-specular shift of the reflected beam as first observed by [*Schoch*, 1952b] using Schlieren photography. [*Brekhovskikh*, 1960] observed displacement along the interface, where it is at its maxima post shear-wave critical angle. *Diachok* [*Diachok*, 1970] attributed this null in the reflected wave to the conversion of the incoming wave to the surface Rayleigh wave. *Tamir and Bertoni* [*Tamir and Bertoni*, 1971; *Bertoni and Tamir*, 1973] proposed an analytic solution for the reflection of the Gaussian ultrasonic wave. They invoked the generation of a leaky surface wave at the Rayleigh angle to explain this phenomenon.

More recently, [*Bouzidi and Schmitt*, 2008a, 2008b] successfully modeled the amplitudes, including near the P-wave critical angle and the Schoch shift null, obtained in a series of ultrasonic bounded pulse reflection tests on well-characterized elastic and porous solids. One important point is that their modeling considers only the appropriate complex reflectivity of the interface to reconstitute the reflected bounded pulse. Importantly, it does this without invoking the generation of inhomogeneous interface modes near critical angles explicitly as this behavior appears to arise from direct use of the complex reflectivities.

Here we review these developments, but provide a computer program that calculates the propagation and reflection of a bounded pulse from the flat interface between liquid and elastic solid half spaces. As inputs, the program requires i) the wavefield of the just-launched bounded pulse, ii) the wave speeds of the liquid and of the reflecting solid, and iii) the appropriate angle-of-incidence dependent complex reflectivity. In the program, each of the source wavefield's

components is propagated to the interface, modulated by the appropriate reflectivity function, and finally propagated back upwards to the observation point. We test this algorithm against laboratory measurements to show that it can accurately reproduce the complicated acoustic reflectivities observed near both the longitudinal P-wave and transverse S-wave critical angles and including the complex behavior near the Rayleigh angle. Our purpose here, however, is not to study directly these counterintuitive phenomena but to provide a tool useful to investigations in ultrasonic goniometry.

3.2 Modeling of the bounded beam

Many researchers have worked to understand the reflectivity from imperfect and non-planar wavefronts. Spherical spreading wavefronts are a special case in which the constant phase surface of the wave increases equally in all directions; the wavefront may be constructed from an ensemble of plane waves propagating in all direction from the central source. *Weyl* [1919], for example, estimated the reflectivity of this spherical wavefront by contour integrating over all the plane-waves.

Plona [*Plona*, 1976] quantitatively explained the bounded beam effect on reflectivity from the liquid-solid interface using *Tamir and Bertoni's* [*Tamir and Bertoni*, 1971] description. Later, *Leroy and Poirèe* [*Leroy and Poirèe*, 1988] showed that the homogenous plane-wave could not account for the observed Rayleigh angle null reflection, however, they could reproduce the bounded beam effect around the Rayleigh angle by defining the bounded beam as an inhomogeneous wave.

The incoming inhomogeneous wave could create a special wavefield, in which the amplitude and oscillation phase are varying in each direction [*Wielandt*, 1993; *Pedersen*, 2006]. *Pedersen* [2006] describes the non-plane wave as a summation of many plane-waves with different amplitude, speeds, and propagation directions, which their interferences could potentially create capricious phases and amplitudes variation. Hence, in the case of reflectivity from a boundary, different wavenumbers are inciting at a different incoming angle to the reflecting interface.

Breazeale [*Breazeale et al.*, 1977; *Ngoc and Mayer*, 1979] and *Ngoc and Mayer* [1979] were among the first to provide a quantitative description of the non-specular reflection

from the bounded beam in the range of frequencies and beam widths. *Declerq and coworkers* [*Declercq et al.*, 2005; *Declercq*, 2006] provide a historical review of the inhomogeneous wave theory and application to null reflection at Rayleigh angle from Gaussian beam. In this Chapter, we present a modified algorithm following the method described by *Bouzidi and Schmitt* [*Bouzidi and Schmitt*, 2008b] to model the propagation and reflection of a bounded beam at any angle of incidence.

3.3 Theory

To better understand and interpret the recorded data in the lab, sometimes it is useful to model the data based on different properties and degrees of symmetries of the subsurface material. The one that shows the best match to the recorded data will be a good representative of subsurface properties.

3.3.1 *Geometry of the Problem*

In this Chapter, we implemented a hybrid algorithm that combines propagation of the bounded pulse with complex reflectivity functions ($R_{pp}(\theta)$) appropriate to the case under study. The geometry of the problem is described in Figure 3-1, where the bounded pulse propagation is modeled inside the box and its reflection is calculated from the water-solid boundary. The top halfspace is liquid with constant velocity ($\boldsymbol{v}$) and density (ρ), while the lower halfspace is a general elastic medium be it isotropic liquid or solid or anisotropic solid. Later, we provide examples of reflectivity curves from isotropic elastic solids but as long as the correct $R_{pp}(\theta)$ is input to the algorithm any of these problems can be addressed (e.g., [*Bouzidi and Schmitt*, 2012; *Malehmir and Schmitt*, 2017]).

The bounded pulse is launched from the profile of the transmitting transducer (yellow line in Figure 3-1) centered at (x_o,z_o=0) within the upper liquid medium. The transmitter is located such that its center extends to the midway point to the receiving transducer (pink box in Figure 3-1) which its center lies at (x_r,z_o=0).

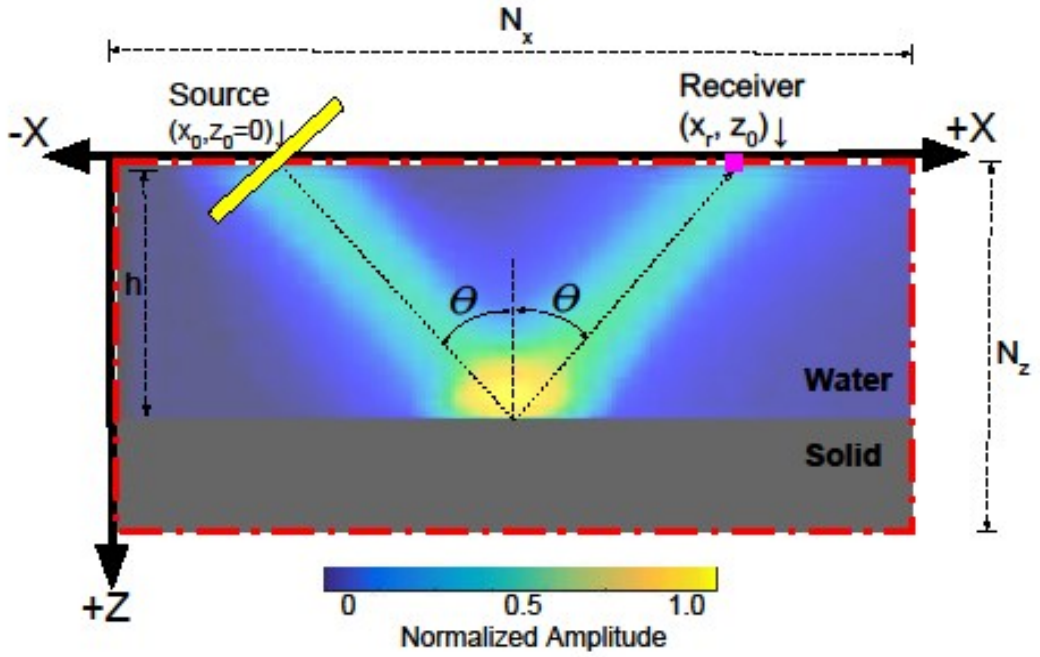

Figure 3.1. The geometry of the bounded beam reflectivity algorithm from the water-solid interface. The algorithm propagates the bounded pulse from the transducer (yellow box) and reflects it from the boundary (z=h) and then propagates it to the receiving transducer (pink box) where it reads the amplitude envelope of the specular reflected bounded beam (overlaid in the background) at the same incident angle (θ). The background color indicates the amplitude of the bounded beam at x, z point when the beam crosses that point.

To explain the methodology, consider a 2D discretized model with two layers with size (N_z, N_x) where N_z is the number of grids in the z-direction and N_x is the number of grids in the x direction, as depicted in Figure 3-1. The number of the gridding points in x- and z- directions is set to minimize the spatial aliasing as well as available memory for computation. The two-dimensional representation of the bounded pulse propagation from the flat and horizontal interface between water-solid significantly reduces the number of calculations without losing valuable information of the wavefield inside the sagittal plane.

3.3.2 *The Properties of the Source Wavefield*

The transmitter centered at ($x_0,z_0=0$) launches the bounded pulse the wavefield of which is described by $\boldsymbol{s}(x,z_0,t)$ in the temporal domain, this wavefield is a necessary input to the algorithm. Later, an example of the launched bounded pulse is provided but the reader can either measure or model their own without any limitation to the algorithm.

While the algorithm takes as input the temporal $s(x_0,z_0=0,t)$ it carries out all of its calculations in the frequency-wavenumber (f-k) domain. $D(k_x,z_0,\omega)$ is the 2D Fourier domain representation of $\boldsymbol{s}(x,z_0,t)$ as calculated using the discrete 2D fast Fourier transform (2D FFT). $\boldsymbol{D}(k_x,z_0,\omega)$ alternatively represents the wavefield in terms of an 2D amplitude spectrum describing the energy associated with each component wavenumber and the 2D phase spectrum connected to the original phase and later phase advance with propagation in space domain.

3.3.3 *Phase Advance Propagation of the Wavefield*

In the construction of the beam, the original $s(x,z_0,t)$ propagates into the medium and is defined at later times by $s(x,z,t)$. We use here a phase advance technique to propagate the wavefield as originally introduced to seismic modeling by Clearbout (1985). In order to propagate the source wavefield centered at (x_0,z_0), to the point in space with the center of ($x,z=z_0+\Delta z$), the phase advance wavefield propagation theory suggests changing the phase of the source wavefield by convolving it with $\delta(x, t - \frac{\Delta z}{\boldsymbol{v}(z_o)})$, in the frequency domain this is effected by,

$$D(k_x, z_0 + \Delta z, \omega) = D(k_x, z_0, \omega)\, e^{i\, k_z\, \Delta z}, \tag{3-1}$$

where k_z is the vertical wavenumber:

$$\boldsymbol{k_z} = \sqrt{\left(\frac{\boldsymbol{\omega}}{\boldsymbol{v}(z_o)}\right)^2 - \boldsymbol{k}_x^2}\,. \tag{3-2}$$

for the component propagating with speed v in the water. Similarly, to effect propagation of the bounded pulse at the angle of incidence θ (Figure 3-1) $D_\theta(k_x, z,\omega)$ is advanced by:

$$D_\theta(k_x, z_o + \Delta z, \omega) = D(k_x,\ z_o, \omega)\, e^{i\, k_z \cos(\theta) \Delta z}. \tag{3-3}$$

When $\Delta z = h - z_o$ the wavefield $D_\theta(k_x, h,\omega)$ has reached the interface between the two halfpaces with $z = h$. At this point each of the components of $\boldsymbol{D}$ is multiplied by its appropriate horizontal

wavenumber dependent reflection co-efficient $R_{pp}(k_x)$ to obtain the incipiently reflected wavefield $D\theta^R(k_x,z=h,\omega)$ through the element by element multiplication of $R_{pp}(k_x)$ with $D\theta(k_x,z=h,\omega)$. It is important to note that $R_{pp}(k_x)$ is in general complex with the complex component introducing a discrete phase shift as necessary to describe fully post-critical reflection behavior.

This reflected wavefield is then upward continued to the measurement surface by applying the phase advance technique:

$$D\theta^R(k_x, z=h-\Delta z, \omega) = R_{pp}(k_x) \ast D\theta(k_x, z=h, \omega)\, e^{-i\, kz\, cos(\theta)\, \Delta z}, \qquad (3\text{-}4)$$

It must be noted that the shift is applied with a negative sign (i.e. $e^{(-i\, \mathbf{kz}\, cos(\theta)\, \Delta z)}$) to move the bounded pulse upward. The measurement surface is reached when $\Delta z = h$ (i.e., $D\theta^R(k_x,z=0,\omega)$) whereupon the inverse 2D FFT transforms $\boldsymbol{D}^R$ to its reconstructed *x-z-t* representation $d\theta^R(x,z=0,t)$. The resulting time series amplitude response from the point $x = x_r$ and $z = 0$ gives the response expected along the locus of the specular reflection. Here, because we use a small receiver as described shortly, this time series is directly compared to the laboratory tests. More usually the aperture of the receiving transducers is larger and its response must be integrated over the appropriate width of $d\theta^R(x,z=0,t)$.

3.3.4 *Applying Complex Reflectivity*

As noted above appropriate knowledge of the angle of incidence dependent reflectivity R_{pp} is needed. The algorithm is intentionally designed to be independent of the calculation of R_{pp}, allowing users to input their reflectivity functions as appropriate. R_{PP} might be provided as a closed form expression such as exists for the interface from an isotropic elastic solid (e.g. Zoeppritz (1919), Bertoni and Tamir (1985)), a liquid saturated porous medium (e.g. Bouzidi and Schmitt, 2012), or suitably oriented anisotropic solids (Christoffel`s (1877), Rokhlin (1986)). In more complicated situations, such as the reflectivity from an arbitrarily oriented anisotropic solid, R_{pp} might only be obtained through numerical means (e.g.,[*Malehmir and Schmitt*, 2016a]).

Although the algorithm takes $R_{pp}(\theta)$ as an input function of incident angle to the normal to the boundary, the dot product is performed in wavenumber domain ($\boldsymbol{k}_x$). So, the calculation of reflection coefficients as a function of the angle of incidence (θ) and/or horizontal wavenumber

($\boldsymbol{k}_x$) is the next step. In order to map input reflectivity into wavenumber domain, $R_{pp}(k_x)$, the algorithm first finds its corresponding incidence angle using

$$\theta(k_x)=sin^{-1}(k_x \boldsymbol{v}(z)\ \boldsymbol{\omega}^{-1}), \qquad (3\text{-}4)$$

then it searches for the corresponding reflectivity from $R_{pp}(\theta)$. In next section, the MATLAB® software flowchart of the bounded beam-modeling algorithm is described.

3.4 Computer program

A flowchart outlining the algorithm as based on the theory above is provided in Figure 3-2 and the various subroutines listed in Table 3-1.

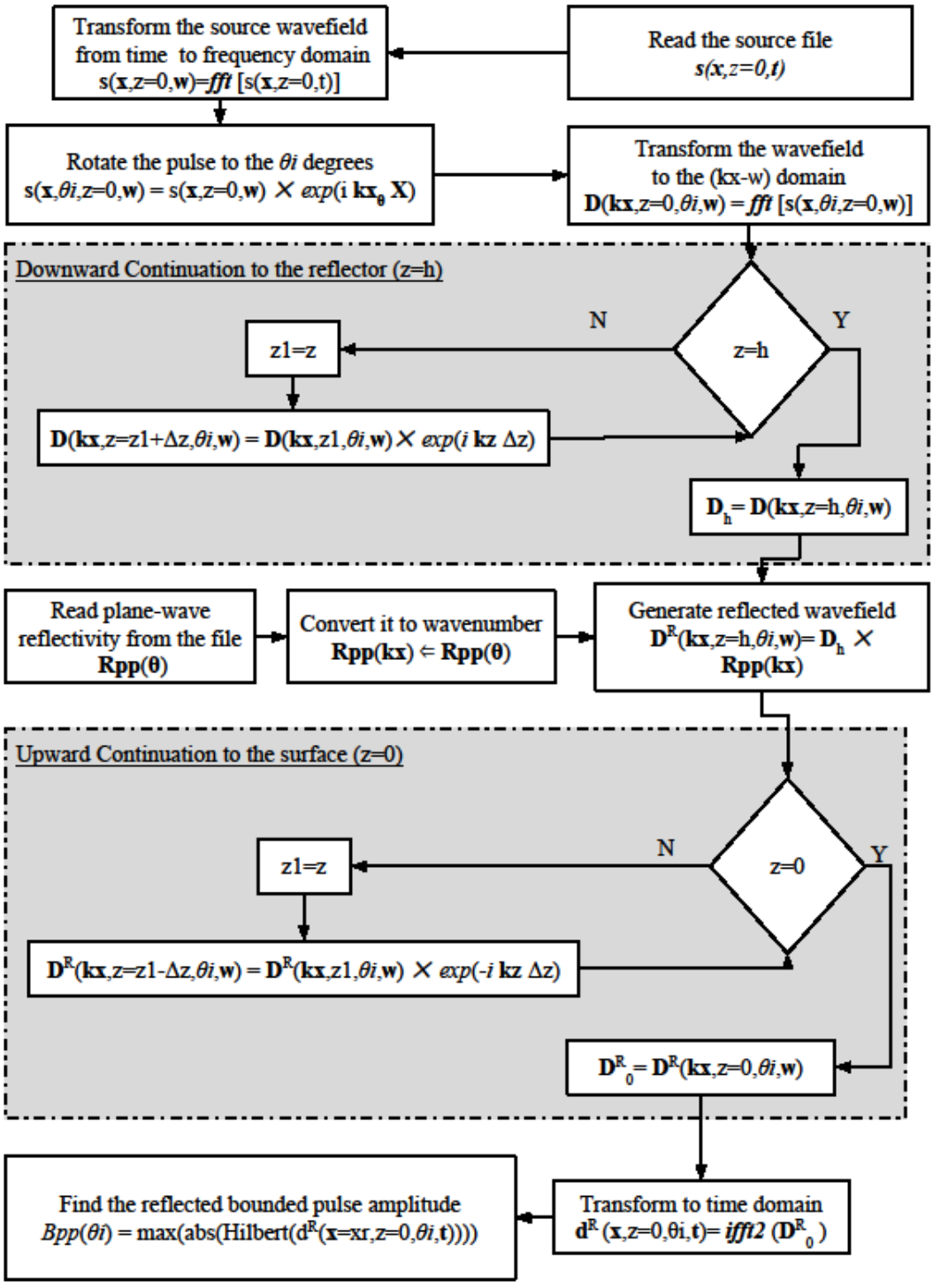

Figure 3.2. Flowchart of the bounded pulse reflectivity algorithm.

Table 3-1. Necessary input arguments required for modeling bounded beam reflectivity from a water-solid interface.

Subroutine	*Description*
Bpp.m	Main function,
Rpp.mat	Input complex acoustic reflectivity $R_{pp}(\theta)$
SRC.mat	Input source wavefield of the transducer s(x,z0,t)
Mpp.mat	Laboratory Measured Reflectivity (optional)
Bpp.mat	Output reflectivity using bounded pulse algorithm,
Bpp.gif	Animation of the bounded pulse propagation (XZ domain)

We provide our MATLAB® code that implements parallel computing power from multi-node processors, which can be extended to graphical processing units for increasing the calculating speed. A version of this algorithm is available in https://www.github.com/malehmir/beam under Apache 2.0 license. In order to run the software, you need MATLAB 2015b (v 8.6) or higher with a minimum 8GB of memory, by executing the main file '*BBM.m'* in MATLAB, which will invoke necessary subroutines as described in the above flowchart, Figure 3-2. Several animations that show the propagation of the wavefield from the water-aluminum interface and water-Copper interface both in temporal and spatial coordinates, measured reflectivities along with the code of the algorithm are all available from the above shared URL and supplementary materials to this Chapter.

To test our algorithm, we repeated measurements of the angle of incidence dependent reflectivities from thick plates of aluminum and copper alloys immersed in water. We chose these to provide examples of reflectivities near the critical angles for the longitudinal, shear (transverse), and Rayleigh wave modes. These observed results are then compared with the modelled output waveform as a test of the algorithm's validity.

3.5 Experimental Configuration

The acoustic goniometer with its specially constructed transmitting and receiving transducers, details of data acquisition, and the calibration procedures are described in detail [*Bouzidi and Schmitt*, 2008a] and only a brief overview is necessary here.

The large ultrasonic transmitter is constructed using a rectangular sheet (80 mm X 100 mm) of piezoelectric PZT ceramic. In contrast, the receiver contains a near-point like PZT receiver whose dimensions (100μm X 100μm) are smaller than the ~1 to 2 mm wavelengths of the bounded pulse in water. Because of the size of the source and other spatial limitations, the allowed incidence angles ranged from 12° to 80°. It is important to note that this study employed a different and smaller transmitter than previous studies [*Bouzidi and Schmitt*, 2008a] and as such, the laboratory reflectivities here will differ slightly due to this variance in geometry.

The reflectivity measurements consist of acquiring a suite of waveforms across a range of angles of incidence and reflection *(θ)* from 12° to 80° in increments of 0.25°. The reflecting face of the test block is aligned horizontally and then centered in the goniometer (Figure 3-3). The small point-shaped receiver is placed at the opposite angle along the central beam axis following the expected direct specular reflection path. A 25*μJ* step provided a pulse with 300 voltage by a Panametrics-NDT® 5800 at a repetition rate of *100Hz* activates the transmitter launching the bounded pulse. The waveforms are temporally sampled at 5 *ns (nano seconds)* using a Tektronix TDS 2000B oscilloscope controlled by a MATLAB® based in-house software. To reduce noise, the final waveform used in the analysis is the average of 1280 individually acquired pulses.

Prior to the measurements, this bounded pulse is recorded laterally every 2 mm. by scanning the receiver a distance of 2 cm for a length of 100 mm along the transmitter's face. The captured wavefield (Figure 3-4c) is mostly planar but exhibits diffractions at its edges. This source wavefield is used as the input *$s(x,z_0,t)$* to the algorithm after proper amplitude normalization and resampling with respect to the model parameters (N_x, and N_z), refer to Figure 3-1.

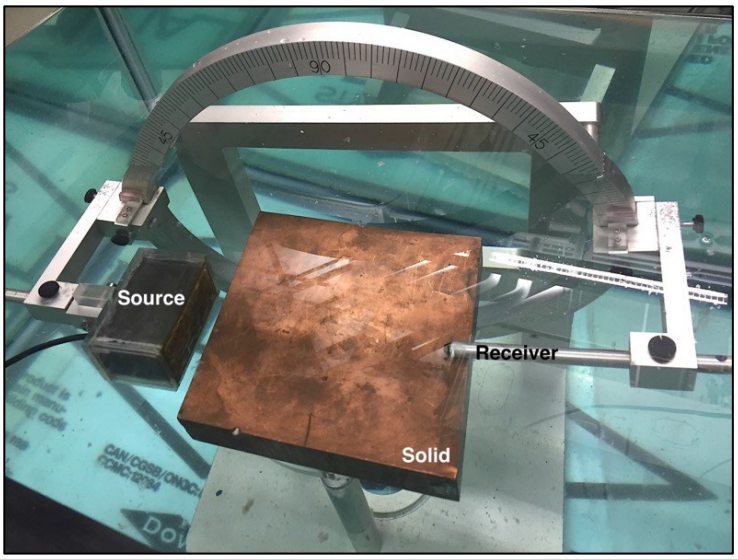

Figure 3.3. Photograph of the laboratory setup for ultrasonic reflectivity measurement with the solid copper alloy sample block and transducers (source and receiver) completely immersed in the water tank. The transmitter and the receiver are moved manually to the exact incidence angles (θ) every 0.25° from 12° to 80° and the reflected wavefield is then recorded on the computer.

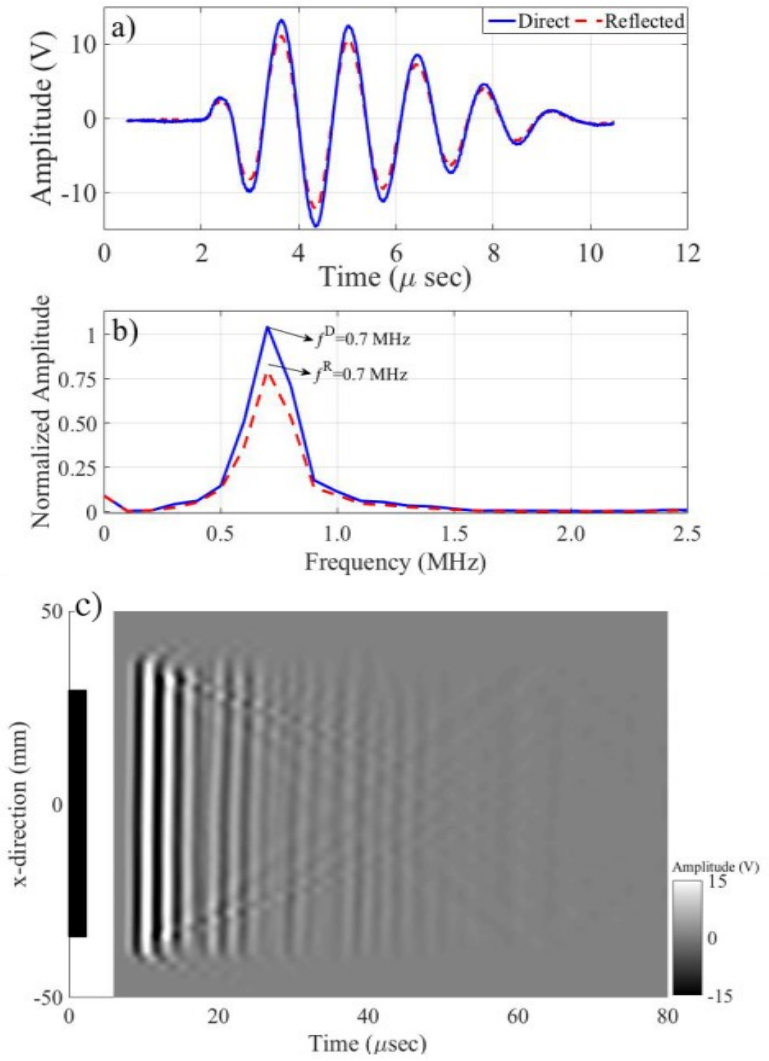

Figure 3.4. a) Example of a comparison between the directly measured waveform (solid line) with one reflected at $\theta = 15°$ (dashed line) from the aluminum block. b) Amplitude spectra calculated for the waveforms in a) indicating a dominant frequency of f=0.7 MHz. c) Observed bounded pulse $s(x,z_0,t)$ as obtained directly by scanning the receiver along the x-axis at a distance of 2 cm from the transmitter (black rectangle) along the x-axis.

The elastic properties of the isotropic materials that we have used in the experiment and the modeling of the reflected waves are shown is Table 3-2 following *Bouzidi and Schmitt* [*Bouzidi and Schmitt*, 2008b].

Table 3.2. Elastic properties of the aluminum, copper alloy and water used for the reflectivity modeling and laboratory experiment, after [Bouzidi and Schmitt, 2008b].

Solid Material	Water density (kg/m^3)	Water V_p (m/s)	Solid density (Kg/m3)	Solid V_p (m/s)	Solid V_s (m/s)	P-critical angle (deg)	S critical angle(deg)	Rayleigh angle(deg)	Rayleigh V_R(m/s)
Aluminum	995 ± 1	1495 ± 5	2695 ± 30	6432 ± 30	3134 ± 2	13.3°±0.1°	28.6° ± 0.1°	29.57 ±0.1°	2938±14
Copper Alloy	995 ±1	1495 ±5	8900 ± 47	4857 ± 18	2296 ± 7	17.3° ± 0.25°	38.3° ± 0.25 °	43.7° ± 0.5°	2930 ± 4

3.6 Results

The suites of reflected waveforms obtained from the aluminum the copper alloys over the range of incidence angles from 12° to 80° are displayed in Figure 3-5a and 3-6a, respectively. The laboratory measured reflectivity data are available in the electronic supplementary material. The corresponding observed amplitude M_{PP} of each reflected waveform, as determined using the amplitude envelope as described above, is plotted versus the angle of incidences in Figure 3-5b and Figure 3-6b, as open squares. These are compared against the classic plane wave elastic reflectivity P_{PP} (dashed line) calculated using the well-known elastic expressions of *Zoepprtiz (1919)* and those B_{PP} (continuous line) modeled with the algorithm developed here. Both P_{PP} and B_{PP} are calculated using the material values in Table 3-2. The difference between the observed M_{PP} and modeled B_{PP} reflectivities is also shown in histogram form.

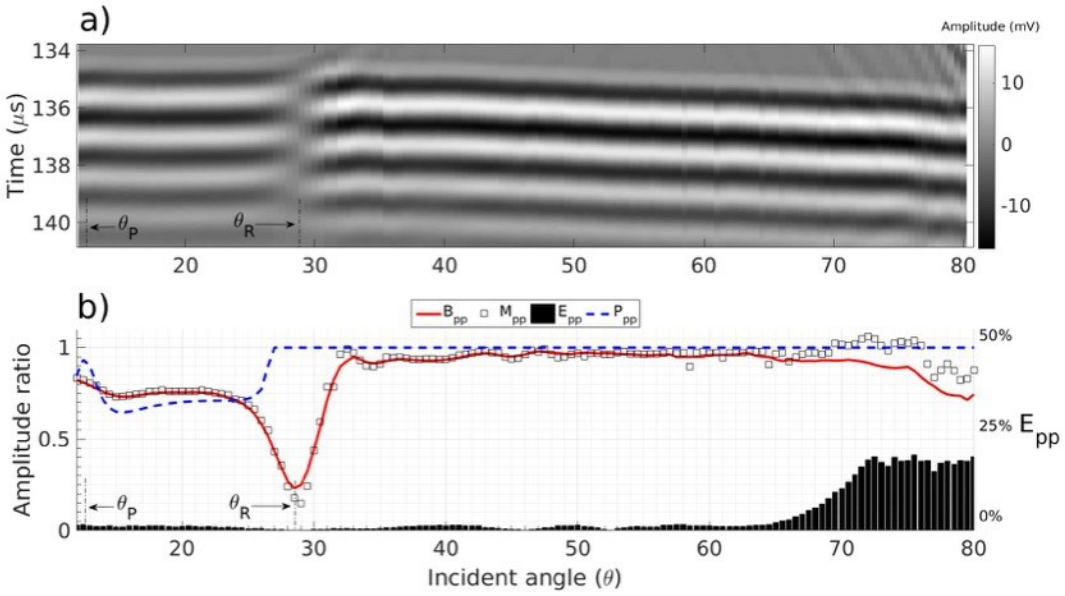

Figure 3.5. a) Waveforms recorded upon reflection from the water-aluminum boundary with the angle of incidence. b) Comparison between the experimentally observed reflectivity (M_{pp}), the calculated theoretical plane wave reflectivity (P_{pp}), and the modeled bounded beam reflectivity (B_{pp}). The percentile error (E_{pp}) is calculated from the difference between M_{pp} and B_{pp} is shown in black bar-plot with a bin for each angle of incidence measured.

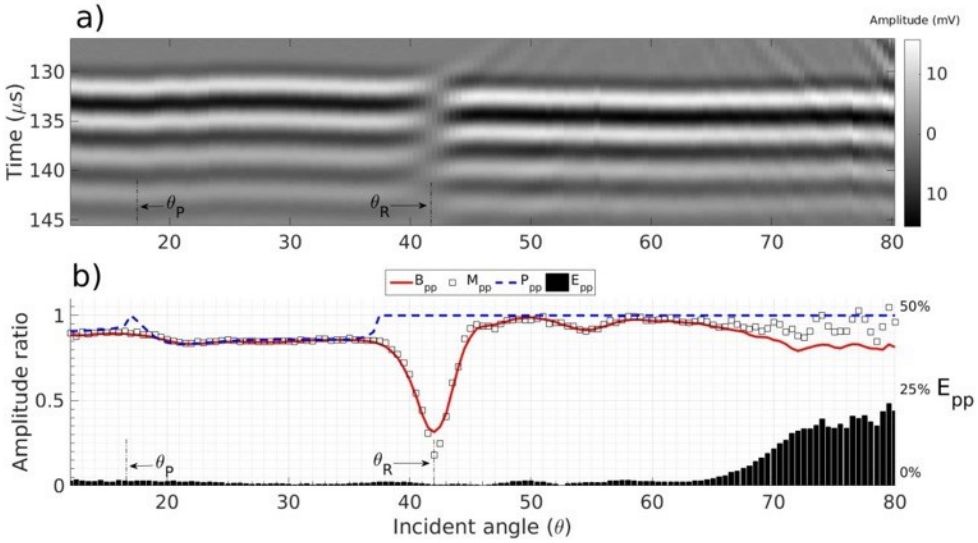

Figure 3.6. a) Waveforms recorded upon reflection from the water-copper alloy boundary with angle of incidence. b) Comparison between the experimentally observed reflectivity (M_{pp}), the calculated theoretical plane wave reflectivity (P_{pp}), and the modeled bounded beam reflectivity (B_{pp}). The error (E_{pp}) as a percentage difference between M_{pp} and B_{pp} is shown in black bar with a bin for each angle of incidence measured.

It is useful to first discuss the differences between the measured reflectivity M_{pp} and the classic plane-wave solution P_{pp} calculated using the *Zoeppritz*, [1919] expressions. P_{PP} displays a sharp, discontinuous peak at the P-wave critical angle that is just apparent in Figure 3-5b and more so in Figure 3-6b. The observed M_{PP} is of lower amplitude and is significantly more rounded. Between the P-wave and S-wave critical angles, the plane wave and observed reflectivities diverge significantly for the aluminum plate while there is a relatively good agreement for the copper plate. This difference is likely related to the impedances between the two materials with density playing the major factor. As such, any reflection from the dense copper plate is already close to unity and the relative divergence is small. In contrast, more character is apparent in the aluminum curves and the two reflectivities diverge significantly. Past the S-wave critical angle, however, P_{PP} and M_{PP} diverge more radically for both samples. P_{PP}, as expected, is unity indicating the total reflection of the plane wave past the S-critical angle. In contrast, M_{PP} shows a null near the critical

angle that is associated with the Rayleigh wave speed. The effect is related to the non-specular Schoch shift [*Schoch*, 1950, 1952a]. *Bouzidi and Schmitt* [2008b] explained that the unaccounted drop in the amplitude of the reflected wave around the Rayleigh angle (θ_R) is due to the phase shifts of the reflected waves compared to the incoming wave, which creates a destructive interference and a non-specular reflection. As such, the existence of this null is well known and, as already reviewed in the introduction, is a part of the complex behavior of observed laboratory reflectivities that has been discussed for some time by many authors. Past this zone the observed reflectivities M_{PP} are close to but oscillate beneath the constant P_{PP} value of unity.

The divergence of the observed from the plane wave theory is expected. More practically, however, this makes it difficult to apply the simpler plane wave theory to the interpretation of observed reflectivity curves. An important goal, for example, might be to use the observed reflectivity to determine the elastic properties of the test solid, this is often used in reflection seismology to infer in situ fluid-saturation states for example. Blind application of the plane wave expressions to the observed M_{PP} over the range of incidences from the P-wave critical angle to the S-wave critical angle for aluminum (Figure 3-5b) could not return correct values for these elastic properties.

Developing a correct experimental reflectivity curve that can be used in quantitative analysis is a key motivation for this work. The modeled B_{PP} and observed M_{PP} reflectivities are also compared in Figure 3-5b and 3-6b, they show good agreement to angles of 65°. At greater incidences the observed waveforms become contaminated with various additional arrivals scattered within the goniometer; and these amplitudes could not be used for analysis. At smaller incidences, however, the agreement is generally better than 93%. Even the small bumps at post Rayleigh critical angles are reproduced as is seen, for example, centered at 56° for the copper allow reflectivity (Figure 3-6b). At post-Rayleigh angles, series of high and low reflectivity pattern are observed in the data (Figure 3-5b and Figure 3-6b) that we initial thought might be from acoustic energy scattered from the laboratory setup. Surprisingly, these small amplitude bumps are well modelled. This is another proof for the integrity of the algorithm in modeling of the reflected wavefield from liquid-solid interfaces.

Another notable difference that exists at the minima for the nulls near the Rayleigh angle (θ_R), where the observed reflectivities are slightly lower than the calculated acoustic reflectivity by this algorithm. Since this difference is relatively constant between the results from water-aluminum and water-Copper, we would attribute this to the temporal and spatial properties of the emitting transducer that might have missed in the sampling of the source ($\boldsymbol{s}(x,z=0,t)$). This would create a larger interference at the Rayleigh angle, which we couldn`t predict it in the bounded pulse algorithm using the sampled source.

Overall, however, the agreement between the observed and the modeled reflectivities is more reliable than direct plane-wave reflectivity solution. This, in turn, suggests that the bounded pulse modeling can be used as a tool to invert observed reflectivities for material properties.

3.7 Conclusions

In this Chapter, we reinforced the long-standing observations that the plane-wave solution for the acoustic reflectivity cannot predict the ultrasonic response from bounded beam reflection from a water-solid boundary. We provide an algorithm that propagates the observed source signal to a receiver after refection. This program accurately reproduces the complicated angle of incidence dependent reflectivity seen in two laboratory tests. The algorithm predicts the blunted reflectivity curve near the longitudinal critical angle as well as the non-intuitive nonspecular behavior near the shear and Rayleigh critical angles. The good agreement between the observed and modelled reflectivities suggests the program could be applied to the determination of more complex material anisotropic or viscoelastic properties. Indeed, we are currently applying this program to the study of the acoustic reflectivity of general anisotropic media as proxies for fractured rock formations in the earth.

References

Aki, K., and P. G. Richards (1980), *Quantitative seismology: Theory and methods, v.1*, W.H. Freeman and Co, San Francisco.

Aleardi, M., and A. Mazzotti (2014), A feasibility study on the expected seismic AVA signatures of deep fractured geothermal reservoirs in an intrusive basement, *J. Geophys. Eng.*, *11*(6),

65008, doi:10.1088/1742-2132/11/6/065008.

Alhussain, M. (2007), Spherical Wave AVO Response of Isotropic and Anisotropic Media : Laboratory Experiment versus Numerical Simulations Mohammed Abdullah K Alhussain, University of Curtin.

Alhussain, M., E. Liu, B. Gurevich, M. Urosevic, and S. U. Rehman (2007), AVOaz response of a fractured medium: Laboratory measurements versus numerical simulations, *SEG Tech. Progr. Expand. Abstr.*, *26*(1), 254–258, doi:10.1190/1.2792421.

Alhussain, M., B. Gurevich, and M. Urosevic (2008), Experimental verification of spherical-wave effect on the AVO response and implications for three-term inversion, *Geophysics*, *73*(2), C7–C12, doi:10.1190/1.2837641.

Almqvist, B. S. G., L. Burlini, D. Mainprice, and A. M. Hirt (2010), Elastic properties of anisotropic synthetic calcite-muscovite aggregates, *J. Geophys. Res. Solid Earth*, *115*(8), 1–15, doi:10.1029/2009JB006523.

Arts, R., P. Rasolofosaon, and B. Zinszner (1991), Complete inversion of the anisotropic elastic tensor in rocks: Experiment versus theory, *1991 SEG Annu. Meet.*, 1538–1541.

Auld, B. A. (1973), *Acoustic fields and waves in solids- Vol 2*, John Wiley & Sons, Inc.

Backus, G. E. (1962), Long-wave elastic anisotropy produced by horizontal layering, *J. Geophys. Res.*, *67*(11), 4427, doi:10.1029/JZ067i011p04427.

Backus, G. E. (1965), Possible forms of seismic anisotropy of the uppermost mantle under oceans, *J. Geophys. Res.*, *70*(14), 3429, doi:10.1029/JZ070i014p03429.

Bakulin, A., V. Grechka, and I. Tsvankin (2000), Estimation of fracture parameters from reflection seismic data—Part II: Fractured models with orthorhombic symmetry, *Geophysics*, *65*(6).

Bao, X., D. W. Eaton, and Y. J. Gu (2016), Rayleigh-wave azimuthally anisotropic phase-velocity maps beneath western Canada, *J. Geophys. Res. Solid Earth*, n/a-n/a, doi:10.1002/2015JB012453.

Bass, J. D. (1995), Elasticity of minerals, glasses, and melts, in *Mineral Physics and Crystallography: A Handbook*, pp. 45–63.

Behura, J., and I. Tsvankin (2006), Small-angle AVO response of PS-waves in tilted transversely

isotropic media, *Geophysics*, *71*(5), C69, doi:10.1190/1.2329865.

Behura, J., and I. Tsvankin (2009), Reflection coefficients in attenuative anisotropic media, *Geophysics*, *74*(5), WB193, doi:10.1190/1.3142874.

Belonoshko, A. B., N. V Skorodumova, A. Rosengren, and B. Johansson (2008), Elastic anisotropy of Earth's inner core., *Science*, *319*(5864), 797–800, doi:10.1126/science.1150302.

Ben-Menahem, A., and A. G. Sena (1990), Seismic source theory in stratified anisotropic media, *J. Geophys. Res.*, *95*(B10), 15395, doi:10.1029/JB095iB10p15395.

Bertoni, H. L., and T. Tamir (1973), Unified theory of Rayleigh-angle phenomena for acoustic beams at liquid-solid interfaces, *Appl. Phys.*, *2*(4), 157–172, doi:10.1007/BF00884205.

Boness, N. L., and M. D. Zoback (2004), Stress-induced seismic velocity anisotropy and physical properties in the SAFOD Pilot Hole in Parkfield, CA, *Geophys. Res. Lett.*, *31*(15), L15S17, doi:10.1029/2003GL019020.

Bortfeld, R. (1961), APPROXIMATIONS TO THE REFLECTION AND TRANSMISSION COEFFICIENTS OF PLANE LONGITUDINAL AND TRANSVERSE WAVES*, *Geophys. Prospect.*, *9*(4), 485–502, doi:10.1111/j.1365-2478.1961.tb01670.x.

Bouzidi, Y., and D. R. Schmitt (2006), A large ultrasonic bounded acoustic pulse transducer for acoustic transmission goniometry: Modeling and calibration, *J. Acoust. Soc. Am.*, *119*(1), 54, doi:10.1121/1.2133683.

Bouzidi, Y., and D. R. Schmitt (2008a), Acoustic reflectivity goniometry of bounded ultrasonic pulses: Experimental verification of numerical models, *J. Appl. Phys.*, *104*(6), doi:10.1063/1.2982094.

Bouzidi, Y., and D. R. Schmitt (2008b), Quantitative modeling of refected ultrasonic bounded beams and a new estimate of the schoch shift, *IEEE Trans. Ultrason. Ferroelectr. Freq. Control*, *55*(12), 2661–2673, doi:10.1109/TUFFC.2008.981.

Bouzidi, Y., and D. R. Schmitt (2012), Incidence-angle-dependent acoustic reflections from liquid-saturated porous solids, *Geophys. J. Int.*, *191*(3), 1427–1440, doi:10.1111/j.1365-246X.2012.05695.x.

Breazeale, M. A., L. Adler, and G. W. Scott (1977), Interaction of ultrasonic waves incident at

the Rayleigh angle onto a liquid-solid interface, *J. Appl. Phys.*, *48*(2), 530–537, doi:10.1063/1.323677.

Brekhovskikh, L. M. (1960), *Waves in layered media.*, Academic Press, New York,.

Brown, R. J., D. C. Lawton, and S. P. Cheadle (1991), Scaled physical modelling of anisotropic wave propagation: multioffset profiles over an orthorhombic medium, *Geophys. J. Int.*, *107*(3), 693–702, doi:10.1111/j.1365-246X.1991.tb01428.x.

Carcione, J. M. (1997), Reflection and transmission of qP-qS plane waves at a plane boundary between viscoelastic transversely isotropic media, *Geophys. J. Int.*, *129*, 669–680.

Castagna, J., and M. Backus (1993), *Offset-dependent refletivity-theory and practice of AVO analysis*, Society of Exploration Geophysicist.

Chattopadhyay, A., P. Kumari, and V. K. Sharma (2015), Reflection and refraction at the interface between distinct generally anisotropic half spaces for three-dimensional plane quasi-P waves, *J. Vib. Control*, *21*, 493–508.

Cheadle, S. P. (1991), Orthorhombic anisotropy: A physical seismic modeling study, *Geophysics*, *56*(10), 1603, doi:10.1190/1.1442971.

Chen, H., J. P. Castagna, R. L. Brown, and A. C. B. Ramos (2001), Three-parameter AVO crossplotting in anisotropic media, *Geophysics*, *66*(5), 1359, doi:10.1190/1.1487081.

Christensen, N. I. (1965), Compressional wave velocities in metamorphic rocks at pressures to 10 kilobars, *J. Geophys. Res.*, *70*(24), 6147–6164, doi:10.1029/JZ070i024p06147.

Christoffel, E. B. (1877), Uber die Fortpflanzung von Stossen durch elastische fest Korper, *Ann. Mater.*, *8*, 193–243.

Claerbout, J. F. (1985), *IMAGING THE EARTH's INTERIOR*, Blackwell Scientific Publications, Oxford, London, Edinburgh, Boston, Palo Alto, Victoria.

Crampin, S. (1985), Evaluation of anisotropy by shear-wave splitting, *Geophysics*, *50*(1), 142, doi:10.1190/1.1441824.

Daley, P. ., and F. Hron (1987), Reflection and transmission coefficients for transversely isotropic media, *Bull. Seism. Soc. Am.*, *67*(3), 661–675.

Daley, P. F. (1979), Reflection and transmission coefficients for seismic waves in ellipsoidally anisotropic media, *Geophysics*, *44*(1), 27, doi:10.1190/1.1440920.

Daley, P. F., and F. Hron (1977a), REFLECTION AND TRANSMISSION COEFFICIENTS TRANSVERSELY ISOTROPIC MEDIA, *BSSA*, *67*(3), 661–675.

Daley, P. F., and F. Hron (1977b), REFLECTION AND TRANSMISSION COEFFICIENTS TRANSVERSELY ISOTROPIC MEDIA, *BSSA*, *67*(3), 661–675.

Declercq, N. F. (2006), Fast beating null strip during the reflection of pulsed Gaussian beams incident at the Rayleigh angle, *Ultrasonics*, *44*(SUPPL.), e1447–e1451, doi:10.1016/j.ultras.2006.05.205.

Declercq, N. F., R. Briers, J. Degrieck, and O. Leroy (2005), The history and properties of ultrasonic inhomogeneous waves, *IEEE Trans. Ultrason. Ferroelectr. Freq. Control*, *52*(5), 776–791, doi:10.1109/TUFFC.2005.1503963.

Descamps, M., and B. Hosten (1991), The effects of viscoelasticity on the reflection and transmission of ultrasonic waves by an orthotropic plate, *J. Acoust. Soc. Am.*, *29*(6), 1763–1770, doi:10.1006/jsvi.1996.0374.

Diachok, O. I. (1970), Conical Reflection of Ultrasound from a Liquid-Solid Interface, *J. Acoust. Soc. Am.*, *47*(1B), 155, doi:10.1121/1.1911450.

Dvorkin, J., M. Gutierrez, and D. Grana (2014), *Seismic Reflections of Rock Properties*.

Ekanem, a. M., J. Wei, X. Y. Li, M. Chapman, and I. G. Main (2013), P-wave attenuation anisotropy in fractured media: A seismic physical modelling study, *Geophys. Prospect.*, *61*(SUPPL.1), 420–433, doi:10.1111/j.1365-2478.2012.01127.x.

Far, M. E., C. M. Sayers, L. Thomsen, D. H. Han, and J. P. Castagna (2013), Seismic characterization of naturally fractured reservoirs using amplitude versus offset and azimuth analysis, *Geophys. Prospect.*, *61*(2), 427–447, doi:10.1111/1365-2478.12011.

Farra, V., and I. Pšenčík (2010), First-order reflection/transmission coefficients for unconverted plane P waves in weakly anisotropic media, *Geophys. J. Int.*, *183*(3), 1443–1454, doi:10.1111/j.1365-246X.2010.04794.x.

Gassmann, F. (1964), Introduction to seismic travel time methods in anisotropic media, *Pure Appl. Geophys. PAGEOPH*, *58*(1), 63–112, doi:10.1007/BF00879140.

Gazdag, J. (1978), Wave equation migration with the phase-shift method, *Geophysics*, *43*(7), 1342, doi:10.1190/1.1440899.

Godfrey, N. J., N. I. Christensen, and D. a. Okaya (2000), Anisotropy of schists: Contribution of crustal anisotropy to active source seismic experiments and shear wave splitting observations, *J. Geophys. Res.*, *105*(B12), 27991–28007, doi:10.1029/2000JB900286.

Golikov, P., and A. Stovas (2010), New weak-contrast approximation for reflection coefficients in transversely isotropic media, *J. Geophys. Eng.*, *7*(4), 343–350, doi:10.1088/1742-2132/7/4/001.

Graebner, M. (1992), Plane-wave reflection and transmission coefficients for a transversely isotropic solid, *GEOPHYSICS*, *57*(11), 1512–1519, doi:10.1190/1.1443219.

Gray, D., G. Roberts, and K. Head (2002), Recent advances in determination of fracture strike and crack density from P-wave seismic data, *Lead. Edge*, *21*(3), 280, doi:10.1190/1.1463778.

Grech, M. G. K., D. C. Lawton, and S. H. Gray (2002), A multioffset vertical seismic profiling experiment for anisotropy analysis and depth imaging, *Geophysics*, *67*(2), 348–354, doi:10.1190/1.1468595.

Grechka, V., and I. Tsvankin (2004), Characterization of dipping fractures in a transverselyisotropic background, *Geophys. Prospect.*, *52*(1), 1–10, doi:10.1046/j.1365-2478.2004.00396.x.

Guest, W. S., and J.-M. Kendall (1993), Modelling waveforms in anisotropic inhomogeneous media using ray and Maslov asymptotic theory: applications to exploration seismology, *Can. J. Expl. Geophys.*, *29*, 78–92.

Guest, W. S., and C. J. Thomson (1992), A SOURCE OF SIGNIFICANT TRANSVERSE ARRIVALS FROM AN ISOTROPIC ANISOTROPIC INTERFACE, eg THE MOHO., *Geophys. J. Int.*, *111*, 309–318.

Guest, W. S., C. J. Thomson, and C. P. Spencer (1993), Anisotropic reflection and transmission calculations with application to a crustal seismic survey from the East Greenland Shelf, *J. Geophys. Res.*, *98*(B8), 14161, doi:10.1029/93JB01156.

Hall, S. A., and J. Kendall (2003), Fracture characterization at Valhall: Application of P-wave amplitude variation with offset and azimuth (AVOA) analysis to a 3D ocean-bottom data set, *Geophysics*, *68*(4), 1150, doi:10.1190/1.1598107.

Helbig, K. (1994), *Foundations of Anisotropy for Exploration Seismics*, Elsevier, Utrecht.

Henneke, E. G. (1972), Reflection-Refraction of a Stress Wave at a Plane Boundary between Anisotropic Media, *J. Acoust. Soc. Am.*, *51*(1B), 210, doi:10.1121/1.1912832.

Henneke, E. G., and G. L. Jones (1976), Erratum: ''Critical angle for reflection at a liquid–solid interface in single crystals'', *J. Acoust. Soc. Am.*, *60*(3), 759, doi:10.1121/1.381248.

Hood, J. A., and M. Schoenberg (1992), NDE of fracture-induced anisotropy, *Rev. Prog. Quant. Nondestruct. Eval. Vol. 11B*, *11*, 2101–2108.

Innanen, K. A., and F. Mahmoudian (2015), Characterizing the degree of amplitude-variation-with-offset nonlinearity in seismic physical modelling reflection data, *Geophys. Prospect.*, *63*(1), 133–140, doi:10.1111/1365-2478.12169.

Isaac, J. H., and D. C. Lawton (1999), Image mispositioning due to dip-ping TI Media: A physical seismic modeling study, *Geophysics*, *64*, 1230–1238.

Jech, J. (1991), Computation of elastic parameters of anisotropic medium from travel times of quasi-compressional waves, *Phys. Earth Planet. Inter.*, *66*(3–4), 153–159, doi:10.1016/0031-9201(91)90074-R.

Ji, S., T. Shao, K. Michibayashi, C. Long, Q. Wang, Y. Kondo, W. Zhao, H. Wang, and M. H. Salisbury (2013), A new calibration of seismic velocities, anisotropy, fabrics, and elastic moduli of amphibole-rich rocks, *J. Geophys. Res. E Planets*, *118*(9), 4699–4728, doi:10.1002/jgrb.50352.

Jocker, J., and D. Smeulders (2007), Minimization of finite beam effects in the determination of reflection and transmission coefficients of an elastic layer, *Ultrasonics*, *46*(1), 42–50, doi:10.1016/j.ultras.2006.10.001.

Kaarsberg, E. A. (1959), Introductory Studies of Natural and Artificial Argillaceous Aggregates by Sound-Propagation and X-ray Diffraction Methods, *J. Geol.*, *67*(4), 447–472, doi:10.1086/626597.

Kebaili, A., and D. R. Schmitt (1997), Ultrasonic anisotropic phase velocity determination with the Radon transformation, *J. Acoust. Soc. Am.*, *101*(6), 3278, doi:10.1121/1.418344.

Keith, C. M., and S. Crampin (1977), Seismic body waves in anisotropic media: Reflection and refraction at a plane interface, *Geophys. J. Roy. Astr. Soc.*, *49*, 181–208.

Kendall, J.-M., and C. J. Thomson (1989), A comment on the form of the geometrical spreading equations, with some numerical examples of seismic ray tracing in inhomogeneous, anisotropic media, *Geophys. J. Int.*, *99*(2), 401–413, doi:10.1111/j.1365-246X.1989.tb01697.x.

Kern, H., and H. R. Wenk (1990), Fabric-related velocity anisotropy and shear wave splitting in rocks from the Santa Rosa Mylonite Zone, California, *J. Geophys. Res. Solid Earth*, *95*(B7), 11213–11223, doi:10.1029/JB095iB07p11213.

Klimes, L. (2003), Weak-contrast reflection–transmission coefficients in a generally anisotropic background, *Geophysics*, *68*(6), 2063, doi:10.1190/1.1635060.

Knott, C. G. (1899), Reflexion and Refraction of Elastic Waves with Seismological Applications, *Philos. Mag.*, *54*(5th series), 64–97.

Krail, P. M., and H. Brysk (1983), Reflection of spherical seismic waves in elastic layered media, *Geophysics*, *48*(6).

Landrø, M., and I. Tsvankin (2006), Seismic critical-angle reflectometry: A method to characterize azimuthal anisotropy?, *Geophysics*, *72*(3), 120–124, doi:10.1190/1.2437145.

Leary, P. C., S. Crampin, and T. V. McEvilly (1990), Evolution of Mid Ocean Ridges, edited by J. M. Sinton, *J. Geophys. Res.*, *95*(B7), 11105–11114, doi:10.1029/GM057.

Di Leo, J. F., A. M. Walker, Z. H. Li, J. Wookey, N. M. Ribe, J. M. Kendall, and A. Tommasi (2014), Development of texture and seismic anisotropy during the onset of subduction, *Geochemistry, Geophys. Geosystems*, *15*(1), 192–212, doi:10.1002/2013GC005032.

Leroy, O., and B. Poirèe (1988), On the Reflection Coefficient of Acoustic Beams, *Acustica*, *66*, 84–89.

Li, L. (2008), Calculation of reflection and transmission coefficients for qP waves incident on a planar interface between isotropic and triclinic media, *Acta Geophys.*, *56*, 518–528.

Liang, K., X. Yin, and G. Wu (2009), Approximate PP reflection coefficient in TTI media, in *Beijing 2009 International Geophysical Conference and Exposition, Beijing, China, 24–27 April 2009*, edited by L. Zhenwu and Y. Sun, pp. 126–126, Society of Exploration Geophysicists.

Lin, F.-C., M. H. Ritzwoller, Y. Yang, M. P. Moschetti, and M. J. Fouch (2011), Complex and

variable crustal and uppermost mantle seismic anisotropy in the western United States, *Nat. Geosci.*, *4*(1), 55–61, doi:10.1038/ngeo1036.

Liu, Y., and D. R. Schmitt (2006), The transition between the scale domains of ray and effective medium theory and anisotropy: Numerical models, *Pure Appl. Geophys.*, *163*(7), 1327–1349, doi:10.1007/s00024-006-0075-5.

Mah, M., and D. R. Schmitt (2001a), Experimental determination of the elastic coefficients of an orthorhombic material, *Geophysics*, *66*(4), 1217, doi:10.1190/1.1487068.

Mah, M., and D. R. Schmitt (2001b), Experimental determination of the elastic coefficients of an orthorhombic material, *Geophysics*, *66*(4), 1217, doi:10.1190/1.1487068.

Mahmoudian, F. (2013), Physical Modeling and Analysis of Seismic Data from a Simulated Fractured Medium, University of Calgary.

Mahmoudian, F., G. Margrave, and P. Daley (2014), Estimation of elastic stiffness coefficients of an orthorhombic physical model using group velocity analysis on transmission data, *Geophysics*, *79*(1), R27–R39, doi:10.1190/geo2013-0203.1.

Mahmoudian, F., G. F. Margrave, J. Wong, and D. C. Henley (2015), Azimuthal amplitude variation with offset analysis of physical modeling data acquired over an azimuthally anisotropic medium, *GEOPHYSICS*, *80*(1), C21–C35, doi:10.1190/geo2014-0070.1.

Mainprice, D., and A. Nicolas (1989), Development of shape and lattice preferred orientations: application to the seismic anisotropy of the lower crust, *J. Struct. Geol.*, *11*(1–2), 175–189, doi:10.1016/0191-8141(89)90042-4.

Malehmir, R., and D. R. Schmitt (2016a), ARTc: Anisotropic reflectivity and transmissivity calculator, *Comput. Geosci.*, *93*, 114–126, doi:10.1016/j.cageo.2016.05.008.

Malehmir, R., and D. R. Schmitt (2016b), Ultrasonic measurement of anisotropic reflectivity from Water-Phenolic CE Interface, *PANGAEA*, doi:10.1594/PANGAEA.864794.

Malehmir, R., and D. R. Schmitt (2017), Acoustic Reflectivity from an Orthorhombic Media : Understanding the Fractured Anisotropic Crust, *J. Geophys. Res.*, Under review.

Malehmir, R., N. Kazemi, and D. R. Schmitt (2017), An Algorithm to Quantitatively Model Reflected Ultrasonic Bounded Beam with Experimental Validation, *Ultrasonics*.

Mallick, S., and L. N. Frazer (1991), REFLECTION-TRANSMISSION COEFFICIENTS AND

AZIMUTHAL ANISOTROPY IN MARINE SEISMIC STUDIES, *Geophys. J. Int.*, *105*, 241–252.

Mallick, S., K. L. Craft, L. J. Meister, and R. E. Chambers (1998), Determination of the principal directions of azimuthal anisotropy from P-wave seismic data, *GEOPHYSICS*, *63*(2), 692–706, doi:10.1190/1.1444369.

Mann, R. W., G. A. Baum, and C. C. Habeger (1980), Determination of all nine orthotropic elastic constants for machine-made paper, *Tappi*, *63*(84), 163–166.

McCamy, K., R. P. Meyer, and T. J. Smith (1962), Generally applicable solutions of Zoeppritz' amplitude equations, *BSSA*, *52*, 923–955.

Merkulov, L. G. (1963), Ultrasonic waves in crystals, *Appl. Mater. Res.*, *2*(4), 231–240.

Musgrave, M. J. P. (1970a), *Crystal Acoustics: Introduction to the Study of Elastic Waves and Vibrations in Crystals*, Holden-Day.

Musgrave, M. J. P. (1970b), *Musgrave M.J.P. Crystal Acoustics 1970.djvu.pdf*, HOLDEN-DAY, San Francisco.

Nakagawa, S., K. T. Nihei, L. R. Myer, and E. L. Majer (2003), Three-dimensional elastic wave scattering by a layer containing vertical periodic fractures, *J. Acoust. Soc. Am.*, *113*(6), 3012, doi:10.1121/1.1572139.

Nayfeh, A. H. (1989), The propagation of horizontally polarized shear waves in multilayered anisotropic media, *J. Acoust. Soc. Am.*, *86*(5), 1–16, doi:10.1121/1.398580.

Ngoc, T. D. K., and W. G. Mayer (1979), Ultrasonic nonspecular reflectivity near longitudinal critical angle, *J. Appl. Phys.*, *50*(12), 7948–7951, doi:10.1063/1.325971.

Nishizawa, O., and K. Kanagawa (2010), Seismic velocity anisotropy of phyllosilicate-rich rocks: characteristics inferred from experimental and crack-model studies of biotite-rich schist, *Geophys. J. Int.*, *182*(1), no-no, doi:10.1111/j.1365-246X.2010.04614.x.

Ortiz-osornio, M., and D. R. Schmitt (2009), Measurements of the reflectivity of a liquid – anisotropic solid interface, in *8th Euro Conference of Rock Physics & Geomechanics*, p. 4pp, Ascona, Switzerland.

Ortiz-osornio, M., and D. R. Schmitt (2010a), The Reflectivity and Transmissivity of Anisotropic Materials : A Physical Modeling Study, in *American Rock Mechanics Association*, p. 5pp.

Ortiz-osornio, M., and D. R. Schmitt (2010b), The reflectivity and transmissivity of anisotropic materials: A physical model study, in *ARMA 44th U.S. Rock Mechanics Symposium*, p. 5 pp, Salt Lake City.

Ortiz-osornio, M., and D. R. Schmitt (2010c), Velocity dispersion of a heavy oil sandstone: A case study, in *Oil Sands and Heavy Oil Technologies Conference, Calgary*, pp. 20–22.

Ortiz-osornio, M., and D. R. Schmitt (2011a), Measurements of the reflectivity and transmissivity of anisotropic materials to test the effect of tilt and azimuth, in *1st Int. Workshop on Rock Physics, August 7-12,* p. 4pp, Golden, CO.

Ortiz-osornio, M., and D. R. Schmitt (2011b), Physical Modeling of the Reflectivity and Transmissivity of Anisotropic Materials, in *73rd EAGE Conference and Exhibition incorporating SPE EUROPEC 2011, Vienna*, p. 4 pp, Vienna.

Ostrander, W. J. (1984), Plane-wave reflection coefficients for gas sands at nonnormal angles of incidence - ostrander1984.pdf, *Geophysics*, *49*(10), 1637–1648.

Ozacar, A. A., and G. Zandt (2004), Crustal seismic anisotropy in central Tibet: Implications for deformational style and flow in the crust, *Geophys. Res. Lett.*, *31*(23), 1–4, doi:10.1029/2004GL021096.

Ozacar, A. A., and G. Zandt (2009), Crustal structure and seismic anisotropy near the San Andreas Fault at Parkfield, California, *Geophys. J. Int.*, *178*(2), 1098–1104, doi:10.1111/j.1365-246X.2009.04198.x.

Pedersen, H. A. (2006), Impacts of non-plane waves on two-station measurements of phase velocities, *Geophys. J. Int.*, *165*(1), 279–287, doi:10.1111/j.1365-246X.2006.02893.x.

Plona, T. J. (1976), Ultrasonic bounded beam reflection and transmission effects at a liquid/ solid-plate/liquid interface, *J. Acoust. Soc. Am.*, *59*(6), 1324, doi:10.1121/1.381011.

Rokhlin, S. I. (1986), Reflection and refraction of elastic waves on a plane interface between two generally anisotropic media, *J. Acoust. Soc. Am.*, *79*(4), 906, doi:10.1121/1.393764.

Rokhlin, S. I., and W. Wang (1992), Double through transmission bulk wave method for ultrasonic phase velocity measurement and determination of elastic constants of composite materials, *Acoust. Soc. Am.*, *91*(6), 3303–3312.

Rüger, A. (1997), P -wave reflection coefficients for transversely isotropic models with vertical

and horizontal axis of symmetry, *Geophysics*, *62*(3), 713–722.

Rüger, A. (1998), Variation of P-wave reflectivity with offset and azimuth in anisotropic media, *Geophysics*, *63*(3), 935, doi:10.1190/1.1444405.

Savage, M. K. (1999), Siesmic anisotropy and mantle deformation, *Rev. Geophys.*, (98), 65–106, doi:10.1029/98RG02075.

Sayers, C. M., and S. Dean (2001), Azimuth-dependent AVO in reservoirs containing non-orthogonal fracture sets gave an analytic expression, valid for, *Geophys. Prospect. Ikelle Ru È ger*, *49*, 100–106.

Sayers, C. M., and M. Kachanov (1995), Microcrack-induced elastic wave anisotropy of brittle rocks, *J. Geophys. Res. Solid Earth*, *100*(B3), 4149–4156, doi:10.1029/94JB03134.

Sayers, C. M., S. Guo, and J. Silva (2015), Sensitivity of the elastic anisotropy and seismic reflection amplitude of the Eagle Ford Shale to the presence of kerogen, *Geophys. Prospect.*, *63*(1), 151–165, doi:10.1111/1365-2478.12153.

Schijns, H., D. R. Schmitt, P. J. Heikkinen, and I. T. Kukkonen (2012a), Seismic anisotropy in the crystalline upper crust: Observations and modelling from the Outokumpu scientific borehole, Finland, *Geophys. J. Int.*, *189*(1), 541–553, doi:10.1111/j.1365-246X.2012.05358.x.

Schijns, H., D. R. Schmitt, P. J. Heikkinen, and I. T. Kukkonen (2012b), Seismic anisotropy in the crystalline upper crust: Observations and modelling from the Outokumpu scientific borehole, Finland, *Geophys. J. Int.*, *189*(1), 541–553, doi:10.1111/j.1365-246X.2012.05358.x.

Schmitt, D. R. (2015), *Geophysical Properties of the Near Surface Earth: Seismic Properties*, Elsevier B.V.

Schoch, A. (1950), Schallreflexion, Schallbrechung und Schallbeugung, in *Ergebnisse der exakten Naturwissenschaften*, vol. 23, pp. 127–234.

Schoch, A. (1952a), b, Seitliche versetzung eines total reflektierten strahles bei ultraschall-wellen, *Acustica*, *2*(17).

Schoch, A. (1952b), Der schallbeugung durch platten, *Acustica*, *1*(2).

Schoenberg, M. (1997), Orthorhombic media: Modeling elastic wave behavior in a vertically

fractured earth, *Geophysics*, *62*(6), 1954, doi:10.1190/1.1444297.

Shadlow, J. (2014), A description of seismic amplitude techniques, *Explor. Geophys.*, *45*(3), 154, doi:10.1071/EG13070.

Shen, F., J. Sierra, D. R. Burns, and M. N. Toksöz (2002), Azimuthal offset-dependent attributes applied to fracture detection in a carbonate reservoir, *GEOPHYSICS*, *67*(2), 355–364, doi:10.1190/1.1468596.

Shuey, R. T. (1985), A simplification of the Zoeppritz equations, *Geophysics*, *50*(4), 609, doi:10.1190/1.1441936.

Skopintseva, L., and T. Alkhalifah (2013), An analysis of AVO inversion for postcritical offsets in HTI media, *GEOPHYSICS*, *78*(3), N11–N20, doi:10.1190/geo2011-0288.1.

Stewart, R. R., N. Dyaur, B. Omoboya, J. J. S. de Figueiredo, M. Willis, and S. Sil (2013), Physical modeling of anisotropic domains: Ultrasonic imaging of laser-etched fractures in glass, *Geophysics*, *78*(1), D11–D19, doi:10.1190/geo2012-0075.1.

Swokowski, E. W. (1979), *Calculus with analytic geometry*, Prindle, Weber & Schmidt.

Tamir, T., and H. L. Bertoni (1971), Lateral Displacement of Optical Beams at Multilayered and Periodic Structures, *J. Opt. Soc. Am.*, *61*(10), 1397–1413, doi:10.1364/JOSA.61.001397.

Thomsen, L. (1986a), Weak elastic anisotropy, *Geophysics*, *51*(10), 1954, doi:10.1190/1.1442051.

Thomsen, L. (1986b), Weak elastic anisotropy, *Geophysics*, *51*(10), 1954, doi:10.1190/1.1442051.

Tsvankin, I. (1997), Anisotropic parameters and P-wave velocity for orthorhombic media, *Geophysics*, *62*(4), 1292, doi:10.1190/1.1444231.

Ursin, B., and G. Haugen (1996), Weak-contrast approximation of the elastic scattering matrix in anisotropic media, *Pure Appl. Geophys.*, *148*(3–4), 685–714.

Vavrycuk, V. (1999), Weak-contrast reflection / transmission coefficients in weakly anisotropic elastic media : P -wave incidence, *Geophys. J. Int.*, *138*, 553–562, doi:10.1046/j.1365-246X.1999.00890.x.

Vavrycuk, V., and I. Pšenčík (1998), PP-reflection coefficients in weakly anisotropic elastic media, *Soc. Expl. Geophys*, *63*(6), 2129–2141.

Vestrum, R. W. (1994), Group and Phase-Velocity Inversions for the General Anisotropic Stiffness Tensor, October.

Vestrum, R. W., and R. J. Brown (1994), *From group or phase velocities stiffness tensor to the general anisotropic Robert W . Vestr um and R . Jame s B ro w n*.

Voigt, W. (1887), Theorie des Lichts für bewegte Medien, *Göttinger Nachrichten*, *7*, 41–51.

Walker, A. M., and J. Wookey (2012a), Computers & Geosciences MSAT — A new toolkit for the analysis of elastic and seismic anisotropy, *Comput. Geosci.*, *49*(October 2012), 81–90, doi:10.1016/j.cageo.2012.05.031.

Walker, A. M., and J. Wookey (2012b), MSAT-A new toolkit for the analysis of elastic and seismic anisotropy, *Comput. Geosci.*, *49*, 81–90, doi:10.1016/j.cageo.2012.05.031.

Wang, X., and I. Tsvankin (2013), Multiparameter TTI tomography of P-wave reflection and VSP data, *Geophysics*, *78*(5), WC51-WC63, doi:10.1190/geo2012-0394.1.

Wenk, H.-R. (1999), A voyage through the deformed Earth with the self-consistent model, *Model. Simul. Mater. Sci. Eng.*, *7*(5), 699–722, doi:10.1088/0965-0393/7/5/304.

Weyl, H. (1919), Ausbreitung elektromagnetischer Wellen über einem ebenen Leiter, *Ann. Phys.*, *365*(21), 481–500, doi:10.1002/andp.19193652104.

Wielandt, E. (1993), Propagation and structural interpretation of non-plane waves, *Geophys. J. Int.*, *113*(1), 45–53, doi:10.1111/j.1365-246X.1993.tb02527.x.

Young, G. B., and L. W. Braile (1976), A computer program for the application of Zoeppritz's amplitude equations and Knott's energy equations, *Bull. Seismol. Soc. Am.*, *66*(6), 1881–1885.

Yousef, B. M., and D. A. Angus (2016), *When do fractured media become seismically anisotropic? Some implications on quantifying fracture properties*.

Zheng, P., and B. Ding (2014), The Generalized Reflection and Transmission Matrix Method for Wave Propagation in Stratified Fluid-Saturated Porous Media, *Transp. Porous Media*, *102*(2), 185–206, doi:10.1007/s11242-014-0271-1.

Zheng, Y. (2006), Seismic azimuthal anisotropy and fracture analysis from PP reflection data, University of Calgary.

Zillmer, M., D. Gajewski, and B. M. Kashtan (1998), Anisotropic reflection coefficients for a

weak-contrast interface, *Geophys. J. Int.*, *132*(1), 159–166.

Zoeppritz, K. (1919), Erdbebenwellen VII. VIIb. Über Reflexion und Durchgang seismischer Wellen durch Unstetigkeitsflächen. Nachrichten von der Königlichen Gesellschaft der Wissenschaften zu Göttingen, *Math. Klasse*, 66–84.

Chapter 4

Acoustic Reflectivity from Variously Oriented Orthorhombic Media: Analogies to Seismic Responses from a Fractured Anisotropic Crust

4.1 Introduction

Many, if not most, rocks and rock masses are anisotropic to the propagation of seismic waves. Conversely, observations of seismic anisotropy inform us about the in-situ metamorphic strain textures [e.g., *Mainprice and Nicolas*, 1989; *Kern and Wenk*, 1990; *Godfrey et al.*, 2000; *Almqvist et al.*, 2010; *Ji et al.*, 2013], layering [e.g., *Backus*, 1962; *Brown et al.*, 1991; *Kebaili and Schmitt*, 1997; *Grech et al.*, 2002], and properties of the natural and induced fracture's network [e.g., *Sayers and Kachanov*, 1995; *Nakagawa et al.*, 2003; *Grechka and Tsvankin*, 2004; *Yousef and Angus*, 2016]. This information is a key to understanding in-situ geological structures and processes, but properly obtaining it requires knowledge of the seismic wavefield behavior in anisotropic media that are addressed both experimentally and numerically.

Observations of seismic waves from different parts of the solid Earth, confirm that elastic anisotropy is a dominant phenomenon, *Belonoshko et al.* [2008] reported about inner core radial anisotropy, *Leary et al.* [1990] and later *Bao et al.* [2016] and many others, showed that preferred alignment of fractures in the crust, under certain conditions, could also create an anisotropic medium, in addition, if the fractures are embedded in an anisotropic rock mass it would exhibit an even more complex anisotropic behavior [e.g., *Nishizawa and Kanagawa*, 2010; *Schijns et al.*, 2012]. Reflected seismic transit times [e.g., *Wang and Tsvankin*, 2013] and amplitudes carry valuable information about the underlying elasticity and its directional dependency are the key to the understanding of elastic anisotropy [e.g., *Guest et al.*, 1993; *Sayers and Dean*, 2001; *Hall and Kendall*, 2003; *Landrø and Tsvankin*, 2006; *Ekanem et al.*, 2013; *Far et al.*, 2013].

The variation in the reflectivity with the angle of incidence from the interface between two isotropic formations is now being used routinely to estimate in situ elastic moduli and fluid content. Observed data are usually evaluated using various levels of approximation of *Zoeppritz's* [1919] original solution for the reflectivity of plane waves from the interface between two isotropic half-spaces. Many researchers [e.g., *Ostrander*, 1984; *Mallick and Frazer*, 1991] have shown that the analysis of the reflected amplitude variation with its corresponding angle of incidence, known as amplitude versus offset (AVO), could reveal important information about the elastic properties of the media. More recently AVO methods have attempted to estimate density by improving the inversion using longer offset (i.e. greater incidence angles) past the compressional wave critical incidence.

However, the use of seismic reflectivity to study anisotropy is less developed. The amplitudes of reflected seismic waves from an anisotropic formations depend not only on the incident angle (θ) of the incoming wave but also on its azimuthal direction (φ); a number of theoretical studies for various situations exist [*Daley*, 1979; *Thomsen*, 1986b; *Schoenberg*, 1997; *Vavrycuk*, 1999]. In practice, *Amplitude versus Azimuth* (*AVAz*) or *Amplitude versus Angle/Amplitude versus Offset* (*AVA/AVO*) investigates the directional dependencies of reflected wavefield to understand the subsurface state of the in-situ or induced stress regime, fracture orientation [e.g., *Mallick et al.*, 1998; *Shen et al.*, 2002; *Zheng*, 2006; *Aleardi and Mazzotti*, 2014].

The analysis of data obtained in *AVAz* field studies are mostly limited to the highly symmetric case of horizontal transverse isotropy (HTI) [*Rüger*, 1997; *Behura and Tsvankin*, 2006]) that might be expected for a geological formation containing a parallel sets of vertically oriented fractures (titling at $\varphi = 90°$) breaking through the otherwise elastically isotropic rock. The popularity of this geometry stems from the relative simplicity of the approximate expressions describing the small angle reflectivity under the weakly anisotropic material assumption [*Thomsen*, 1986b]. These simplified expressions have been used extensively [e.g., *Innanen and Mahmoudian*, 2015] although questions remain as to its range of validity [e.g., *Mallick et al.*, 1998]. These two cases do not rigorously apply should the symmetry planes of the TI rock mass be tilted which is likely to be encountered more often in real geological situations.

There are also many cases in which we would expect the symmetry of the rock mass to be less than transversely isotropic. Metamorphic rocks displaying both strong lineation and foliation are expected to have orthorhombic symmetry [e.g., *Christensen*, 1965; *Schijns et al.*, 2012]. So are isotropic rocks containing uniformly oriented orthogonal microcracks subject to anisotropic stress states [e.g., *Sayers and Dean*, 2001], and rocks or rock masses containing multiple fracture sets [e.g., *Hall and Kendall*, 2003]. Reflectivity from orthorhombic materials, however, remains poorly studied and the few solutions that do exist remain limited to cases aligned with the principal symmetry axes in analogy to the VTI-HTI geometries. As such, extending *AVAz* studies beyond the classic transversely isotropic geometries to more realistic situations that consider lower symmetry formations is necessary, and of the available possibilities, orthorhombic symmetry may be the most representative, [*Bakulin et al.*, 2000].

Here, we describe and model a series of laboratory reflectivity measurements from blocks orthorhombic material. The symmetry of the blocks are variously tilted making an analogy to a geological formation containing coherent fracture sets with different dips. First, we review the theory of elastic wave propagation and its reflection in anisotropic materials, and then describe the laboratory setup and properties of the anisotropic samples. We repeated measurements of ultrasonic acoustic reflectivity from thick blocks of a composite material with orthorhombic symmetry following the original reflectivity observations of *Ortiz-osornio and Schmitt* [2009, 2010a, 2010b, 2011a, 2011b]. These measurements were carried out on samples with a variety of tilt angles (ψ) of the symmetry axis beam incidence angles (θ), and azimuthal angles (φ). We go further describing a method to model the observed reflectivities that accounts for the effects related to real beam propagation at both pre- and post-critical incidence angles. The modeling, which incorporates a recent solution for reflectivity from anisotropic media, reproduces well the observed reflectivities. The observations illustrate the potential importance of including critical angle information. However, this must be done with the realization that once past a limited range of steep pre-critical angles of incidence the real observations will diverge from the theoretical plane wave solutions, solutions that are almost exclusively used to analyze reflectivity in the field. This has long been known but usually ignored in practice, and the current laboratory observations reinforce

that the characteristics of the wave field emitted from a real seismic source need to be considered as the critical angle is approached and exceeded.

4.2 Theory

In this experiment, the acoustic reflectivity of a bounded ultrasonic pulse from blocks of orthorhombic material is measured. A proper analysis of the observations requires, first, that the complex plane-wave reflectivity is properly calculated and, second, that the real beam diffraction effects are properly accounted for. A real-valued plane-wave solution is usually believed to suffice at small angles of incidence, but in a real world situation where the source has a finite aperture, the plane-wave solution fails even well before the first critical angle is reached. A proper quantitative modeling of the observed responses necessitates that the complex reflectivities be incorporated to the beam propagation. The details may be found in the recent descriptions [*Malehmir et al.*, 2017] but are briefly discussed here; however, the main contribution here is focusing on the experimental observations.

4.2.1 Essential Concepts of Elastic Wave Anisotropy

The theory describing the propagation and reflection of mechanical waves in anisotropic elastic media is well developed with numerous resources available [e.g., *Musgrave*, 1970; *Auld*, 1973] and only the essential elements need be provided. We assume Hooke's elastic law holds whereby the stresses $\boldsymbol{\tau}$ are related to strains $\boldsymbol{\varepsilon}$ in Voigt's reduced notation within the principal material reference coordinate frame *x-y-z* (Figure 4-1a) is:

$$\sigma_{ij} = C_{ijkl}\ \varepsilon_{kl} \tag{4-1}$$

with elastic tensor stiffnesses $\boldsymbol{C}_{ijkl}$ in the reduced $\boldsymbol{C}_{IJ}$ form according to the cyclical indicial shorthand notation 11→1, 22→2, 33→3, 23→4, 13→5, 12 →6. For the orthorhombic material studied here with the number of independent stiffnesses reduces to nine. The solution of the wave equation with the constitutive Equation 4-1 leads to a Christoffel's theorem:

$$[\Lambda_{ij} - \rho\ v^2\ \delta_{ij}\ ]\ [\xi_j] = 0 \tag{4-2}$$

with Christoffel matrix $\boldsymbol{\Lambda}$ that depends on the stiffness and direction (refer to [*Auld*, 1973]), mass density ρ, phase wave speed $\boldsymbol{v}$, and polarization direction component ξ. Equation 4-2 is a standard eigenvalue, eigenvector problem the solution of which is given for any propagation direction

through the material gives, and as is well known in general, three distinct wave phase speeds with corresponding particle motion polarizations, these modes are associated with plane wave propagation. Usually, this gives one wave-mode that has nearly longitudinal and two other modes that are nearly transverse and referred to as q-P, q-S1, and 1-S2, respectively. Algorithms to calculate these directionally controlled phase wave speeds and polarizations are readily available [e.g., *Walker and Wookey*, 2012], an example of such variations calculated using the algorithms in [*Malehmir and Schmitt*, 2016a] for the material studied here is given in Figure 4-1 b-d. One additional key aspect of elastic wave propagation in anisotropic media is that generally in any direction within the anisotropic medium in addition to the three phase or plane wave, modes there is associated *at least* 3 corresponding group (or ray) speeds the directions and magnitudes of which differ.

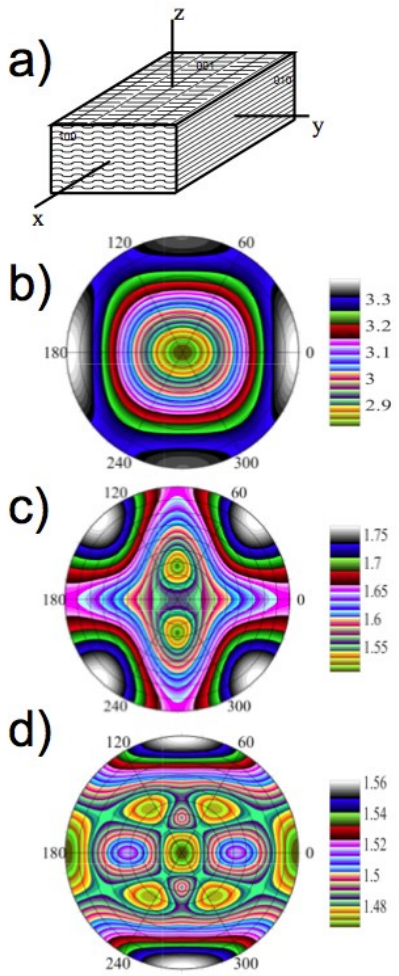

Figure 4.1.a) Orthorhombic material within its x-y-z coordinate frame. Remaining panels show directionally dependent waves speeds (km per second) calculated for the material used in the measurements plotted on an equal area (0.2°) polar projection with z-axis vertical and x-axis at 0° for modes b) qP, c) qS1, and d) qS2.

The material co-ordinates *x-y-z* do not necessarily align with the global coordinates *X-Y-Z* with the reflecting interface contained within the *X-Y* plane (Figure 4-2). The stiffness matrix $\boldsymbol{C}$ must be rotated into the global coordinate system providing $\boldsymbol{C}^{rot}$ [*Swokowski*, 1979]:

$$\boldsymbol{C}^{rot} = \boldsymbol{R}\,\boldsymbol{C}\,\boldsymbol{R}^{T} \tag{4-3}$$

where the transformations matrix $\boldsymbol{R}$ is calculated from the tilt cosine matrix:

$$\boldsymbol{r}_y = \begin{bmatrix} \cos\psi & 0 & sin\,\psi \\ 0 & 1 & 0 \\ -sin\psi & 0 & cos\psi \end{bmatrix} \tag{4-4}$$

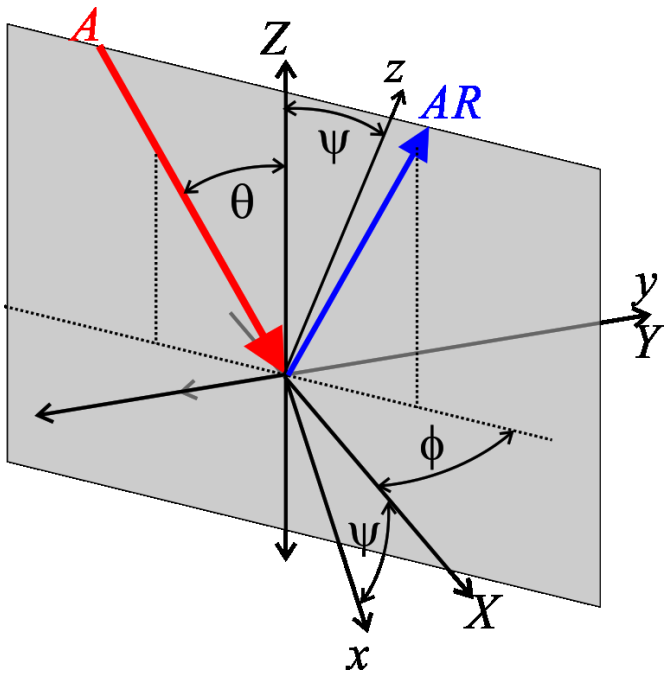

Figure 4.2. The relationship between material's coordinates x-y-z and experimental coordinates X-Y-Z with the reflecting plane coinciding with plane X-Y. The incoming plane wave of amplitude A is incident at angle θ with azimuth φ. For the specific geometry of the measurements, the Y and y-axes coincide around which the material tilt angle ψ is given.

4.2.2 *Reflectivity from Anisotropic Media*

An appropriate full solution to the reflectivity between two arbitrarily oriented anisotropic half-spaces is needed in order to properly compare the observations to theory. The complete plane-wave solution to this problem has been described earlier [e.g., *Henneke*, 1972; *Keith and Crampin*, 1977; *Rokhlin*, 1986] and for the most general case of two welded anisotropic half spaces there are in total 36 combinations of incident and converted transmission and reflection plane wave solutions

possible. The continuity of both displacements and stress across the welded interface, set the boundary conditions. *Knott* [1899] and *Zoeppritz* [1919] used the same boundary conditions to solve for two elastically isotropic half-spaces.

For the general anisotropic case, however, the boundary conditions are further complicated by additional scattered modes that must be considered, the problems of finding reflection and refraction angles, and the general misalignment between particle polarizations and propagation directions. The solution is described in Chapter 2. The open source algorithm ARTc provides the plane-wave reflectivities and transmissivities as functions of incidence θ and azimuth φ for all modes incident to the welded interface. This algorithm is employed here to model the observations. Conversely, the observations serve to test this algorithm's adequacy.

In the experiments, the uppermost medium is liquid water that admits only a pure longitudinal P-wave and only this single reflection is of concern for analysis of the data. For incident plane waves from the liquid layer there are four possible scattered plane waves: one is a reflected P-wave which travels back into the liquid, and three are transmitted into the solid as qP-, qS1-, and qS2-waves, this problem has been studied by numerous researchers [e.g., *Nayfeh*, 1989; *Descamps and Hosten*, 1991]. The solid material consists of blocks with differing tilts ψ for which the appropriately, rotated stiffnesses must be input. The pattern of plane-wave reflectivity P_{PP} from this water-solid interface is calculated for the complete set angles of incidence $0 \leq \theta \leq \pi/2$ and azimuth $0 \leq \varphi \leq 2\pi$ in terms of the reflected particle motion reflectivity R_{PP} and corresponding phase shifts Δ_{pp} (Figure 4-3). The compressional wave critical angle (θ_c) depends on both azimuth φ and tilt ψ and at this incidence R_{PP} (θ_c) = 1. Because the reflectivity is purely real before its critical angle, the phase shift (Δ_{pp}) is zeros however it only takes on nontrivial values past critical angle as the reflectivity becomes complex, [Knott, 1899; Aki and Richards, 1980]. R_{PP} also is independent of frequency where the elastic case assumed. The theoretical plane wave critical angle (θ_c) will become an important point of discussion later.

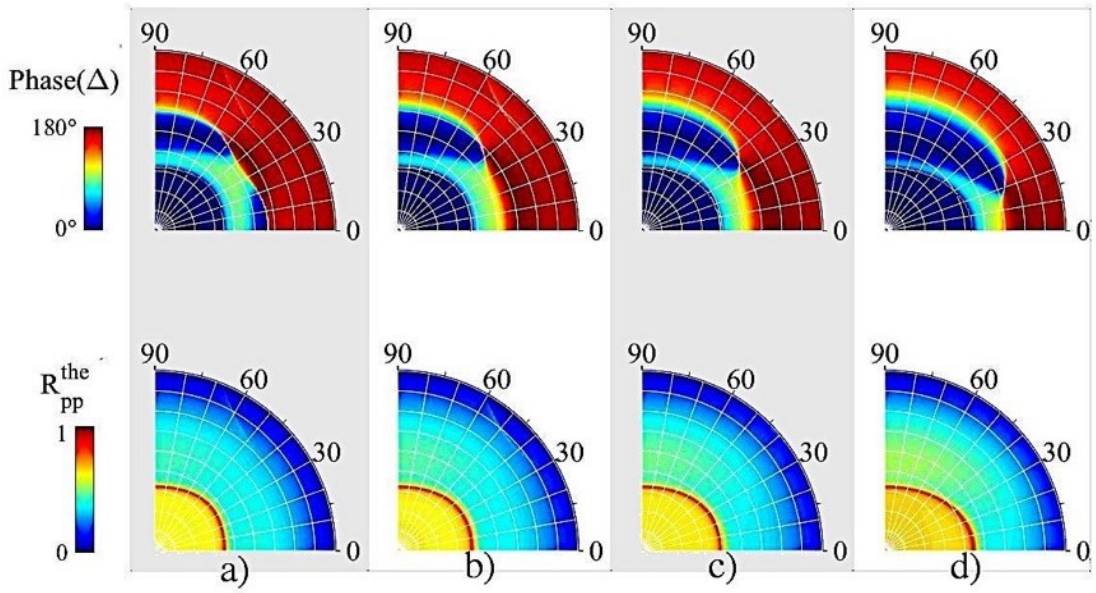

Figure 4.3. Calculated plane wave reflection phase shift $\Delta_{PP}(\theta,\varphi)$ (top) and amplitude $R_{PP}(\theta,\varphi)$ (bottom) for tilts ψ of a) 0°, b) 30°, c) 40°, and d) 90° shown on an equal angle polar projection down the Z axis with the X and Y axes aligned with 0° and 90° respectively. Only 1 quadrant need be shown due to rotational symmetry around Z-axis. The locus of P-P critical angles is traced in red where $R_{PP}(\theta,\varphi)$ near to 1.

4.2.3 *Theory of Bounded Pulse Propagation and Reflection*

It is important to stress that the experiment is carried out under real but not ideal plane wave conditions with a transmitter of finite size. In other words, it is impossible to fully observe the plane wave reflectivity of Figure 4-3, but these difficulties can be accounted for. The transmitter, even though much larger than normally employed in ultrasonic testing [see review in *Bouzidi and Schmitt*, 2006], provides a 'bounded pulse' that is limited both spatially and temporally. This has a number of implications for the pulse's spreading and reflectivity.

Bouzidi and Schmitt [2008a, 2008b] suggested that the pulse can essentially be considered as the summation of a distribution of plane waves of differing propagation directions and frequencies; this may alternatively be interpreted as a distribution of wave numbers. This means

that even though most of the energy of the pulse consists of plane waves propagating at the desired incidence θ it also must contain plane-waves with both larger and smaller incidences. All of these component plane waves are also reflected and transmitted as the bounded pulse strikes the interface. An unavoidable consequence is that some of the component plane waves will already be post-critical before the primary incidence θ. The phase of these post-critical components (Figure 4-3) is shifted upon reflection and at the observation point interfere causing in distortion of the observed waveform such that the amplitudes are modified so that what is actually observed will be here referred to as an observed effective reflectivity denoted $P_{PP}(\theta)$. Similarly, if θ is post-critical there are still components of the pulse that will be at the pre-critical incidence and P_{PP} still differs from R_{PP}.

Such effects have been long known in the acoustics community and produce a variety of unexpected behaviors. For example, past the shear wave critical angle the beam appears to be displaced relative to its expected specular reflection as first observed by *Schoch* [1950] and now referred to as the Schoch shift. *Declercq et al.* [2005] provided a relatively recent overview of the topic. In seismology, the similar problem of the effective reflection coefficients observed from a point source reappears periodically in the geophysical literature [see *Krail and Brysk*, 1983] for a survey up to that time) but these nontrivial effects are usually ignored in the analysis of seismic reflectivity. As will be shown shortly in comparisons between the theoretical plane wave R_{PP} and the observed P_{PP}, these effects are manifest here by smoothing of the observed reflectivity in the vicinity of and past θ_c.

A full description of how $P_{PP}(\theta)$ is quantitatively modeled including the algorithm developed is given by *Malehmir et al.* [2017] adapted after [*Bouzidi and Schmitt*, 2008b] for an anisotropic media with preferred anisotropic symmetry. Briefly, however, the algorithm models the propagation of the bounded pulse launched from the source to the interface and finally the receiver by phase advance for each of its component plane waves [*Gazdag*, 1978; *Claerbout*, 1985]. During the propagation, each component is modulated by its appropriate complex R_{PP}. Finally, the reflected wavefield is reconstructed and from this step, the time series of the pressure at the location of the receiver is extracted that we hereafter refer to as the modeled effective reflectivity M_{PP}. This is not, perhaps, the most elegant solution and it is computationally expensive as a large number of

wavenumbers must be used. This cost, however, is offset in that it allows us to make a fully quantitative calculation of the reflected response without any limiting assumptions or approximations [e.g., *Bertoni and Tamir*, 1973]. It must be pointed out that it requires knowledge of the experimental geometry as well as the spatial and temporal profile of the bounded pulse in order to calculate its propagation. The algorithm also relies on having knowledge of the complex plane wave reflection coefficients, $R_{PP}(\theta)$, as provided by the algorithm described earlier in Chapter 2, [*Malehmir and Schmitt*, 2016a].

4.3 Description of the Anisotropic Samples

In this research, custom made tiles cut from a large block of Phenolic CE of orthotropic anisotropic symmetry [e.g., *Brown et al.*, 1991; *Mah and Schmitt*, 2001] were used as the experimental samples. Figure 4-4 displays the zero tilt ($\psi = 0°$) experimental Phenolic block with enlarged microscopic pictures from different sections which show the composition of canvas fabric that glued with phenolic resin. We re-used the four rectangular blocks machined by *Ortiz-osornio and Schmitt* [2009] (5 cm thick by 12.5 cm) each with different tilt angles ψ denoted P^{T0} ($\psi = 0°$), P^{T30} ($\psi = 30°$), P^{T45} ($\psi = 45°$), and P^{T90} ($\psi = 90°$) as shown in Figure 4-5. There have only been a limited number of similar studies that have attempted to quantitatively measure the reflectivity from tilted composites [e.g., *Descamps and Hosten*, 1991; *Rokhlin and Wang*, 1992; *Innanen and Mahmoudian*, 2015] but to our knowledge, no studies have examined tilts other than *0°* or *90°*. A thin layer of water-resistant lacquer was sprayed to seal the samples against water damage.

Figure 4.4. The texture of CE canvas fabric phenolic laminate with views along a) x-axis displaying warp and layering, b) y-axis displaying layering and weft, and c) z-axis displaying warp and weft. Arrows in each panel are 2 cm in length. d) Block of zero tilted ($\psi = 0°$) Phenolic sample that is 5 cm * 12.5 cm * 12.5 cm.

The measured mass density of the sample is 1393 kg/m^3, and *Mah and Schmitt* [2001] reported that the thickness of the fabric and resin are about 0.4mm and 1-2.5mm, respectively. The latest revision of the stiffness tensor that we measured for the phenolic sample which has been immersed in water is calculated and given:

$$C = \begin{bmatrix} 16.9 & 7.18 & 6.80 & 0 & 0 & 0 \\ 7.18 & 19.5 & 6.94 & 0 & 0 & 0 \\ 6.80 & 6.94 & 11.1 & 0 & 0 & 0 \\ 0 & 0 & 0 & 3.47 & 0 & 0 \\ 0 & 0 & 0 & 0 & 3.12 & 0 \\ 0 & 0 & 0 & 0 & 0 & 3.84 \end{bmatrix} GPa \qquad (4\text{-}5)$$

which the arrangement of elastic modules indicates that the samples possess orthotropic anisotropic symmetry, [Musgrave, 1970].

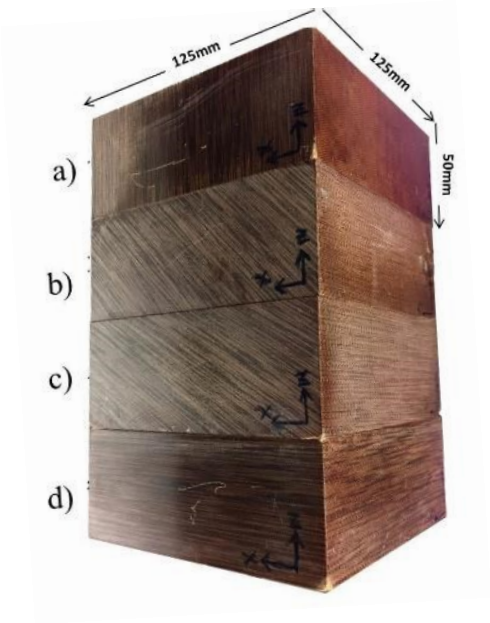

Figure 4.5. Side view of the four Phenolic CE blocks stacked on top of each other for purposes of comparison of the various tilts that were used in the laboratory reflectivity measurements with a) ψ= 90° b) ψ=30°, c) ψ=45° and d) ψ=0°.

4.4 Experimental Setup

The acoustic goniometer technique which we employed here has long been employed in the acoustics community for fundamental studies of reflectivity and transmissivity, although focus mostly on reflections from thin plates [e.g., *Plona*, 1976; *Declercq*, 2006] and determination of elastic properties [e.g., *Mann et al.*, 1980]. The measurements here employ the acoustic goniometer described by *Bouzidi and Schmitt* [2006] and developed initially to quantitatively test theories related to the reflectivity of a liquid-saturated porous material, [*Bouzidi and Schmitt*, 2012]. This apparatus was further modified by incorporating a horizontal rotating stage [*Ortiz-osornio and Schmitt*, 2010b] that allows the blocks to be rotated around the Z-axis providing ready access to the complete range of azimuths $0 \leq \varphi \leq 2\pi$. The transmitter and receiver are mounted within the vertical circular rim, perpendicular to the rotating stage, and aligned with the receiver along the

expected specular travel path at the incident angle (θ) originating from the center of the transmitter (Figure 4-6b). The source- receiver distance is 21.3cm remains unchanged throughout the experiment.

The goniometer is immersed in a deionized water bath, and the measurements are carried out at standard pressure and the room temperature of 22°C.

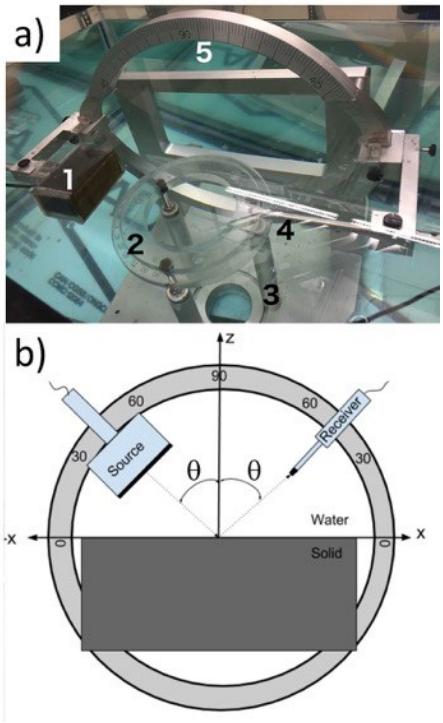

Figure 4.6. a) Photograph of the acoustic goniometer showing (1) the transmitter, (2) the rotating stage, (3) the adjusting pillars, (4) the receiver and vertical goniometer, b) side view schematic of the laboratory setup.

The system is further novel in that it employs a large transmitter (50 mm × 60 mm) but only a small receiver (2 mm×2 mm). There are a number of reasons for configuration. First, the larger transmitter produces a strong bounded pulse whose wavefront remains substantially planar, as seen in Figure 4-7c, over the length of the travel paths of the experiment. Second, the small transducer acts as a near point receiver. This combination significantly reduces the complicating corrections

necessary for proper quantitative analysis of the most usual configuration that uses two transducers with the same dimensions for the transmitter and receiver [e.g., *Alhussain et al.*, 2008; *Mahmoudian et al.*, 2014]. We note that the transmitter employed here is smaller than that used in *Ortiz-osornio and Schmitt* [2009, 2010a] initial studies allowing waveforms to be acquired here over a larger range of incidence angles. On each of the four samples with differing tilts we collected the reflected amplitudes in the four azimuthal directions of $\varphi = 0°$, 30°, 60°, and 90° over the range of incidence angles from 15° to 60° at increments of 0.25°; this produced 181 individual ultrasonic traces at each azimuth.

The transmitter was activated by a voltage spike of 2.8 Volts repeated at 100 Hz. The resulting voltages produced by the receiver were sampled with a rate of 40 *n*s/sample for a total of 2500 samples (i.e. 100 μs). Examples of records obtained directly from the transmitter to the receiver during calibration and upon reflection (Figure 4-7 a,b) show the loss of amplitude due to reflection. The shapes of amplitude spectra of the two records also do not change upon reflection, the peak frequency of 0.70 MHz is close to the resonant thickness frequency of the piezoelectric ceramic sheet that comprises the transmitter's central element. The apparent reflectivities P_{PP} reported later are the ratio of the peak values of the amplitude envelopes as calculated using the Hilbert transform between the reflected and the direct (i.e. non-reflected) waveforms.

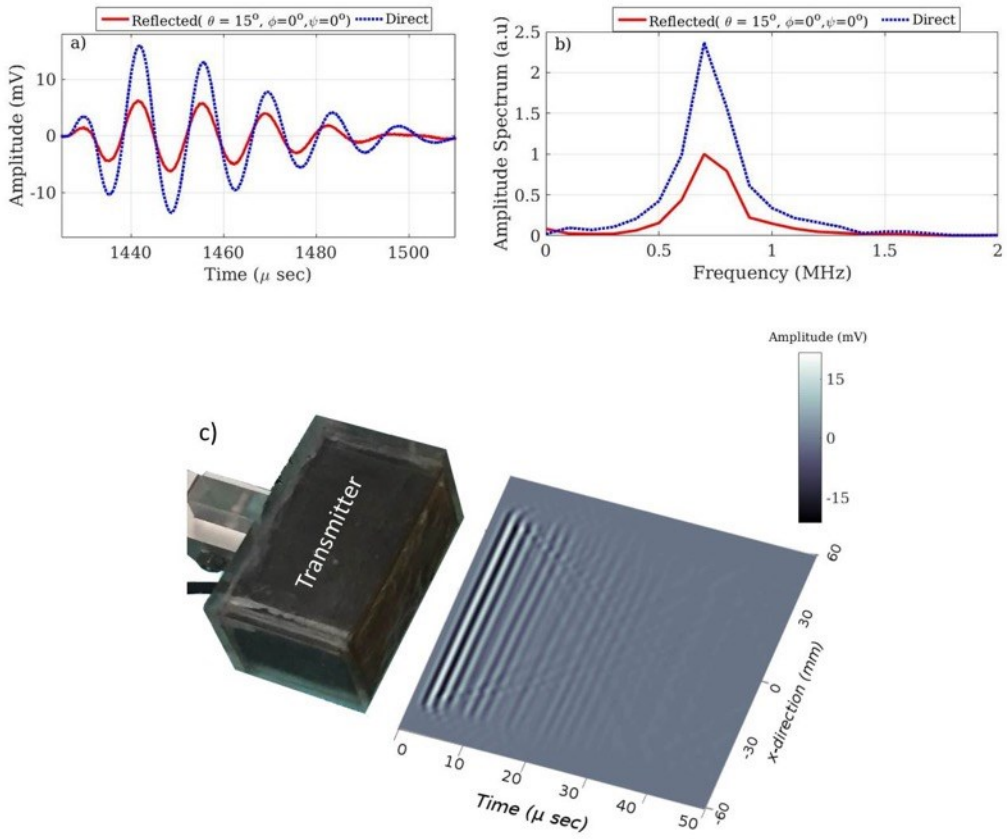

Figure 4.7. a) Comparison of direct and reflected (P^{T0} at θ = 15° and φ = 0°) waveform records in the time domain with the Hilbert amplitude envelope of the reflected waveform is shown b) Corresponding amplitude spectrum for the records in a. c) Scanned profile of the launched bounded pulse as recorded at 20 mm from the transmitter face. The aperture of the transmitter is shown. High-frequency noise generated when the transmitter is activated is muted for the first 100 ns.

The wavelengths of the insonifying sound waves must be considered. As we expect the wave speed in the water to be close to 1483 m/s under the laboratory conditions then predominant wavelengths in the water will be ~ 2 mm. This is important as it means that the ratio between the scales of the wavelengths to the layering (~ 0.4 mm) (Figure 4-3) is well above two; this indicates that for purposes of these measurements the phenolic acts as an effective medium [*Liu and Schmitt*, 2006].

As indicated above, the modeling requires that the actually bounded pulse launched towards the sample be obtained. This is accomplished by scanning the receiver across the width of the transmitter with the results (Figure 4-7c) illustrating the mostly planar wavefront. The end diffractions show the departure of the bounded pulse from a plane wave.

4.5 Results and Discussion

As noted, the raw data set consists of 16 individual suites each of 181 ultrasonic waveforms obtained at four azimuths (φ) on each of the four blocks of different tilts (ψ). The raw data together with the corresponding values of the theoretical and observed reflectivities are publicly available [*Malehmir and Schmitt*, 2016b][1].

4.5.1 *Observed vs Theoretical Plane Wave Reflectivity*

A suite of raw waveform records (Figure 4-8a) and their corresponding Hilbert amplitude envelopes (Figure 4-8b) collected over the range $15° \leq \theta \leq 60°$ highlight the variation in both amplitude and phase of the reflected waveform that causes an apparent time shift [see *Bouzidi and Schmitt*, 2008a, 2008b]. Already at about 55° directly arriving diffractions from the edge of the transmitter begin to interfere with and contaminate the reflections.

The apparent reflectivities P_{PP} are obtained from the peak amplitude of each record in Figure 4-8b and compared to the theoretical plane wave R_{PP} (Figure 4-8c) calculated using the procedures described earlier. R_{PP} predicts P_{PP} to better than 92% over the incidence ranges of 15° to 24° but the two diverge past this point with P_{PP} initially increasing and reaching a peak at θ_E = 27.2°± 0.25°. As expected the calculated R_{PP} reaches a peak value of 1 at the plane wave critical angle θ_c = 28.73°. The difference in the two peaks was unexpected, and it further emphasizes that great care must be taken in trying to interpret amplitude peaks observed in real data as being at the

critical angle. The discrepancy continues to larger angles of incidence indicating that plane wave calculations cannot adequately describe the observed reflectivity at shallower angles of incidence.

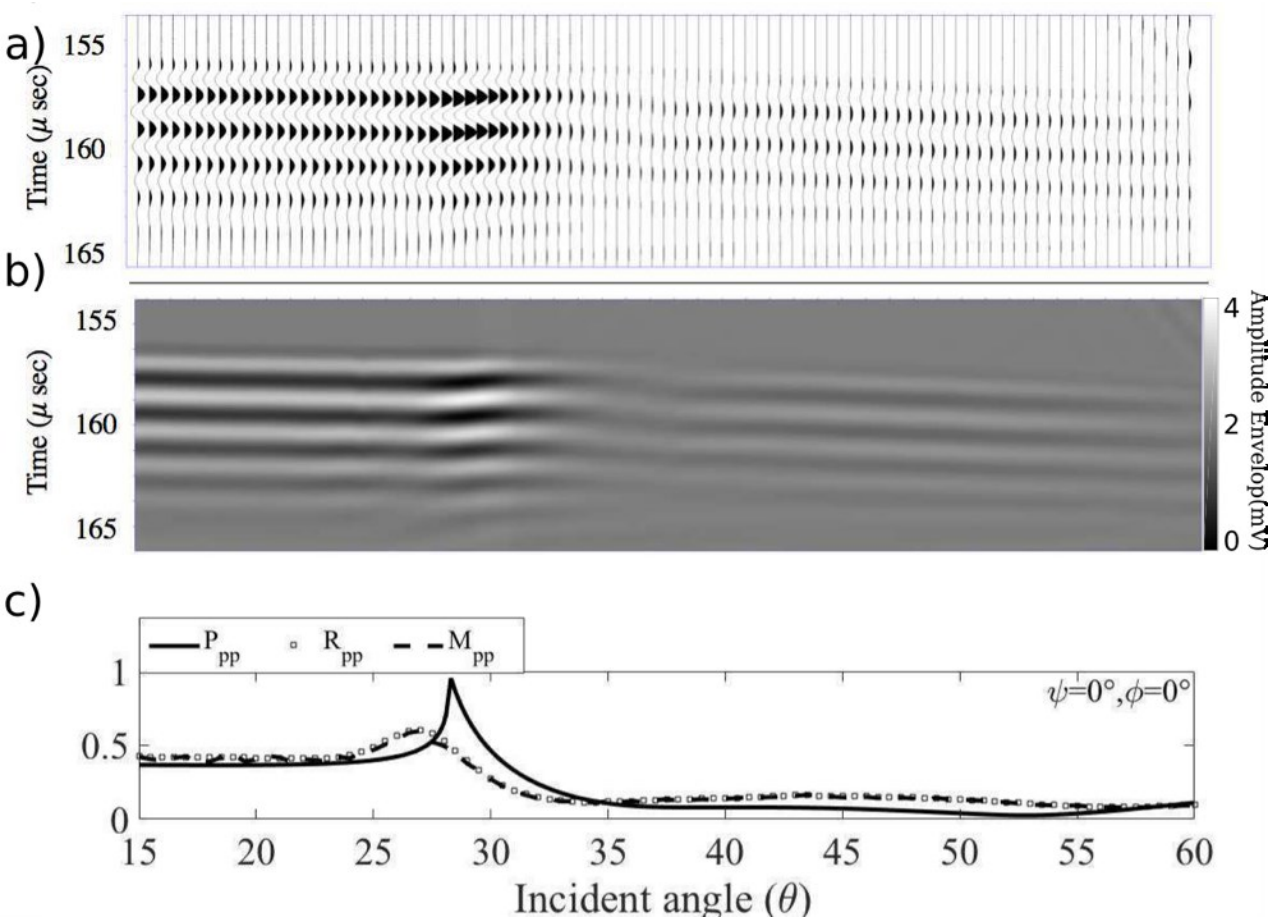

Figure 4.8. Reflected waveforms obtained from block P^{T0} at φ = 0° over a range of incident angles from 15° to 60° displayed as a) directly recorded voltage time series and b) corresponding color representation of the normalized reflected waveform. About incident angle of 60° interferences from direct arrival is observed and are excluded from the amplitude analysis. Displayed waveforms records are windowed to isolate the pulse c) comparison of observed effective reflectivity waveform amplitudes of amplitude envelope against calculated plane wave reflectivity R_{PP} and with the modeled effective reflectivity M_{PP}.

The entire set of collected reflection coefficients (Figure 4-8) from 16 suites of $P_{PP}(\theta,\varphi)$ displays the strong influence of both azimuth φ and material tilt ψ and confirm the earlier observations by *Ortiz-osornio and Schmitt* [2009, 2010a] with the variations due to the differing experimental configurations kept in mind. The corresponding theoretical plane wave $R_{PP}(\theta, \varphi)$ are also given for the sake of comparison. A number of observations can be made: Following the example of Figure 4-8c, R_{PP} agrees well with P_{PP} for steep incidences (small θ) but the two diverge well before the critical angle θ_c. R_{PP} does appear to predict P_{PP} for cases at post critical angles but this is not true in general and at $\psi = 0°$ they do not match. The maxima of the $P_{PP}(\theta, \varphi)$ does follow the order of the expected from the critical angles seen for $R_{PP}(\theta, \varphi)$.

It is clear from Figure 4-9 that the value of the critical angle changes with tilt and azimuth. The variation with azimuth becomes increasingly larger with tilt ψ. According to Snell's law, shifting of such maxima with the angle of incidence indicates significant change of the impedance contrast. As the incidence medium in our measurements is always the same water, therefore variations in the critical angle indicate velocity variations in the anisotropic sample. Consequently, the larger the critical angle, the slower the refracted propagation velocity of the sample. For the different reflectivity curves we observe that, as anticipated, those of the zero tilted sample (as seen in Figure 4-9) remain nearly the same for the different azimuths, which confirms the conclusion that Phenolic CE is weakly orthorhombic.

At a tilt of $\psi = 30°$ the reflectivity displays a greater dependence on the azimuth although the largest variations are in the post-critical amplitudes, there is also some amplitude variation just before the critical angle. In this case, θ_c (critical incident angle) spreads between 28° and 32.5° and it increases as we increase φ. A similar set of features can be observed for phenolic sample $\psi = 45°$ (Figure 4-9c), but now the spreading zone for θ_c goes from 28° to 32.5°, also the transition from pre-critical to post-critical reflections is smoother, and amplitude variation is larger and more prominent in the post-critical zone. Finally sample $\psi = 90°$ showed, as it was expected, the largest azimuthal variation of the reflectivity (Figure 4-9d), the spreading zone of θ_c is increased to more than 10° as it spreads from 27.75° to 39.25°, and the error between θ_c and the peak P_{PP} is small at larger azimuths and impressively increases as we decrease the azimuth. This data set also shows the largest variation of the amplitude at post-critical reflections. Furthermore, the incident angle of

the critical longitudinal reflection from the interface decreases with azimuthal direction. This means that the velocity of the samples increases with the azimuthal direction of the measurement, which is in agreement with Figure 4-3. For a given tilt ψ there is not a strong variation in $P_{PP}(\theta,\varphi)$ ($\approx R_{PP}(\theta,\varphi)$) with θ or φ at steep angles of incidence.

4.5.2 *Bounded Pulse Modelling of Observed Reflectivity*

The last section demonstrated that the theoretical plane wave reflectivity R_{PP} only predicts that observed P_{PP} at small angles of incidence well before the critical angle. At face value, this could be interpreted as an error in the calculation of R_{PP}, an experimental deficiency while obtaining P_{PP}, or even a failure of both. In this section, we demonstrate that both the experimental observations and the algorithm used to calculate the plane wave reflectivity are valid. This is accomplished by directly modeling the reflected wave field of the reflected bounded pulse as described earlier in order to obtain the modeled effective reflectivity $M_{PP}(\theta, \varphi)$ and contrasting it with the observed $P_{PP}(\theta, \varphi)$.

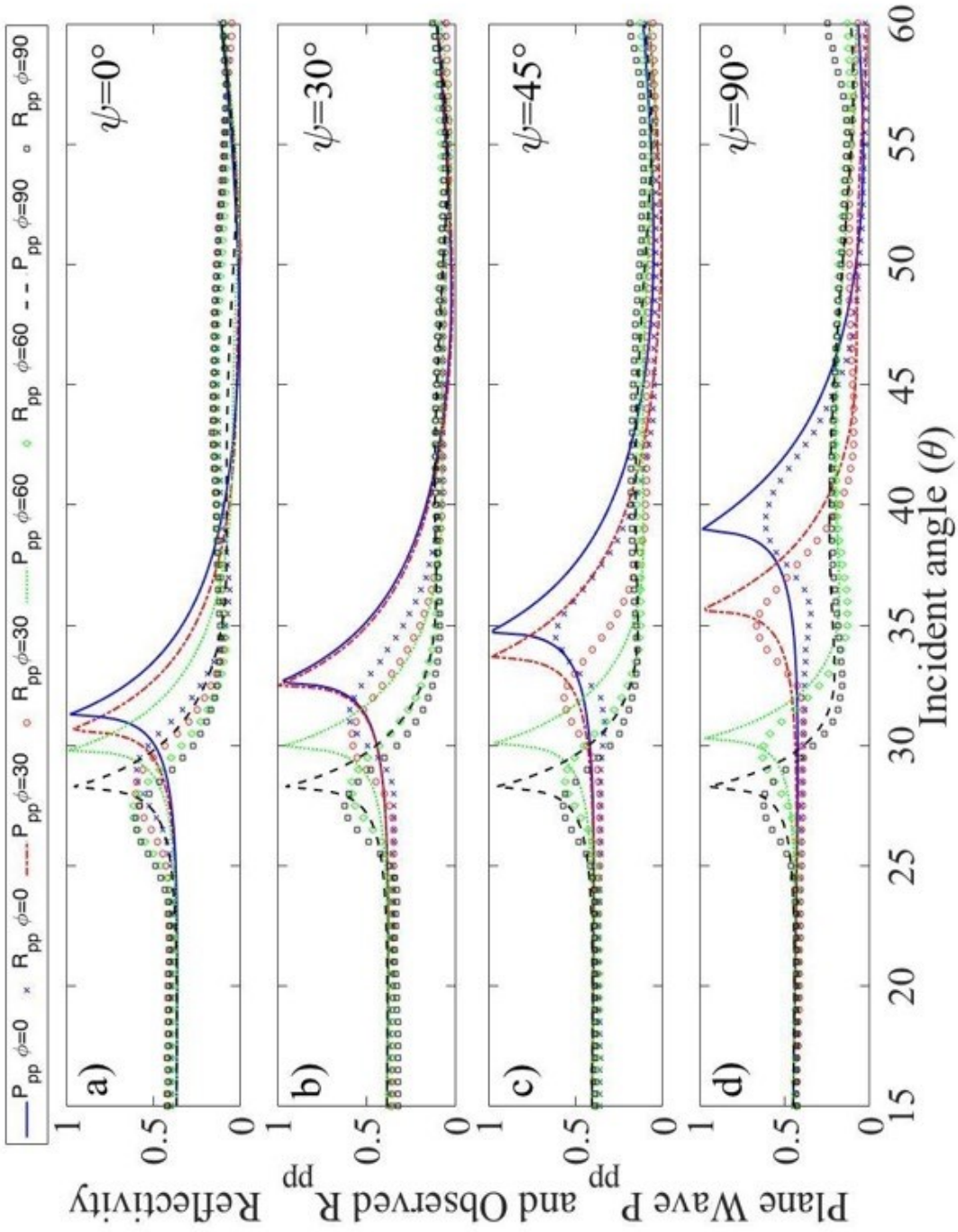

Figure 4.9. Complete set of observed apparent reflectivities P_{PP} compared with the corresponding calculated plane wave reflectivities M_{PP} for tilts a) 0°, b) 30°, c) 45°, and d) 90°.

The observed and modeled (Figure 4-10) responses from block ψ = 30° at azimuth φ are difficult to distinguish from one another. The corresponding observed $P_{PP}(\theta)$ and modeled $M_{PP}(\theta)$ apparent reflectivities (Figure 4-8c) agree well differing from each other by at most 4.75% (Figure 4-7d). This good comparison extends to the entire data set (Figure 4-10).

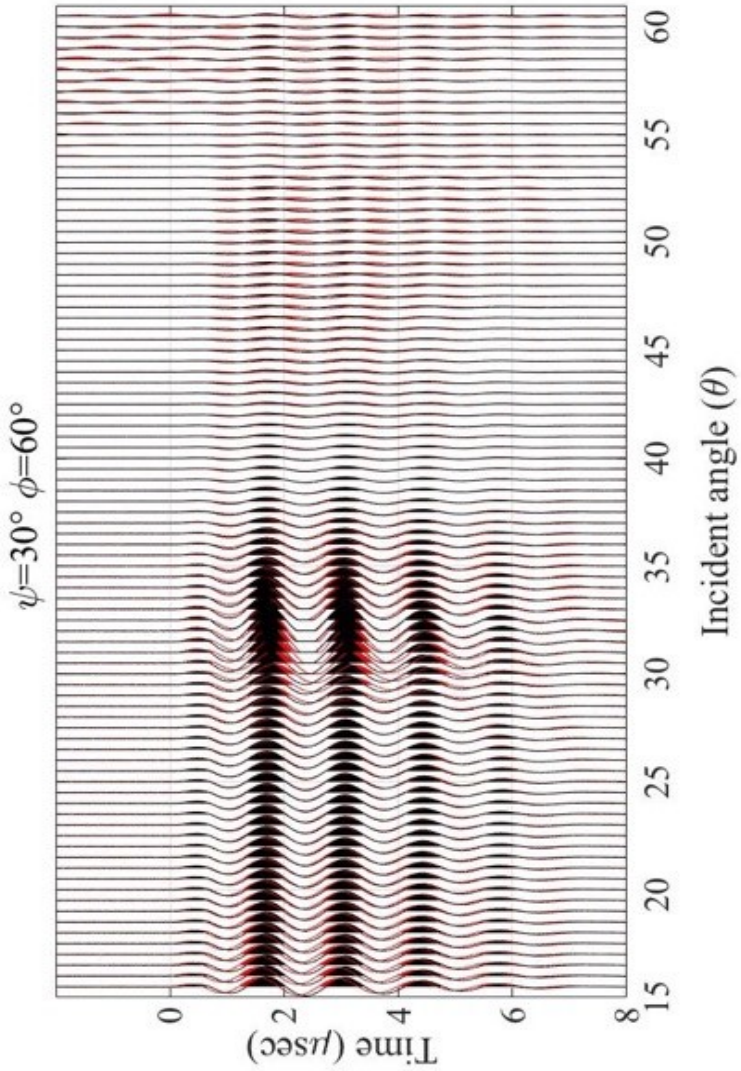

Figure 4.10. Wiggle trace representation of observed (black wiggle) and modeled (red wiggle) waveforms from the water-phenolic TI30° sample in the azimuthal direction of 60°.

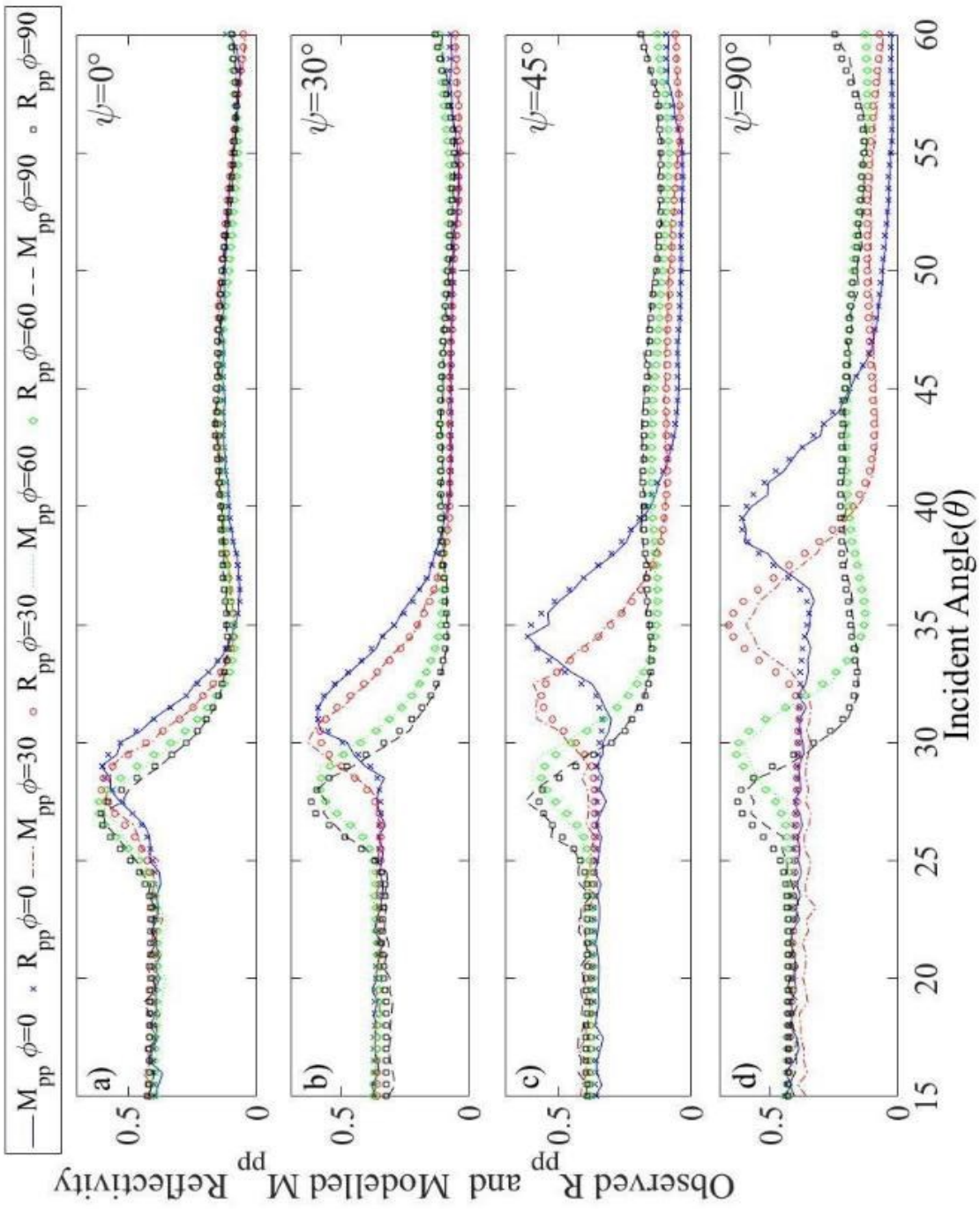

Figure 4.11. Complete set of observed apparent reflectivities R_{PP} compared with corresponding bounded pulse modeled M_{PP} reflectivities for tilts a) 0°, b) 30°, c) 45°, and d) 90°.

The results summarized in Figure 4-11 are significant for two reasons. First and more pragmatically, they show that the methodologies established earlier by *Bouzidi and Schmitt* [2008b] for modeling of the reflections of bounded pulses can be applied to the case of reflectivity from an anisotropic medium. For more details about bounded pulse modeling, see [*Malehmir et al*, 2017]. Second and more fundamentally, however, they demonstrate that the forward calculation of the complex R_{PP} is accurate and as such provides experimental evidence that the solution to this problem is valid. This is comforting as we have largely accepted such solutions to be legitimate without empirical proof.

4.6 Implications for Seismological Investigations

AVAz investigations seek to find the directions of anisotropy that in turn could be interpreted in terms of orientations of metamorphic texture, fractures or stress. The present laboratory tests, even though having a geometry is not exactly that one would expect when recording seismic reflections in the earth, do provide some insight into field experiments.

4.6.1 Insensitivity of Reflectivity to Azimuth

One, perhaps unexpected, observation is that for a given tilt there the theoretical plane wave reflectivity R_{PP} does not depend strongly on the azimuth φ. This occurs despite the large azimuthal variations in acoustic wave speed that one can encounter around the *X*-*Y* plane even for the most extreme case with the tilt of 90° and similar results are observed by *Alhussain et al.* [2007] in numerical models of HTI reflectivity. In a field situation, these relatively small azimuthal variations make properly detecting such variations challenging given a noisy environment and the additional corrections that must be applied to such data. The changes in the observed effective reflectivity R_{PP} with φ are also not large but do vary significantly more, and this would allow for more robust inversions of the data. The ostensible success of real AVAz operations may rely more on this effect if it also applies to real wavefields produced by surface point sources.

4.6.2 *Exploiting the Critical Angle*

The azimuthal variations in the critical angles and correspondingly the peak values for the observed $R_{PP}(\theta,\varphi)$ are the most distinctive feature of these data (Figure 4-11). As such, these variations must contain important information. To review, for isotropic materials the critical angle is well understood to be the incidence at which the plane wave is refracted horizontally along the interface with a refraction angle of 90° and is simply obtained using Snell's law:

$$\theta_c = sin^{-1}(\frac{v_i}{v_r}), \tag{4-7}$$

where v_i and v_r are the compressional wave speeds in half-spaces of incidence and refraction, respectively. Determinations of θ_c by reflection have long been employed in the acoustics community as a means to obtain the wave speeds in isotropic materials [*Ngoc and Mayer*, 1979]. They attributed the blunting of observed R_{PP} in the vicinity of the θ_c to non-specular reflection and were successfully able to model it using a numerical procedure. *Henneke and Jones* [1976] tested this concept and confirmed that his observed θ_c could be used to find the refracted wave speed. More recently, in a series of tests on blocks of well characterized isotropic solids, *Bouzidi and Schmitt* [2008a] too found a very small discrepancy between the peak of their observed effective reflectivities P_{PP} and the θ_c predicted applying Eq.4-7, with the known water and the material wave speeds. Critically, their $R_{PP}(\theta)$ curves were rounded in the vicinity of θ_c similarly to those observed here (Figure 4-11) but the peak of these curves aligned with θ_c. The $P_{PP}(\theta)$ were also well reproduced by the calculated $M_{PP}(\theta)$ establishing the robustness of the modeling procedures also employed here.

However, to understand the critical reflection in anisotropic media, we refer to [*Henneke*, 1972; *Henneke and Jones*, 1976], who pointed out that more generally θ_c occurs not when $\theta_r = 90°$ for the phase velocity along the interface, but for the phase velocity whose corresponding energy-flux follows the interface. Consequently, for this anisotropic case, one cannot simply use observed critical angle (θ_E) and Eq. 4-7, to determine the phase speed parallel to the interface. This difference between θ_E and θ_c may be another example of phenomena arising because of the differences between the group and phase speeds in anisotropic materials. For the anisotropic case, it cannot be found without prior knowledge of the material's stiffnesses thus negating the utility of using θ_c to find v_r. This concern together with our observations that $\theta_E \neq \theta_c$ suggests that attempting to

determine in-situ elastic constants on the basis of observed critical angles would require extreme caution. *Alhussain et al.* [2008] and *Innanen and Mahmoudian* [2015] also reported the difference between θ_E and θ_c from an anisotropic layer, by using identical round transducers for source and receiver.

Another important factor that we need to consider in the analysis of θ_E, is the effect that size of the source has on the observed reflected amplitudes. As discussed before, the small size source may not satisfy plane-wave propagation, in the pre-critical reflection, near θ_c the signal that is generated from the sides of the transducer (Figure 4-7c), are critically reflected, while the wavenumbers from the center of the beam are in pre-critical condition. Also, when the wavenumbers from the center of the source are inciting the boundary at the critical angle, the others are in post-critical angle.

Nevertheless, we are able to model the observed reflectivity data (Figure 4-10 and 4-11) by using the combination of full waveform propagation of the pulse (Figure 4-6c) and then producing the reflected beam by combining the individually calculated reflection of each wavenumber. This technique is computationally expensive and requires a detailed understanding of the elasticity of the medium, geometry of the acquisition and properties of the source signal as discussed earlier.

4.6.3 *Qualitative Analogies to Fractured Formations*

One of the most important implications of studying the reflectivity from these anisotropic blocks is to provide a laboratory analog for field studies of seismic reflectivity from fractured formations. Orthogonal sets of fractures in the layered medium are considered to produce an elastic anisotropic medium with orthotropic symmetry, and in the case of non-orthogonal fracture sets, would create a lower symmetric elastic anisotropic medium, where the fracture spacing and layering thickness are bigger than the elastic wavelength.

Obtaining knowledge of the tilt (or dipping angle) and azimuth of fracture sets in the earth is important in many fields. Having prior information on fractures orientations in hydrocarbon or geothermal systems would allow us to efficiently produce oil, gas or steam. In the present reflectivity data set, with having the access to four tilting angles and long offset coverage of reflectivity, one can use the critical reflectivity data and find their associated velocities and map out the faster and slower direction for which the wave propagates in the phenolic sample.

Considering that elastic waves propagate faster along the direction of fractures, is a great attribute to find the azimuthal orientation of a fracture.

First, we recorded the observed critical angle from Figure 4-9, and created Table 4-1. Simply by rearranging the Eq.6, we calculate the apparent refracted velocity traveling horizontally through the phenolic medium at the critical angle of qP wave reflection, [*Skopintseva and Alkhalifah*, 2013]. Figure 4-12, displays the calculated apparent horizontal velocity variation with azimuth and tilt from the critical angle of R_{PP} and P_{PP} in Table 4-1.

Table 4-1.Observed apparent critical angle (angle of peak amplitude in observed reflectivity profiles) of the qP-wave reflection from water-Phenolic CE sample in different azimuth (φ) and tilt (ψ) direction.

	ψ = 0°	**ψ = 30°**	**ψ = 45°**	**ψ = 90°**
φ = 0°	29.0 ± 0.25°	31.5 ± 0.25°	35.0 ± 0.25°	39.5 ± 0.25°
φ = 30°	28.5 ± 0.25°	30.5 ± 0.25°	32.0 ± 0.25°	35.0 ± 0.25°
φ = 60°	27.5 ± 0.25°	28.5 ± 0.25°	29.0 ± 0.25°	30.0 ± 0.25°
φ = 90°	27.5 ± 0.25°	28 .0± 0.25°	28.0 ± 0.25°	28.0 ± 0.25°

Evidently, the direction which qP-wave travels faster in the anisotropic medium, at all tilt angles is at $\varphi = 90°$, that matches with the micro-layering (or fractures) direction of the phenolic samples. We observe a significant azimuthal velocity variation at $\psi = 90°$, of 26.3% compared to the 4.63% at $\psi = 0°$. This substantial difference between the velocity variations implies that within the same medium, the 90° tilt shows strongest velocity and amplitude variation with azimuth (*VVAz* and *AVAz*), hence has a better application to understand the orientation of anisotropic features, compared to tilt 0°.

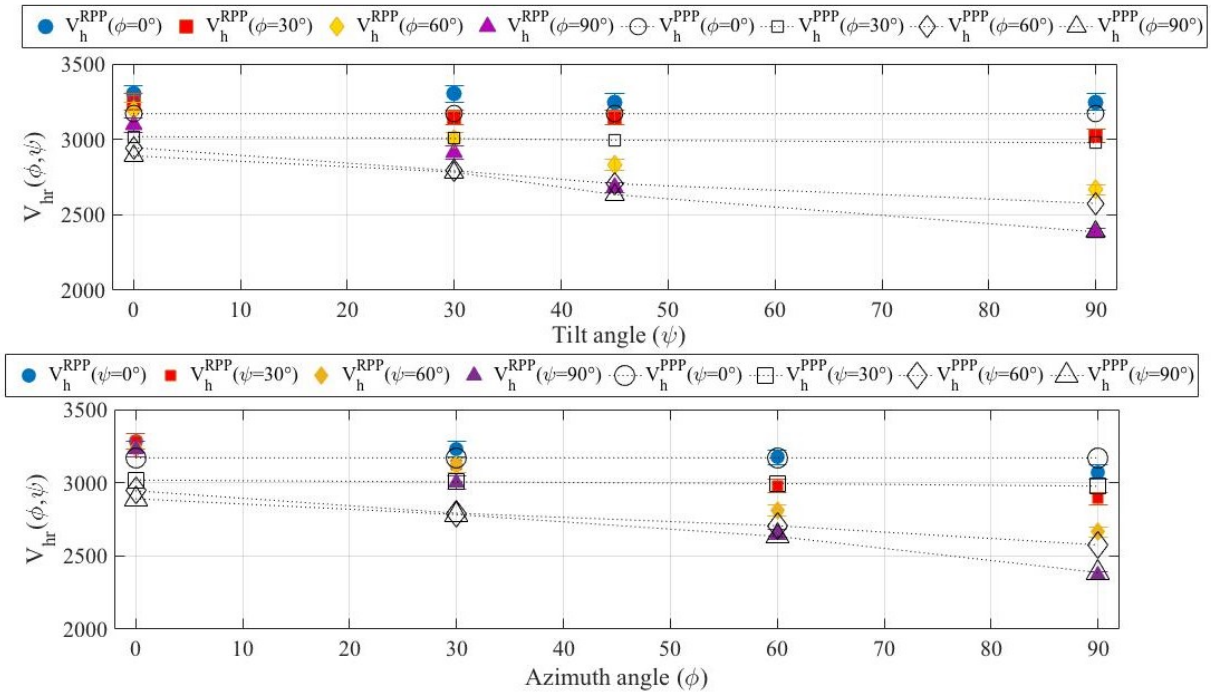

Figure 4.12. Displays the apparent horizontal phase velocity (V_{hr}) in the Phenolic sample variation with a) tilt (ψ) and b) azimuth (φ), which are calculated from the critical angle of the observed reflectivity (R_{PP}) and plane-wave solution ($\boldsymbol{P}_{PP}$) reflectivity. It is clear that the direction of which qP-wave travels quickest is along the azimuth of $\varphi = 0°$ and slowest in azimuth $\varphi = 90°$. Also we observe the biggest variation in apparent velocity at $\psi = 90°$, at around 26.3%, compared to the 4.63% at $\psi = 0°$.

Unfortunately, in most wide azimuthally acquired seismic reflection data, we are unable to collect or locate critical reflection, due to acquisition geometry or poor signal–to-noise ratio at the far offset. Furthermore, if in such a rare condition, we would be able to collect seismic data from post-critical reflection, we can only find the azimuth of the fast and slow direction, which it would not be sufficient to find the tilt angle of a fractured medium (known as dipping angle). Because, naturally, we can only collect seismic data from the subsurface medium, from a single tilt angle. However, as explained in the previous section, quantitative calculation of the elastic coefficients

of the anisotropic media, from the calculated apparent phase velocity, requires further detailed study.

4.7 Conclusion

, We observed and modeled as functions of the angles of incidence and azimuth the acoustic reflectivity from the interface between water and orthotropic composite material samples at four different tilt angles. These ultrasonic reflectivities display complex patterns first observed, but not fully explained, by *Ortiz-osornio and Schmitt* [2009, 2010a].

The only difference between the four blocks was the tilt of the composite layering with respect to their surfaces. Nevertheless, the observed angle-of-incidence dependent reflecitivities collected along constant azimuth angle profiles display variations in amplitude and, most noticeably, large shifts in their maximum value. The observed reflectivities could not be described by a previously developed plane-wave solution alone. However, this solution when employed together with a model that accounts for the full geometry and character of the bounded ultrasonic pulses along their reflection propagation path. This convergence of theory and observation validates the general anisotropic reflectivity algorithm developed earlier in Chapter 2. This algorithm should be useful to real field seismic studies that consider azimuthal and incidence angle amplitudes, often referred to as *AVAz* in the literature, providing complementary solutions the structurally limited approximations used in common practice.

The results of the laboratory measurements may also highlight some difficulties inherent to field studies that are intended to provide quantitative information on in situ fracture networks. For one, at small angles of incidence well before the critical angle, the variations with azimuth while measurable are not large. This suggests that properly extracting azimuthal variations in noisy field data needs to be carried out carefully. On top of this, it may be difficult to extract any information about the tilt of fracture sets from the observed seismic responses even with a complete set of data at all azimuths and incidences. Additional geological knowledge about in situ fractures and rock anisotropy should be included in order to avoid overinterpretation of the data. Too, workers should take care when associating the peak value of reflectivity observed in real field data directly to the critical angle obtained from plane wave solutions.

Despite these caveats, however, qualitative observations of the apparent critical angles from field data do align along projections to the surface of the material's principal symmetry directions; that is one can infer slow and fast directions. This information is insufficient to determine the dips of fracture sets of geological layers but one can in principal infer dip azimuth. This alone can be of substantial value towards understanding subsurface structures.

References

Aki, K., and P. G. Richards (1980), *Quantitative seismology: Theory and methods, v.1*, W.H. Freeman and Co, San Francisco.

Aleardi, M., and A. Mazzotti (2014), A feasibility study on the expected seismic AVA signatures of deep fractured geothermal reservoirs in an intrusive basement, *J. Geophys. Eng.*, *11*(6), 65008, doi:10.1088/1742-2132/11/6/065008.

Alhussain, M. (2007), Spherical Wave AVO Response of Isotropic and Anisotropic Media : Laboratory Experiment versus Numerical Simulations Mohammed Abdullah K Alhussain, University of Curtin.

Alhussain, M., E. Liu, B. Gurevich, M. Urosevic, and S. U. Rehman (2007), AVOaz response of a fractured medium: Laboratory measurements versus numerical simulations, *SEG Tech. Progr. Expand. Abstr.*, *26*(1), 254–258, doi:10.1190/1.2792421.

Alhussain, M., B. Gurevich, and M. Urosevic (2008), Experimental verification of spherical-wave effect on the AVO response and implications for three-term inversion, *Geophysics*, *73*(2), C7–C12, doi:10.1190/1.2837641.

Almqvist, B. S. G., L. Burlini, D. Mainprice, and A. M. Hirt (2010), Elastic properties of anisotropic synthetic calcite-muscovite aggregates, *J. Geophys. Res. Solid Earth*, *115*(8), 1–15, doi:10.1029/2009JB006523.

Arts, R., P. Rasolofosaon, and B. Zinszner (1991), Complete inversion of the anisotropic elastic tensor in rocks: Experiment versus theory, *1991 SEG Annu. Meet.*, 1538–1541.

Auld, B. A. (1973), *Acoustic fields and waves in solids- Vol 2*, John Wiley & Sons, Inc.

Backus, G. E. (1962), Long-wave elastic anisotropy produced by horizontal layering, *J. Geophys. Res.*, *67*(11), 4427, doi:10.1029/JZ067i011p04427.

Backus, G. E. (1965), Possible forms of seismic anisotropy of the uppermost mantle under oceans, *J. Geophys. Res.*, *70*(14), 3429, doi:10.1029/JZ070i014p03429.

Bakulin, A., V. Grechka, and I. Tsvankin (2000), Estimation of fracture parameters from reflection seismic data—Part II: Fractured models with orthorhombic symmetry, *Geophysics*, *65*(6).

Bao, X., D. W. Eaton, and Y. J. Gu (2016), Rayleigh-wave azimuthally anisotropic phase-velocity maps beneath western Canada, *J. Geophys. Res. Solid Earth*, n/a-n/a, doi:10.1002/2015JB012453.

Bass, J. D. (1995), Elasticity of minerals, glasses, and melts, in *Mineral Physics and Crystallography: A Handbook*, pp. 45–63.

Behura, J., and I. Tsvankin (2006), Small-angle AVO response of PS-waves in tilted transversely isotropic media, *Geophysics*, *71*(5), C69, doi:10.1190/1.2329865.

Behura, J., and I. Tsvankin (2009), Reflection coefficients in attenuative anisotropic media, *Geophysics*, *74*(5), WB193, doi:10.1190/1.3142874.

Belonoshko, A. B., N. V Skorodumova, A. Rosengren, and B. Johansson (2008), Elastic anisotropy of Earth's inner core., *Science*, *319*(5864), 797–800, doi:10.1126/science.1150302.

Ben-Menahem, A., and A. G. Sena (1990), Seismic source theory in stratified anisotropic media, *J. Geophys. Res.*, *95*(B10), 15395, doi:10.1029/JB095iB10p15395.

Bertoni, H. L., and T. Tamir (1973), Unified theory of Rayleigh-angle phenomena for acoustic beams at liquid-solid interfaces, *Appl. Phys.*, *2*(4), 157–172, doi:10.1007/BF00884205.

Boness, N. L., and M. D. Zoback (2004), Stress-induced seismic velocity anisotropy and physical properties in the SAFOD Pilot Hole in Parkfield, CA, *Geophys. Res. Lett.*, *31*(15), L15S17, doi:10.1029/2003GL019020.

Bortfeld, R. (1961), APPROXIMATIONS TO THE REFLECTION AND TRANSMISSION COEFFICIENTS OF PLANE LONGITUDINAL AND TRANSVERSE WAVES*, *Geophys. Prospect.*, *9*(4), 485–502, doi:10.1111/j.1365-2478.1961.tb01670.x.

Bouzidi, Y., and D. R. Schmitt (2006), A large ultrasonic bounded acoustic pulse transducer for acoustic transmission goniometry: Modeling and calibration, *J. Acoust. Soc. Am.*, *119*(1),

54, doi:10.1121/1.2133683.

Bouzidi, Y., and D. R. Schmitt (2008a), Acoustic reflectivity goniometry of bounded ultrasonic pulses: Experimental verification of numerical models, *J. Appl. Phys.*, *104*(6), doi:10.1063/1.2982094.

Bouzidi, Y., and D. R. Schmitt (2008b), Quantitative modeling of refected ultrasonic bounded beams and a new estimate of the schoch shift, *IEEE Trans. Ultrason. Ferroelectr. Freq. Control*, *55*(12), 2661–2673, doi:10.1109/TUFFC.2008.981.

Bouzidi, Y., and D. R. Schmitt (2012), Incidence-angle-dependent acoustic reflections from liquid-saturated porous solids, *Geophys. J. Int.*, *191*(3), 1427–1440, doi:10.1111/j.1365-246X.2012.05695.x.

Breazeale, M. A., L. Adler, and G. W. Scott (1977), Interaction of ultrasonic waves incident at the Rayleigh angle onto a liquid-solid interface, *J. Appl. Phys.*, *48*(2), 530–537, doi:10.1063/1.323677.

Brekhovskikh, L. M. (1960), *Waves in layered media.*, Academic Press, New York,.

Brown, R. J., D. C. Lawton, and S. P. Cheadle (1991), Scaled physical modelling of anisotropic wave propagation: multioffset profiles over an orthorhombic medium, *Geophys. J. Int.*, *107*(3), 693–702, doi:10.1111/j.1365-246X.1991.tb01428.x.

Carcione, J. M. (1997), Reflection and transmission of qP-qS plane waves at a plane boundary between viscoelastic transversely isotropic media, *Geophys. J. Int.*, *129*, 669–680.

Castagna, J., and M. Backus (1993), *Offset-dependent refletivity-theory and practice of AVO analysis*, Society of Exploration Geophysicist.

Chattopadhyay, A., P. Kumari, and V. K. Sharma (2015), Reflection and refraction at the interface between distinct generally anisotropic half spaces for three-dimensional plane quasi-P waves, *J. Vib. Control*, *21*, 493–508.

Cheadle, S. P. (1991), Orthorhombic anisotropy: A physical seismic modeling study, *Geophysics*, *56*(10), 1603, doi:10.1190/1.1442971.

Chen, H., J. P. Castagna, R. L. Brown, and A. C. B. Ramos (2001), Three-parameter AVO crossplotting in anisotropic media, *Geophysics*, *66*(5), 1359, doi:10.1190/1.1487081.

Christensen, N. I. (1965), Compressional wave velocities in metamorphic rocks at pressures to 10

kilobars, *J. Geophys. Res.*, *70*(24), 6147–6164, doi:10.1029/JZ070i024p06147.

Christoffel, E. B. (1877), Uber die Fortpflanzung von Stossen durch elastische fest Korper, *Ann. Mater.*, *8*, 193–243.

Claerbout, J. F. (1985), *IMAGING THE EARTH's INTERIOR*, Blackwell Scientific Publications, Oxford, London, Edinburgh, Boston, Palo Alto, Victoria.

Crampin, S. (1985), Evaluation of anisotropy by shear-wave splitting, *Geophysics*, *50*(1), 142, doi:10.1190/1.1441824.

Daley, P. ., and F. Hron (1987), Reflection and transmission coefficients for transversely isotropic media, *Bull. Seism. Soc. Am.*, *67*(3), 661–675.

Daley, P. F. (1979), Reflection and transmission coefficients for seismic waves in ellipsoidally anisotropic media, *Geophysics*, *44*(1), 27, doi:10.1190/1.1440920.

Daley, P. F., and F. Hron (1977a), REFLECTION AND TRANSMISSION COEFFICIENTS TRANSVERSELY ISOTROPIC MEDIA, *BSSA*, *67*(3), 661–675.

Daley, P. F., and F. Hron (1977b), REFLECTION AND TRANSMISSION COEFFICIENTS TRANSVERSELY ISOTROPIC MEDIA, *BSSA*, *67*(3), 661–675.

Declercq, N. F. (2006), Fast beating null strip during the reflection of pulsed Gaussian beams incident at the Rayleigh angle, *Ultrasonics*, *44*(SUPPL.), e1447–e1451, doi:10.1016/j.ultras.2006.05.205.

Declercq, N. F., R. Briers, J. Degrieck, and O. Leroy (2005), The history and properties of ultrasonic inhomogeneous waves, *IEEE Trans. Ultrason. Ferroelectr. Freq. Control*, *52*(5), 776–791, doi:10.1109/TUFFC.2005.1503963.

Descamps, M., and B. Hosten (1991), The effects of viscoelasticity on the reflection and transmission of ultrasonic waves by an orthotropic plate, *J. Acoust. Soc. Am.*, *29*(6), 1763–1770, doi:10.1006/jsvi.1996.0374.

Diachok, O. I. (1970), Conical Reflection of Ultrasound from a Liquid-Solid Interface, *J. Acoust. Soc. Am.*, *47*(1B), 155, doi:10.1121/1.1911450.

Dvorkin, J., M. Gutierrez, and D. Grana (2014), *Seismic Reflections of Rock Properties*.

Ekanem, a. M., J. Wei, X. Y. Li, M. Chapman, and I. G. Main (2013), P-wave attenuation anisotropy in fractured media: A seismic physical modelling study, *Geophys. Prospect.*,

61(SUPPL.1), 420–433, doi:10.1111/j.1365-2478.2012.01127.x.

Far, M. E., C. M. Sayers, L. Thomsen, D. H. Han, and J. P. Castagna (2013), Seismic characterization of naturally fractured reservoirs using amplitude versus offset and azimuth analysis, *Geophys. Prospect.*, *61*(2), 427–447, doi:10.1111/1365-2478.12011.

Farra, V., and I. Pšenčík (2010), First-order reflection/transmission coefficients for unconverted plane P waves in weakly anisotropic media, *Geophys. J. Int.*, *183*(3), 1443–1454, doi:10.1111/j.1365-246X.2010.04794.x.

Gassmann, F. (1964), Introduction to seismic travel time methods in anisotropic media, *Pure Appl. Geophys. PAGEOPH*, *58*(1), 63–112, doi:10.1007/BF00879140.

Gazdag, J. (1978), Wave equation migration with the phase-shift method, *Geophysics*, *43*(7), 1342, doi:10.1190/1.1440899.

Godfrey, N. J., N. I. Christensen, and D. a. Okaya (2000), Anisotropy of schists: Contribution of crustal anisotropy to active source seismic experiments and shear wave splitting observations, *J. Geophys. Res.*, *105*(B12), 27991–28007, doi:10.1029/2000JB900286.

Golikov, P., and A. Stovas (2010), New weak-contrast approximation for reflection coefficients in transversely isotropic media, *J. Geophys. Eng.*, *7*(4), 343–350, doi:10.1088/1742-2132/7/4/001.

Graebner, M. (1992), Plane-wave reflection and transmission coefficients for a transversely isotropic solid, *GEOPHYSICS*, *57*(11), 1512–1519, doi:10.1190/1.1443219.

Gray, D., G. Roberts, and K. Head (2002), Recent advances in determination of fracture strike and crack density from P-wave seismic data, *Lead. Edge*, *21*(3), 280, doi:10.1190/1.1463778.

Grech, M. G. K., D. C. Lawton, and S. H. Gray (2002), A multioffset vertical seismic profiling experiment for anisotropy analysis and depth imaging, *Geophysics*, *67*(2), 348–354, doi:10.1190/1.1468595.

Grechka, V., and I. Tsvankin (2004), Characterization of dipping fractures in a transverselyisotropic background, *Geophys. Prospect.*, *52*(1), 1–10, doi:10.1046/j.1365-2478.2004.00396.x.

Guest, W. S., and J.-M. Kendall (1993), Modelling waveforms in anisotropic inhomogeneous

media using ray and Maslov asymptotic theory: applications to exploration seismology, *Can. J. Expl. Geophys.*, *29*, 78–92.

Guest, W. S., and C. J. Thomson (1992), A SOURCE OF SIGNIFICANT TRANSVERSE ARRIVALS FROM AN ISOTROPIC ANISOTROPIC INTERFACE, eg THE MOHO., *Geophys. J. Int.*, *111*, 309–318.

Guest, W. S., C. J. Thomson, and C. P. Spencer (1993), Anisotropic reflection and transmission calculations with application to a crustal seismic survey from the East Greenland Shelf, *J. Geophys. Res.*, *98*(B8), 14161, doi:10.1029/93JB01156.

Hall, S. A., and J. Kendall (2003), Fracture characterization at Valhall: Application of P-wave amplitude variation with offset and azimuth (AVOA) analysis to a 3D ocean-bottom data set, *Geophysics*, *68*(4), 1150, doi:10.1190/1.1598107.

Helbig, K. (1994), *Foundations of Anisotropy for Exploration Seismics*, Elsevier, Utrecht.

Henneke, E. G. (1972), Reflection-Refraction of a Stress Wave at a Plane Boundary between Anisotropic Media, *J. Acoust. Soc. Am.*, *51*(1B), 210, doi:10.1121/1.1912832.

Henneke, E. G., and G. L. Jones (1976), Erratum: ''Critical angle for reflection at a liquid–solid interface in single crystals'', *J. Acoust. Soc. Am.*, *60*(3), 759, doi:10.1121/1.381248.

Hood, J. A., and M. Schoenberg (1992), NDE of fracture-induced anisotropy, *Rev. Prog. Quant. Nondestruct. Eval. Vol. 11B*, *11*, 2101–2108.

Innanen, K. A., and F. Mahmoudian (2015), Characterizing the degree of amplitude-variation-with-offset nonlinearity in seismic physical modelling reflection data, *Geophys. Prospect.*, *63*(1), 133–140, doi:10.1111/1365-2478.12169.

Isaac, J. H., and D. C. Lawton (1999), Image mispositioning due to dip-ping TI Media: A physical seismic modeling study, *Geophysics*, *64*, 1230–1238.

Jech, J. (1991), Computation of elastic parameters of anisotropic medium from travel times of quasi-compressional waves, *Phys. Earth Planet. Inter.*, *66*(3–4), 153–159, doi:10.1016/0031-9201(91)90074-R.

Ji, S., T. Shao, K. Michibayashi, C. Long, Q. Wang, Y. Kondo, W. Zhao, H. Wang, and M. H. Salisbury (2013), A new calibration of seismic velocities, anisotropy, fabrics, and elastic moduli of amphibole-rich rocks, *J. Geophys. Res. E Planets*, *118*(9), 4699–4728,

doi:10.1002/jgrb.50352.

Jocker, J., and D. Smeulders (2007), Minimization of finite beam effects in the determination of reflection and transmission coefficients of an elastic layer, *Ultrasonics*, *46*(1), 42–50, doi:10.1016/j.ultras.2006.10.001.

Kaarsberg, E. A. (1959), Introductory Studies of Natural and Artificial Argillaceous Aggregates by Sound-Propagation and X-ray Diffraction Methods, *J. Geol.*, *67*(4), 447–472, doi:10.1086/626597.

Kebaili, A., and D. R. Schmitt (1997), Ultrasonic anisotropic phase velocity determination with the Radon transformation, *J. Acoust. Soc. Am.*, *101*(6), 3278, doi:10.1121/1.418344.

Keith, C. M., and S. Crampin (1977), Seismic body waves in anisotropic media: Reflection and refraction at a plane interface, *Geophys. J. Roy. Astr. Soc.*, *49*, 181–208.

Kendall, J.-M., and C. J. Thomson (1989), A comment on the form of the geometrical spreading equations, with some numerical examples of seismic ray tracing in inhomogeneous, anisotropic media, *Geophys. J. Int.*, *99*(2), 401–413, doi:10.1111/j.1365-246X.1989.tb01697.x.

Kern, H., and H. R. Wenk (1990), Fabric-related velocity anisotropy and shear wave splitting in rocks from the Santa Rosa Mylonite Zone, California, *J. Geophys. Res. Solid Earth*, *95*(B7), 11213–11223, doi:10.1029/JB095iB07p11213.

Klimeš, L. (2003), Weak-contrast reflection–transmission coefficients in a generally anisotropic background, *Geophysics*, *68*(6), 2063, doi:10.1190/1.1635060.

Knott, C. G. (1899), Reflexion and Refraction of Elastic Waves with Seismological Applications, *Philos. Mag.*, *54*(5th series), 64–97.

Krail, P. M., and H. Brysk (1983), Reflection of spherical seismic waves in elastic layered media, *Geophysics*, *48*(6).

Landrø, M., and I. Tsvankin (2006), Seismic critical-angle reflectometry: A method to characterize azimuthal anisotropy?, *Geophysics*, *72*(3), 120–124, doi:10.1190/1.2437145.

Leary, P. C., S. Crampin, and T. V. McEvilly (1990), Evolution of Mid Ocean Ridges, edited by J. M. Sinton, *J. Geophys. Res.*, *95*(B7), 11105–11114, doi:10.1029/GM057.

Di Leo, J. F., A. M. Walker, Z. H. Li, J. Wookey, N. M. Ribe, J. M. Kendall, and A. Tommasi

(2014), Development of texture and seismic anisotropy during the onset of subduction, *Geochemistry, Geophys. Geosystems*, *15*(1), 192–212, doi:10.1002/2013GC005032.

Leroy, O., and B. Poirèe (1988), On the Reflection Coefficient of Acoustic Beams, *Acustica*, *66*, 84–89.

Li, L. (2008), Calculation of reflection and transmission coefficients for qP waves incident on a planar interface between isotropic and triclinic media, *Acta Geophys.*, *56*, 518–528.

Liang, K., X. Yin, and G. Wu (2009), Approximate PP reflection coefficient in TTI media, in *Beijing 2009 International Geophysical Conference and Exposition, Beijing, China, 24–27 April 2009*, edited by L. Zhenwu and Y. Sun, pp. 126–126, Society of Exploration Geophysicists.

Lin, F.-C., M. H. Ritzwoller, Y. Yang, M. P. Moschetti, and M. J. Fouch (2011), Complex and variable crustal and uppermost mantle seismic anisotropy in the western United States, *Nat. Geosci.*, *4*(1), 55–61, doi:10.1038/ngeo1036.

Liu, Y., and D. R. Schmitt (2006), The transition between the scale domains of ray and effective medium theory and anisotropy: Numerical models, *Pure Appl. Geophys.*, *163*(7), 1327–1349, doi:10.1007/s00024-006-0075-5.

Mah, M., and D. R. Schmitt (2001a), Experimental determination of the elastic coefficients of an orthorhombic material, *Geophysics*, *66*(4), 1217, doi:10.1190/1.1487068.

Mah, M., and D. R. Schmitt (2001b), Experimental determination of the elastic coefficients of an orthorhombic material, *Geophysics*, *66*(4), 1217, doi:10.1190/1.1487068.

Mahmoudian, F. (2013), Physical Modeling and Analysis of Seismic Data from a Simulated Fractured Medium, University of Calgary.

Mahmoudian, F., G. Margrave, and P. Daley (2014), Estimation of elastic stiffness coefficients of an orthorhombic physical model using group velocity analysis on transmission data, *Geophysics*, *79*(1), R27–R39, doi:10.1190/geo2013-0203.1.

Mahmoudian, F., G. F. Margrave, J. Wong, and D. C. Henley (2015), Azimuthal amplitude variation with offset analysis of physical modeling data acquired over an azimuthally anisotropic medium, *GEOPHYSICS*, *80*(1), C21–C35, doi:10.1190/geo2014-0070.1.

Mainprice, D., and A. Nicolas (1989), Development of shape and lattice preferred orientations:

application to the seismic anisotropy of the lower crust, *J. Struct. Geol.*, *11*(1–2), 175–189, doi:10.1016/0191-8141(89)90042-4.

Malehmir, R., and D. R. Schmitt (2016a), ARTc: Anisotropic reflectivity and transmissivity calculator, *Comput. Geosci.*, *93*, 114–126, doi:10.1016/j.cageo.2016.05.008.

Malehmir, R., and D. R. Schmitt (2016b), Ultrasonic measurement of anisotropic reflectivity from Water-Phenolic CE Interface, *PANGAEA*, doi:10.1594/PANGAEA.864794.

Malehmir, R., and D. R. Schmitt (2017), Acoustic Reflectivity from an Orthorhombic Media : Understanding the Fractured Anisotropic Crust, *J. Geophys. Res.*, Under review.

Malehmir, R., N. Kazemi, and D. R. Schmitt (2017), An Algorithm to Quantitatively Model Reflected Ultrasonic Bounded Beam with Experimental Validation, *Ultrasonics*.

Mallick, S., and L. N. Frazer (1991), REFLECTION-TRANSMISSION COEFFICIENTS AND AZIMUTHAL ANISOTROPY IN MARINE SEISMIC STUDIES, *Geophys. J. Int.*, *105*, 241–252.

Mallick, S., K. L. Craft, L. J. Meister, and R. E. Chambers (1998), Determination of the principal directions of azimuthal anisotropy from P-wave seismic data, *GEOPHYSICS*, *63*(2), 692–706, doi:10.1190/1.1444369.

Mann, R. W., G. A. Baum, and C. C. Habeger (1980), Determination of all nine orthotropic elastic constants for machine-made paper, *Tappi*, *63*(84), 163–166.

McCamy, K., R. P. Meyer, and T. J. Smith (1962), Generally applicable solutions of Zoeppritz' amplitude equations, *BSSA*, *52*, 923–955.

Merkulov, L. G. (1963), Ultrasonic waves in crystals, *Appl. Mater. Res.*, *2*(4), 231–240.

Musgrave, M. J. P. (1970a), *Crystal Acoustics: Introduction to the Study of Elastic Waves and Vibrations in Crystals*, Holden-Day.

Musgrave, M. J. P. (1970b), *Musgrave M.J.P. Crystal Acoustics 1970.djvu.pdf*, HOLDEN-DAY, San Francisco.

Nakagawa, S., K. T. Nihei, L. R. Myer, and E. L. Majer (2003), Three-dimensional elastic wave scattering by a layer containing vertical periodic fractures, *J. Acoust. Soc. Am.*, *113*(6), 3012, doi:10.1121/1.1572139.

Nayfeh, A. H. (1989), The propagation of horizontally polarized shear waves in multilayered

anisotropic media, *J. Acoust. Soc. Am.*, *86*(5), 1–16, doi:10.1121/1.398580.

Ngoc, T. D. K., and W. G. Mayer (1979), Ultrasonic nonspecular reflectivity near longitudinal critical angle, *J. Appl. Phys.*, *50*(12), 7948–7951, doi:10.1063/1.325971.

Nishizawa, O., and K. Kanagawa (2010), Seismic velocity anisotropy of phyllosilicate-rich rocks: characteristics inferred from experimental and crack-model studies of biotite-rich schist, *Geophys. J. Int.*, *182*(1), no-no, doi:10.1111/j.1365-246X.2010.04614.x.

Ortiz-osornio, M., and D. R. Schmitt (2009), Measurements of the reflectivity of a liquid – anisotropic solid interface, in *8th Euro Conference of Rock Physics & Geomechanics*, p. 4pp, Ascona, Switzerland.

Ortiz-osornio, M., and D. R. Schmitt (2010a), The Reflectivity and Transmissivity of Anisotropic Materials : A Physical Modeling Study, in *American Rock Mechanics Association*, p. 5pp.

Ortiz-osornio, M., and D. R. Schmitt (2010b), The reflectivity and transmissivity of anisotropic materials: A physical model study, in *ARMA 44th U.S. Rock Mechanics Symposium*, p. 5 pp, Salt Lake City.

Ortiz-osornio, M., and D. R. Schmitt (2010c), Velocity dispersion of a heavy oil sandstone: A case study, in *Oil Sands and Heavy Oil Technologies Conference, Calgary*, pp. 20–22.

Ortiz-osornio, M., and D. R. Schmitt (2011a), Measurements of the reflectivity and transmissivity of anisotropic materials to test the effect of tilt and azimuth, in *1st Int. Workshop on Rock Physics, August 7-12,* p. 4pp, Golden, CO.

Ortiz-osornio, M., and D. R. Schmitt (2011b), Physical Modeling of the Reflectivity and Transmissivity of Anisotropic Materials, in *73rd EAGE Conference and Exhibition incorporating SPE EUROPEC 2011, Vienna*, p. 4 pp, Vienna.

Ostrander, W. J. (1984), Plane-wave reflection coefficients for gas sands at nonnormal angles of incidence - ostrander1984.pdf, *Geophysics*, *49*(10), 1637–1648.

Ozacar, A. A., and G. Zandt (2004), Crustal seismic anisotropy in central Tibet: Implications for deformational style and flow in the crust, *Geophys. Res. Lett.*, *31*(23), 1–4, doi:10.1029/2004GL021096.

Ozacar, A. A., and G. Zandt (2009), Crustal structure and seismic anisotropy near the San Andreas Fault at Parkfield, California, *Geophys. J. Int.*, *178*(2), 1098–1104,

doi:10.1111/j.1365-246X.2009.04198.x.

Pedersen, H. A. (2006), Impacts of non-plane waves on two-station measurements of phase velocities, *Geophys. J. Int.*, *165*(1), 279–287, doi:10.1111/j.1365-246X.2006.02893.x.

Plona, T. J. (1976), Ultrasonic bounded beam reflection and transmission effects at a liquid/ solid-plate/liquid interface, *J. Acoust. Soc. Am.*, *59*(6), 1324, doi:10.1121/1.381011.

Rokhlin, S. I. (1986), Reflection and refraction of elastic waves on a plane interface between two generally anisotropic media, *J. Acoust. Soc. Am.*, *79*(4), 906, doi:10.1121/1.393764.

Rokhlin, S. I., and W. Wang (1992), Double through transmission bulk wave method for ultrasonic phase velocity measurement and determination of elastic constants of composite materials, *Acoust. Soc. Am.*, *91*(6), 3303–3312.

Rüger, A. (1997), P -wave reflection coefficients for transversely isotropic models with vertical and horizontal axis of symmetry, *Geophysics*, *62*(3), 713–722.

Rüger, A. (1997), P -wave reflection coefficients for transversely isotropic models with vertical and horizontal axis of symmetry, *Geophysics*, *62*(3), 713–722.

Rüger, A. (1998), Variation of P-wave reflectivity with offset and azimuth in anisotropic media, *Geophysics*, *63*(3), 935, doi:10.1190/1.1444405.

Savage, M. K. (1999), Siesmic anisotropy and mantle deformation, *Rev. Geophys.*, (98), 65–106, doi:10.1029/98RG02075.

Sayers, C. M., and S. Dean (2001), Azimuth-dependent AVO in reservoirs containing non-orthogonal fracture sets gave an analytic expression, valid for, *Geophys. Prospect. Ikelle Ru È ger*, *49*, 100–106.

Sayers, C. M., and M. Kachanov (1995), Microcrack-induced elastic wave anisotropy of brittle rocks, *J. Geophys. Res. Solid Earth*, *100*(B3), 4149–4156, doi:10.1029/94JB03134.

Sayers, C. M., S. Guo, and J. Silva (2015), Sensitivity of the elastic anisotropy and seismic reflection amplitude of the Eagle Ford Shale to the presence of kerogen, *Geophys. Prospect.*, *63*(1), 151–165, doi:10.1111/1365-2478.12153.

Schijns, H., D. R. Schmitt, P. J. Heikkinen, and I. T. Kukkonen (2012a), Seismic anisotropy in the crystalline upper crust: Observations and modelling from the Outokumpu scientific borehole, Finland, *Geophys. J. Int.*, *189*(1), 541–553, doi:10.1111/j.1365-

246X.2012.05358.x.

Schijns, H., D. R. Schmitt, P. J. Heikkinen, and I. T. Kukkonen (2012b), Seismic anisotropy in the crystalline upper crust: Observations and modelling from the Outokumpu scientific borehole, Finland, *Geophys. J. Int.*, *189*(1), 541–553, doi:10.1111/j.1365-246X.2012.05358.x.

Schmitt, D. R. (2015), *Geophysical Properties of the Near Surface Earth: Seismic Properties*, Elsevier B.V.

Schoch, A. (1950), Schallreflexion, Schallbrechung und Schallbeugung, in *Ergebnisse der exakten Naturwissenschaften*, vol. 23, pp. 127–234.

Schoch, A. (1952a), b, Seitliche versetzung eines total reflektierten strahles bei ultraschall-wellen, *Acustica*, *2*(17).

Schoch, A. (1952b), Der schallbeugung durch platten, *Acustica*, *1*(2).

Schoenberg, M. (1997), Orthorhombic media: Modeling elastic wave behavior in a vertically fractured earth, *Geophysics*, *62*(6), 1954, doi:10.1190/1.1444297.

Shadlow, J. (2014), A description of seismic amplitude techniques, *Explor. Geophys.*, *45*(3), 154, doi:10.1071/EG13070.

Shen, F., J. Sierra, D. R. Burns, and M. N. Toksöz (2002), Azimuthal offset-dependent attributes applied to fracture detection in a carbonate reservoir, *GEOPHYSICS*, *67*(2), 355–364, doi:10.1190/1.1468596.

Shuey, R. T. (1985), A simplification of the Zoeppritz equations, *Geophysics*, *50*(4), 609, doi:10.1190/1.1441936.

Skopintseva, L., and T. Alkhalifah (2013), An analysis of AVO inversion for postcritical offsets in HTI media, *GEOPHYSICS*, *78*(3), N11–N20, doi:10.1190/geo2011-0288.1.

Stewart, R. R., N. Dyaur, B. Omoboya, J. J. S. de Figueiredo, M. Willis, and S. Sil (2013), Physical modeling of anisotropic domains: Ultrasonic imaging of laser-etched fractures in glass, *Geophysics*, *78*(1), D11–D19, doi:10.1190/geo2012-0075.1.

Swokowski, E. W. (1979), *Calculus with analytic geometry*, Prindle, Weber & Schmidt.

Tamir, T., and H. L. Bertoni (1971), Lateral Displacement of Optical Beams at Multilayered and Periodic Structures, *J. Opt. Soc. Am.*, *61*(10), 1397–1413, doi:10.1364/JOSA.61.001397.

Thomsen, L. (1986a), Weak elastic anisotropy, *Geophysics*, *51*(10), 1954, doi:10.1190/1.1442051.

Thomsen, L. (1986b), Weak elastic anisotropy, *Geophysics*, *51*(10), 1954, doi:10.1190/1.1442051.

Tsvankin, I. (1997), Anisotropic parameters and P-wave velocity for orthorhombic media, *Geophysics*, *62*(4), 1292, doi:10.1190/1.1444231.

Ursin, B., and G. Haugen (1996), Weak-contrast approximation of the elastic scattering matrix in anisotropic media, *Pure Appl. Geophys.*, *148*(3–4), 685–714.

Vavrycuk, V. (1999), Weak-contrast reflection / transmission coefficients in weakly anisotropic elastic media : P -wave incidence, *Geophys. J. Int.*, *138*, 553–562, doi:10.1046/j.1365-246X.1999.00890.x.

Vavrycuk, V., and I. Pšenčík (1998), PP-reflection coefficients in weakly anisotropic elastic media, *Soc. Expl. Geophys*, *63*(6), 2129–2141.

Vestrum, R. W. (1994), Group and Phase-Velocity Inversions for the General Anisotropic Stiffness Tensor, October.

Vestrum, R. W., and R. J. Brown (1994), *From group or phase velocities stiffness tensor to the general anisotropic Robert W . Vestr um and R . Jame s B ro w n*.

Voigt, W. (1887), Theorie des Lichts für bewegte Medien, *Göttinger Nachrichten*, *7*, 41–51.

Walker, A. M., and J. Wookey (2012a), Computers & Geosciences MSAT — A new toolkit for the analysis of elastic and seismic anisotropy, *Comput. Geosci.*, *49*(October 2012), 81–90, doi:10.1016/j.cageo.2012.05.031.

Walker, A. M., and J. Wookey (2012b), MSAT-A new toolkit for the analysis of elastic and seismic anisotropy, *Comput. Geosci.*, *49*, 81–90, doi:10.1016/j.cageo.2012.05.031.

Wang, X., and I. Tsvankin (2013), Multiparameter TTI tomography of P-wave reflection and VSP data, *Geophysics*, *78*(5), WC51-WC63, doi:10.1190/geo2012-0394.1.

Wenk, H.-R. (1999), A voyage through the deformed Earth with the self-consistent model, *Model. Simul. Mater. Sci. Eng.*, *7*(5), 699–722, doi:10.1088/0965-0393/7/5/304.

Weyl, H. (1919), Ausbreitung elektromagnetischer Wellen über einem ebenen Leiter, *Ann. Phys.*, *365*(21), 481–500, doi:10.1002/andp.19193652104.

Wielandt, E. (1993), Propagation and structural interpretation of non-plane waves, *Geophys. J. Int.*, *113*(1), 45–53, doi:10.1111/j.1365-246X.1993.tb02527.x.

Young, G. B., and L. W. Braile (1976), A computer program for the application of Zoeppritz's amplitude equations and Knott's energy equations, *Bull. Seismol. Soc. Am.*, *66*(6), 1881–1885.

Yousef, B. M., and D. A. Angus (2016), *When do fractured media become seismically anisotropic? Some implications on quantifying fracture properties*.

Zheng, P., and B. Ding (2014), The Generalized Reflection and Transmission Matrix Method for Wave Propagation in Stratified Fluid-Saturated Porous Media, *Transp. Porous Media*, *102*(2), 185–206, doi:10.1007/s11242-014-0271-1.

Zheng, Y. (2006), Seismic azimuthal anisotropy and fracture analysis from PP reflection data, University of Calgary.

Zillmer, M., D. Gajewski, and B. M. Kashtan (1998), Anisotropic reflection coefficients for a weak-contrast interface, *Geophys. J. Int.*, *132*(1), 159–166.

Zoeppritz, K. (1919), Erdbebenwellen VII. VIIb. Über Reflexion und Durchgang seismischer Wellen durch Unstetigkeitsflächen. Nachrichten von der Königlichen Gesellschaft der Wissenschaften zu Göttingen, *Math. Klasse*, 66–84.

Chapter 5
Conclusions and directions for future research

5.1 Contributions of Work Described Here

It has long been known that large proportions of the Earth's crust, mantle, and inner core are anisotropic, and that this anisotropy must influence seismic wave propagation, transmission, and reflection. Despite this, seismic transmissivity and reflectivity is usually described using either Zoeppritz's isotropic formulae or approximations valid only for specifically oriented transversely isotropic substrates. This over-simplification may create artifacts in the seismic image, target mis-positioning and hence flawed interpretation. This thesis seeks to better understand the behavior of reflected seismic waves in anisotropic formations.

This thesis makes three distinct contributions by providing i) an algorithm that calculates the reflectivity from the welded interface between any two anisotropic elastic solids and ii) an algorithm to model the propagation and reflection of a bounded beam from a water-solid interface, and by iii) carrying out and fully modelling a set of reflectivities from anisotropic media obtained in laboratory experiments.

First, we contribute an algorithm that solves for the reflectivity and transmissivity from the interface between two anisotropic slabs of arbitrary orientation and symmetry up to and including triclinic. The algorithm solves the full elastic wave equation and yields the polarizations, slowness and amplitudes of all six of the possible wave-modes generated at the welded interface between two anisotropic half-spaces. The utility of the algorithm, provided as a series of MATLAB® based programs called Anisotropic Reflectivity Transmissivity calculator (ARTc) is illustrated in a number of different cases of increasing complexity. ARTc is coded in MATLAB® and bundled with an interactive GUI and bash script to run on single or multi-processor computers.

Second, the study of the reflected acoustic waves plays an important role in our understanding of media. We provide an algorithm to propagate the ultrasonic bounded beam source and study its reflection from any horizontal and homogenous water-solid boundary. This algorithm implements a hybrid combination of the phase-advance wavefield continuation in the frequency domain and the complex analytic solution for the acoustic reflectivity. The peak amplitude of the specularly reflected beam is in agreement with the laboratory measured acoustic reflection from water-Aluminum and water-Copper alloy boundaries. The algorithm is able to model the observed critical reflection as well as the null in the amplitude at the Rayleigh critical angle from the acoustic wave. This algorithm is a crucial tool to understand the full reflected wave from material immersed in water in any azimuthal or incidental angles. The software of this algorithm and acoustic reflectivity from both solid materials are provided. This algorithm will be of interest to both the Geophysical and Nondestructive Testing communities.

The variations in the strength of seismic reflections with both angles of incidence and azimuth are being used to constrain the orientations and degrees of mechanical anisotropy of geological formations. This information is often used in turn to infer the directions of fracturing and stress usually assuming simplified geological structures that in many cases are not realistic. In order to further understand this problem, the reflectivities from a set of variously titled samples cut from a single block of a common anisotropic composite material are measured with both angles of incidence and azimuth in the laboratory. Each sample is analogous to a formation in which the fracture sets increasingly dip. The observed responses differ from plane wave theory due to the finite nature of the experiment, but the deviations are well accounted for by modeling the expected responses for the behavior of a bounded pulse. As expected, the reflectivities vary with the sample tilt, the angle of incidence, and the azimuth at which the measurements are made. However, some of these responses, such as the pre-critical reflectivities, do not appear to strongly vary with azimuth for a given sample. Critical angle phenomena, too, must be used cautiously as the observed peaks do not lie at the exact critical angle. These results suggest that reflectivities do provide important information with regards to orientations of anisotropy but may not be able to provide further details without making assumptions with regards to the structure of the formation. Although these are laboratory observations, their interpretation may impact field practice.

5.2 Suggestions for future research

Much of this thesis required us to develop tools for the study of anisotropic reflectivity and for bounded beam propagation. The latter will provide workers with a new tool to assist in the interpretation of laboratory beam propagation and reflection. This certainly will be valuable to the specialist nondestructive test community although there is potential to extend the method to some forms of modeling of seismic responses. The former, however, by providing a relatively straightforward manner to determine the reflectivity and transmissivity of an otherwise rather complex problem opens a number of future potential research studies. The following is a list of activities that we did not have time to complete, but remain to be done:

- We studied the role of elastic anisotropy on the acoustical reflectivity variation with incidental and azimuthal direction (chapter 2) and expressed a hybrid method to consider source mechanism on the post-critical reflectivity and Schoch shift effect from liquid-solid interface (chapter 3). There is a great potential to study the properties of the quasi-shear wave in anisotropic medium by analyzing the converted waves in the transmission.
- Investigate the application of the Reflectivity and transmissivity calculator (ARTc-chapter 2) in ray-tracing of the layered subsurface model and its application on seismic data migration.
- We studied the role of fractured medium on the acoustic reflectivity (chapter 4) using blocks of phenolic with grade CE with different tilting angles. Additionally, 3D-printed blocks of isotropic material could be implemented with difference fracture density and spacing and filling to investigate their role on reflected wavefield.
- We have studied the role of trigonal symmetric anisotropy from a z-cut single crystal alpha-quartz on acoustic reflectivity. Our measured acoustic reflectivity from water-quartz interface displays a complex pattern in which we observed double null reflection at far incident angles. To the best knowledge of the author, this pattern has never been reported in the scientific community, and we will use this dataset to understand the role of the elastic anisotropy and the bounded beam on the double Schoch shifts.

Bibliography

Aki, K., and P. G. Richards (1980), *Quantitative seismology: Theory and methods, v.1*, W.H. Freeman and Co, San Francisco.

Aleardi, M., and A. Mazzotti (2014), A feasibility study on the expected seismic AVA signatures of deep fractured geothermal reservoirs in an intrusive basement, *J. Geophys. Eng.*, *11*(6), 65008, doi:10.1088/1742-2132/11/6/065008.

Alhussain, M. (2007), Spherical Wave AVO Response of Isotropic and Anisotropic Media : Laboratory Experiment versus Numerical Simulations Mohammed Abdullah K Alhussain, University of Curtin.

Alhussain, M., E. Liu, B. Gurevich, M. Urosevic, and S. U. Rehman (2007), AVOaz response of a fractured medium: Laboratory measurements versus numerical simulations, *SEG Tech. Progr. Expand. Abstr.*, *26*(1), 254–258, doi:10.1190/1.2792421.

Alhussain, M., B. Gurevich, and M. Urosevic (2008), Experimental verification of spherical-wave effect on the AVO response and implications for three-term inversion, *Geophysics*, *73*(2), C7–C12, doi:10.1190/1.2837641.

Almqvist, B. S. G., L. Burlini, D. Mainprice, and A. M. Hirt (2010), Elastic properties of anisotropic synthetic calcite-muscovite aggregates, *J. Geophys. Res. Solid Earth*, *115*(8), 1–15, doi:10.1029/2009JB006523.

Arts, R., P. Rasolofosaon, and B. Zinszner (1991), Complete inversion of the anisotropic elastic tensor in rocks: Experiment versus theory, *1991 SEG Annu. Meet.*, 1538–1541.

Auld, B. A. (1973), *Acoustic fields and waves in solids- Vol 2*, John Wiley & Sons, Inc.

Backus, G. E. (1962), Long-wave elastic anisotropy produced by horizontal layering, *J. Geophys. Res.*, *67*(11), 4427, doi:10.1029/JZ067i011p04427.

Backus, G. E. (1965), Possible forms of seismic anisotropy of the uppermost mantle under oceans, *J. Geophys. Res.*, *70*(14), 3429, doi:10.1029/JZ070i014p03429.

Bakulin, A., V. Grechka, and I. Tsvankin (2000), Estimation of fracture parameters from reflection seismic data—Part II: Fractured models with orthorhombic symmetry, *Geophysics*, *65*(6).

Bao, X., D. W. Eaton, and Y. J. Gu (2016), Rayleigh-wave azimuthally anisotropic phase-velocity maps beneath western Canada, *J. Geophys. Res. Solid Earth*, n/a-n/a, doi:10.1002/2015JB012453.

Bass, J. D. (1995), Elasticity of minerals, glasses, and melts, in *Mineral Physics and Crystallography: A Handbook*, pp. 45–63.

Behura, J., and I. Tsvankin (2006), Small-angle AVO response of PS-waves in tilted transversely isotropic media, *Geophysics*, *71*(5), C69, doi:10.1190/1.2329865.

Behura, J., and I. Tsvankin (2009), Reflection coefficients in attenuative anisotropic media, *Geophysics*, *74*(5), WB193, doi:10.1190/1.3142874.

Belonoshko, A. B., N. V Skorodumova, A. Rosengren, and B. Johansson (2008), Elastic anisotropy of Earth's inner core., *Science*, *319*(5864), 797–800, doi:10.1126/science.1150302.

Ben-Menahem, A., and A. G. Sena (1990), Seismic source theory in stratified anisotropic media, *J. Geophys. Res.*, *95*(B10), 15395, doi:10.1029/JB095iB10p15395.

Bertoni, H. L., and T. Tamir (1973), Unified theory of Rayleigh-angle phenomena for acoustic beams at liquid-solid interfaces, *Appl. Phys.*, *2*(4), 157–172, doi:10.1007/BF00884205.

Boness, N. L., and M. D. Zoback (2004), Stress-induced seismic velocity anisotropy and physical properties in the SAFOD Pilot Hole in Parkfield, CA, *Geophys. Res. Lett.*, *31*(15), L15S17, doi:10.1029/2003GL019020.

Bortfeld, R. (1961), APPROXIMATIONS TO THE REFLECTION AND TRANSMISSION COEFFICIENTS OF PLANE LONGITUDINAL AND TRANSVERSE WAVES*, *Geophys. Prospect.*, *9*(4), 485–502, doi:10.1111/j.1365-2478.1961.tb01670.x.

Bouzidi, Y., and D. R. Schmitt (2006), A large ultrasonic bounded acoustic pulse transducer for acoustic transmission goniometry: Modeling and calibration, *J. Acoust. Soc. Am.*, *119*(1), 54, doi:10.1121/1.2133683.

Bouzidi, Y., and D. R. Schmitt (2008a), Acoustic reflectivity goniometry of bounded ultrasonic pulses: Experimental verification of numerical models, *J. Appl. Phys.*, *104*(6), doi:10.1063/1.2982094.

Bouzidi, Y., and D. R. Schmitt (2008b), Quantitative modeling of refected ultrasonic bounded

beams and a new estimate of the schoch shift, *IEEE Trans. Ultrason. Ferroelectr. Freq. Control*, *55*(12), 2661–2673, doi:10.1109/TUFFC.2008.981.

Bouzidi, Y., and D. R. Schmitt (2012), Incidence-angle-dependent acoustic reflections from liquid-saturated porous solids, *Geophys. J. Int.*, *191*(3), 1427–1440, doi:10.1111/j.1365-246X.2012.05695.x.

Breazeale, M. A., L. Adler, and G. W. Scott (1977), Interaction of ultrasonic waves incident at the Rayleigh angle onto a liquid-solid interface, *J. Appl. Phys.*, *48*(2), 530–537, doi:10.1063/1.323677.

Brekhovskikh, L. M. (1960), *Waves in layered media.*, Academic Press, New York,.

Brown, R. J., D. C. Lawton, and S. P. Cheadle (1991), Scaled physical modelling of anisotropic wave propagation: multioffset profiles over an orthorhombic medium, *Geophys. J. Int.*, *107*(3), 693–702, doi:10.1111/j.1365-246X.1991.tb01428.x.

Carcione, J. M. (1997), Reflection and transmission of qP-qS plane waves at a plane boundary between viscoelastic transversely isotropic media, *Geophys. J. Int.*, *129*, 669–680.

Castagna, J., and M. Backus (1993), *Offset-dependent refletivity-theory and practice of AVO analysis*, Society of Exploration Geophysicist.

Chattopadhyay, A., P. Kumari, and V. K. Sharma (2015), Reflection and refraction at the interface between distinct generally anisotropic half spaces for three-dimensional plane quasi-P waves, *J. Vib. Control*, *21*, 493–508.

Cheadle, S. P. (1991), Orthorhombic anisotropy: A physical seismic modeling study, *Geophysics*, *56*(10), 1603, doi:10.1190/1.1442971.

Chen, H., J. P. Castagna, R. L. Brown, and A. C. B. Ramos (2001), Three-parameter AVO crossplotting in anisotropic media, *Geophysics*, *66*(5), 1359, doi:10.1190/1.1487081.

Christensen, N. I. (1965), Compressional wave velocities in metamorphic rocks at pressures to 10 kilobars, *J. Geophys. Res.*, *70*(24), 6147–6164, doi:10.1029/JZ070i024p06147.

Christoffel, E. B. (1877), Uber die Fortpflanzung von Stossen durch elastische fest Korper, *Ann. Mater.*, *8*, 193–243.

Claerbout, J. F. (1985), *IMAGING THE EARTH's INTERIOR*, Blackwell Scientific Publications, Oxford, London, Edinburgh, Boston, Palo Alto, Victoria.

Crampin, S. (1985), Evaluation of anisotropy by shear-wave splitting, *Geophysics*, *50*(1), 142, doi:10.1190/1.1441824.

Daley, P. ., and F. Hron (1987), Reflection and transmission coefficients for transversely isotropic media, *Bull. Seism. Soc. Am.*, *67*(3), 661–675.

Daley, P. F. (1979), Reflection and transmission coefficients for seismic waves in ellipsoidally anisotropic media, *Geophysics*, *44*(1), 27, doi:10.1190/1.1440920.

Daley, P. F., and F. Hron (1977a), REFLECTION AND TRANSMISSION COEFFICIENTS TRANSVERSELY ISOTROPIC MEDIA, *BSSA*, *67*(3), 661–675.

Daley, P. F., and F. Hron (1977b), REFLECTION AND TRANSMISSION COEFFICIENTS TRANSVERSELY ISOTROPIC MEDIA, *BSSA*, *67*(3), 661–675.

Declercq, N. F. (2006), Fast beating null strip during the reflection of pulsed Gaussian beams incident at the Rayleigh angle, *Ultrasonics*, *44*(SUPPL.), e1447–e1451, doi:10.1016/j.ultras.2006.05.205.

Declercq, N. F., R. Briers, J. Degrieck, and O. Leroy (2005), The history and properties of ultrasonic inhomogeneous waves, *IEEE Trans. Ultrason. Ferroelectr. Freq. Control*, *52*(5), 776–791, doi:10.1109/TUFFC.2005.1503963.

Descamps, M., and B. Hosten (1991), The effects of viscoelasticity on the reflection and transmission of ultrasonic waves by an orthotropic plate, *J. Acoust. Soc. Am.*, *29*(6), 1763–1770, doi:10.1006/jsvi.1996.0374.

Diachok, O. I. (1970), Conical Reflection of Ultrasound from a Liquid-Solid Interface, *J. Acoust. Soc. Am.*, *47*(1B), 155, doi:10.1121/1.1911450.

Dvorkin, J., M. Gutierrez, and D. Grana (2014), *Seismic Reflections of Rock Properties*.

Ekanem, a. M., J. Wei, X. Y. Li, M. Chapman, and I. G. Main (2013), P-wave attenuation anisotropy in fractured media: A seismic physical modelling study, *Geophys. Prospect.*, *61*(SUPPL.1), 420–433, doi:10.1111/j.1365-2478.2012.01127.x.

Far, M. E., C. M. Sayers, L. Thomsen, D. H. Han, and J. P. Castagna (2013), Seismic characterization of naturally fractured reservoirs using amplitude versus offset and azimuth analysis, *Geophys. Prospect.*, *61*(2), 427–447, doi:10.1111/1365-2478.12011.

Farra, V., and I. Pšenčík (2010), First-order reflection/transmission coefficients for unconverted

plane P waves in weakly anisotropic media, *Geophys. J. Int.*, *183*(3), 1443–1454, doi:10.1111/j.1365-246X.2010.04794.x.

Gassmann, F. (1964), Introduction to seismic travel time methods in anisotropic media, *Pure Appl. Geophys. PAGEOPH*, *58*(1), 63–112, doi:10.1007/BF00879140.

Gazdag, J. (1978), Wave equation migration with the phase-shift method, *Geophysics*, *43*(7), 1342, doi:10.1190/1.1440899.

Godfrey, N. J., N. I. Christensen, and D. a. Okaya (2000), Anisotropy of schists: Contribution of crustal anisotropy to active source seismic experiments and shear wave splitting observations, *J. Geophys. Res.*, *105*(B12), 27991–28007, doi:10.1029/2000JB900286.

Golikov, P., and A. Stovas (2010), New weak-contrast approximation for reflection coefficients in transversely isotropic media, *J. Geophys. Eng.*, *7*(4), 343–350, doi:10.1088/1742-2132/7/4/001.

Graebner, M. (1992), Plane-wave reflection and transmission coefficients for a transversely isotropic solid, *GEOPHYSICS*, *57*(11), 1512–1519, doi:10.1190/1.1443219.

Gray, D., G. Roberts, and K. Head (2002), Recent advances in determination of fracture strike and crack density from P-wave seismic data, *Lead. Edge*, *21*(3), 280, doi:10.1190/1.1463778.

Grech, M. G. K., D. C. Lawton, and S. H. Gray (2002), A multioffset vertical seismic profiling experiment for anisotropy analysis and depth imaging, *Geophysics*, *67*(2), 348–354, doi:10.1190/1.1468595.

Grechka, V., and I. Tsvankin (2004), Characterization of dipping fractures in a transverselyisotropic background, *Geophys. Prospect.*, *52*(1), 1–10, doi:10.1046/j.1365-2478.2004.00396.x.

Guest, W. S., and J.-M. Kendall (1993), Modelling waveforms in anisotropic inhomogeneous media using ray and Maslov asymptotic theory: applications to exploration seismology, *Can. J. Expl. Geophys.*, *29*, 78–92.

Guest, W. S., and C. J. Thomson (1992), A SOURCE OF SIGNIFICANT TRANSVERSE ARRIVALS FROM AN ISOTROPIC ANISOTROPIC INTERFACE, eg THE MOHO., *Geophys. J. Int.*, *111*, 309–318.

Guest, W. S., C. J. Thomson, and C. P. Spencer (1993), Anisotropic reflection and transmission calculations with application to a crustal seismic survey from the East Greenland Shelf, *J. Geophys. Res.*, *98*(B8), 14161, doi:10.1029/93JB01156.

Hall, S. A., and J. Kendall (2003), Fracture characterization at Valhall: Application of P-wave amplitude variation with offset and azimuth (AVOA) analysis to a 3D ocean-bottom data set, *Geophysics*, *68*(4), 1150, doi:10.1190/1.1598107.

Helbig, K. (1994), *Foundations of Anisotropy for Exploration Seismics*, Elsevier, Utrecht.

Henneke, E. G. (1972), Reflection-Refraction of a Stress Wave at a Plane Boundary between Anisotropic Media, *J. Acoust. Soc. Am.*, *51*(1B), 210, doi:10.1121/1.1912832.

Henneke, E. G., and G. L. Jones (1976), Erratum: ''Critical angle for reflection at a liquid–solid interface in single crystals'', *J. Acoust. Soc. Am.*, *60*(3), 759, doi:10.1121/1.381248.

Hood, J. A., and M. Schoenberg (1992), NDE of fracture-induced anisotropy, *Rev. Prog. Quant. Nondestruct. Eval. Vol. 11B*, *11*, 2101–2108.

Innanen, K. A., and F. Mahmoudian (2015), Characterizing the degree of amplitude-variation-with-offset nonlinearity in seismic physical modelling reflection data, *Geophys. Prospect.*, *63*(1), 133–140, doi:10.1111/1365-2478.12169.

Isaac, J. H., and D. C. Lawton (1999), Image mispositioning due to dip-ping TI Media: A physical seismic modeling study, *Geophysics*, *64*, 1230–1238.

Jech, J. (1991), Computation of elastic parameters of anisotropic medium from travel times of quasi-compressional waves, *Phys. Earth Planet. Inter.*, *66*(3–4), 153–159, doi:10.1016/0031-9201(91)90074-R.

Ji, S., T. Shao, K. Michibayashi, C. Long, Q. Wang, Y. Kondo, W. Zhao, H. Wang, and M. H. Salisbury (2013), A new calibration of seismic velocities, anisotropy, fabrics, and elastic moduli of amphibole-rich rocks, *J. Geophys. Res. E Planets*, *118*(9), 4699–4728, doi:10.1002/jgrb.50352.

Jocker, J., and D. Smeulders (2007), Minimization of finite beam effects in the determination of reflection and transmission coefficients of an elastic layer, *Ultrasonics*, *46*(1), 42–50, doi:10.1016/j.ultras.2006.10.001.

Kaarsberg, E. A. (1959), Introductory Studies of Natural and Artificial Argillaceous Aggregates

by Sound-Propagation and X-ray Diffraction Methods, *J. Geol.*, *67*(4), 447–472, doi:10.1086/626597.

Kebaili, A., and D. R. Schmitt (1997), Ultrasonic anisotropic phase velocity determination with the Radon transformation, *J. Acoust. Soc. Am.*, *101*(6), 3278, doi:10.1121/1.418344.

Keith, C. M., and S. Crampin (1977), Seismic body waves in anisotropic media: Reflection and refraction at a plane interface, *Geophys. J. Roy. Astr. Soc.*, *49*, 181–208.

Kendall, J.-M., and C. J. Thomson (1989), A comment on the form of the geometrical spreading equations, with some numerical examples of seismic ray tracing in inhomogeneous, anisotropic media, *Geophys. J. Int.*, *99*(2), 401–413, doi:10.1111/j.1365-246X.1989.tb01697.x.

Kern, H., and H. R. Wenk (1990), Fabric-related velocity anisotropy and shear wave splitting in rocks from the Santa Rosa Mylonite Zone, California, *J. Geophys. Res. Solid Earth*, *95*(B7), 11213–11223, doi:10.1029/JB095iB07p11213.

Klimes, L. (2003), Weak-contrast reflection–transmission coefficients in a generally anisotropic background, *Geophysics*, *68*(6), 2063, doi:10.1190/1.1635060.

Knott, C. G. (1899), Reflexion and Refraction of Elastic Waves with Seismological Applications, *Philos. Mag.*, *54* (5th series), 64–97.

Krail, P. M., and H. Brysk (1983), Reflection of spherical seismic waves in elastic layered media, *Geophysics*, *48*(6).

Landrø, M., and I. Tsvankin (2006), Seismic critical-angle reflectometry: A method to characterize azimuthal anisotropy?, *Geophysics*, *72*(3), 120–124, doi:10.1190/1.2437145.

Leary, P. C., S. Crampin, and T. V. McEvilly (1990), Evolution of Mid Ocean Ridges, edited by J. M. Sinton, *J. Geophys. Res.*, *95*(B7), 11105–11114, doi:10.1029/GM057.

Di Leo, J. F., A. M. Walker, Z. H. Li, J. Wookey, N. M. Ribe, J. M. Kendall, and A. Tommasi (2014), Development of texture and seismic anisotropy during the onset of subduction, *Geochemistry, Geophys. Geosystems*, *15*(1), 192–212, doi:10.1002/2013GC005032.

Leroy, O., and B. Poirèe (1988), On the Reflection Coefficient of Acoustic Beams, *Acustica*, *66*, 84–89.

Li, L. (2008), Calculation of reflection and transmission coefficients for qP waves incident on a

planar interface between isotropic and triclinic media, *Acta Geophys.*, *56*, 518–528.

Liang, K., X. Yin, and G. Wu (2009), Approximate PP reflection coefficient in TTI media, in *Beijing 2009 International Geophysical Conference and Exposition, Beijing, China, 24–27 April 2009*, edited by L. Zhenwu and Y. Sun, pp. 126–126, Society of Exploration Geophysicists.

Lin, F.-C., M. H. Ritzwoller, Y. Yang, M. P. Moschetti, and M. J. Fouch (2011), Complex and variable crustal and uppermost mantle seismic anisotropy in the western United States, *Nat. Geosci.*, *4*(1), 55–61, doi:10.1038/ngeo1036.

Liu, Y., and D. R. Schmitt (2006), The transition between the scale domains of ray and effective medium theory and anisotropy: Numerical models, *Pure Appl. Geophys.*, *163*(7), 1327–1349, doi:10.1007/s00024-006-0075-5.

Mah, M., and D. R. Schmitt (2001a), Experimental determination of the elastic coefficients of an orthorhombic material, *Geophysics*, *66*(4), 1217, doi:10.1190/1.1487068.

Mah, M., and D. R. Schmitt (2001b), Experimental determination of the elastic coefficients of an orthorhombic material, *Geophysics*, *66*(4), 1217, doi:10.1190/1.1487068.

Mahmoudian, F. (2013), Physical Modeling and Analysis of Seismic Data from a Simulated Fractured Medium, University of Calgary.

Mahmoudian, F., G. Margrave, and P. Daley (2014), Estimation of elastic stiffness coefficients of an orthorhombic physical model using group velocity analysis on transmission data, *Geophysics*, *79*(1), R27–R39, doi:10.1190/geo2013-0203.1.

Mahmoudian, F., G. F. Margrave, J. Wong, and D. C. Henley (2015), Azimuthal amplitude variation with offset analysis of physical modeling data acquired over an azimuthally anisotropic medium, *GEOPHYSICS*, *80*(1), C21–C35, doi:10.1190/geo2014-0070.1.

Mainprice, D., and A. Nicolas (1989), Development of shape and lattice preferred orientations: application to the seismic anisotropy of the lower crust, *J. Struct. Geol.*, *11*(1–2), 175–189, doi:10.1016/0191-8141(89)90042-4.

Malehmir, R., and D. R. Schmitt (2016a), ARTc: Anisotropic reflectivity and transmissivity calculator, *Comput. Geosci.*, *93*, 114–126, doi:10.1016/j.cageo.2016.05.008.

Malehmir, R., and D. R. Schmitt (2016b), Ultrasonic measurement of anisotropic reflectivity

from Water-Phenolic CE Interface, *PANGAEA*, doi:10.1594/PANGAEA.864794.

Malehmir, R., and D. R. Schmitt (2017), Acoustic Reflectivity from an Orthorhombic Media : Understanding the Fractured Anisotropic Crust, *J. Geophys. Res.*, Under review.

Malehmir, R., N. Kazemi, and D. R. Schmitt (2017), An Algorithm to Quantitatively Model Reflected Ultrasonic Bounded Beam with Experimental Validation, *Ultrasonics*.

Mallick, S., and L. N. Frazer (1991), REFLECTION-TRANSMISSION COEFFICIENTS AND AZIMUTHAL ANISOTROPY IN MARINE SEISMIC STUDIES, *Geophys. J. Int.*, *105*, 241–252.

Mallick, S., K. L. Craft, L. J. Meister, and R. E. Chambers (1998), Determination of the principal directions of azimuthal anisotropy from P-wave seismic data, *GEOPHYSICS*, *63*(2), 692–706, doi:10.1190/1.1444369.

Mann, R. W., G. A. Baum, and C. C. Habeger (1980), Determination of all nine orthotropic elastic constants for machine-made paper, *Tappi*, *63*(84), 163–166.

McCamy, K., R. P. Meyer, and T. J. Smith (1962), Generally applicable solutions of Zoeppritz' amplitude equations, *BSSA*, *52*, 923–955.

Merkulov, L. G. (1963), Ultrasonic waves in crystals, *Appl. Mater. Res.*, *2*(4), 231–240.

Musgrave, M. J. P. (1970a), *Crystal Acoustics: Introduction to the Study of Elastic Waves and Vibrations in Crystals*, Holden-Day.

Musgrave, M. J. P. (1970b), *Musgrave M.J.P. Crystal Acoustics 1970.djvu.pdf*, HOLDEN-DAY, San Francisco.

Nakagawa, S., K. T. Nihei, L. R. Myer, and E. L. Majer (2003), Three-dimensional elastic wave scattering by a layer containing vertical periodic fractures, *J. Acoust. Soc. Am.*, *113*(6), 3012, doi:10.1121/1.1572139.

Nayfeh, A. H. (1989), The propagation of horizontally polarized shear waves in multilayered anisotropic media, *J. Acoust. Soc. Am.*, *86*(5), 1–16, doi:10.1121/1.398580.

Ngoc, T. D. K., and W. G. Mayer (1979), Ultrasonic nonspecular reflectivity near longitudinal critical angle, *J. Appl. Phys.*, *50*(12), 7948–7951, doi:10.1063/1.325971.

Nishizawa, O., and K. Kanagawa (2010), Seismic velocity anisotropy of phyllosilicate-rich rocks: characteristics inferred from experimental and crack-model studies of biotite-rich schist,

Geophys. J. Int., *182*(1), no-no, doi:10.1111/j.1365-246X.2010.04614.x.

Ortiz-osornio, M., and D. R. Schmitt (2009), Measurements of the reflectivity of a liquid – anisotropic solid interface, in *8th Euro Conference of Rock Physics & Geomechanics*, p. 4pp, Ascona, Switzerland.

Ortiz-osornio, M., and D. R. Schmitt (2010a), The Reflectivity and Transmissivity of Anisotropic Materials : A Physical Modeling Study, in *American Rock Mechanics Association*, p. 5pp.

Ortiz-osornio, M., and D. R. Schmitt (2010b), The reflectivity and transmissivity of anisotropic materials: A physical model study, in *ARMA 44th U.S. Rock Mechanics Symposium*, p. 5 pp, Salt Lake City.

Ortiz-osornio, M., and D. R. Schmitt (2010c), Velocity dispersion of a heavy oil sandstone: A case study, in *Oil Sands and Heavy Oil Technologies Conference, Calgary*, pp. 20–22.

Ortiz-osornio, M., and D. R. Schmitt (2011a), Measurements of the reflectivity and transmissivity of anisotropic materials to test the effect of tilt and azimuth, in *1st Int. Workshop on Rock Physics, August 7-12,* p. 4pp, Golden, CO.

Ortiz-osornio, M., and D. R. Schmitt (2011b), Physical Modeling of the Reflectivity and Transmissivity of Anisotropic Materials, in *73rd EAGE Conference and Exhibition incorporating SPE EUROPEC 2011, Vienna*, p. 4 pp, Vienna.

Ostrander, W. J. (1984), Plane-wave reflection coefficients for gas sands at nonnormal angles of incidence - ostrander1984.pdf, *Geophysics*, *49*(10), 1637–1648.

Ozacar, A. A., and G. Zandt (2004), Crustal seismic anisotropy in central Tibet: Implications for deformational style and flow in the crust, *Geophys. Res. Lett.*, *31*(23), 1–4, doi:10.1029/2004GL021096.

Ozacar, A. A., and G. Zandt (2009), Crustal structure and seismic anisotropy near the San Andreas Fault at Parkfield, California, *Geophys. J. Int.*, *178*(2), 1098–1104, doi:10.1111/j.1365-246X.2009.04198.x.

Pedersen, H. A. (2006), Impacts of non-plane waves on two-station measurements of phase velocities, *Geophys. J. Int.*, *165*(1), 279–287, doi:10.1111/j.1365-246X.2006.02893.x.

Plona, T. J. (1976), Ultrasonic bounded beam reflection and transmission effects at a liquid/ solid-plate/liquid interface, *J. Acoust. Soc. Am.*, *59*(6), 1324, doi:10.1121/1.381011.

Rokhlin, S. I. (1986), Reflection and refraction of elastic waves on a plane interface between two generally anisotropic media, *J. Acoust. Soc. Am.*, *79*(4), 906, doi:10.1121/1.393764.

Rokhlin, S. I., and W. Wang (1992), Double through transmission bulk wave method for ultrasonic phase velocity measurement and determination of elastic constants of composite materials, *Acoust. Soc. Am.*, *91*(6), 3303–3312.

Rüger, A. (1997), P -wave reflection coefficients for transversely isotropic models with vertical and horizontal axis of symmetry, *Geophysics*, *62*(3), 713–722.

Rüger, A. (1998), Variation of P-wave reflectivity with offset and azimuth in anisotropic media, *Geophysics*, *63*(3), 935, doi:10.1190/1.1444405.

Savage, M. K. (1999), Siesmic anisotropy and mantle deformation, *Rev. Geophys.*, (98), 65–106, doi:10.1029/98RG02075.

Sayers, C. M., and S. Dean (2001), Azimuth-dependent AVO in reservoirs containing non-orthogonal fracture sets gave an analytic expression, valid for, *Geophys. Prospect. Ikelle Ru È ger*, *49*, 100–106.

Sayers, C. M., and M. Kachanov (1995), Microcrack-induced elastic wave anisotropy of brittle rocks, *J. Geophys. Res. Solid Earth*, *100*(B3), 4149–4156, doi:10.1029/94JB03134.

Sayers, C. M., S. Guo, and J. Silva (2015), Sensitivity of the elastic anisotropy and seismic reflection amplitude of the Eagle Ford Shale to the presence of kerogen, *Geophys. Prospect.*, *63*(1), 151–165, doi:10.1111/1365-2478.12153.

Schijns, H., D. R. Schmitt, P. J. Heikkinen, and I. T. Kukkonen (2012a), Seismic anisotropy in the crystalline upper crust: Observations and modelling from the Outokumpu scientific borehole, Finland, *Geophys. J. Int.*, *189*(1), 541–553, doi:10.1111/j.1365-246X.2012.05358.x.

Schijns, H., D. R. Schmitt, P. J. Heikkinen, and I. T. Kukkonen (2012b), Seismic anisotropy in the crystalline upper crust: Observations and modelling from the Outokumpu scientific borehole, Finland, *Geophys. J. Int.*, *189*(1), 541–553, doi:10.1111/j.1365-246X.2012.05358.x.

Schmitt, D. R. (2015), *Geophysical Properties of the Near Surface Earth: Seismic Properties*, Elsevier B.V.

Schoch, A. (1950), Schallreflexion, Schallbrechung und Schallbeugung, in *Ergebnisse der exakten Naturwissenschaften*, vol. 23, pp. 127–234.

Schoch, A. (1952a), b, Seitliche versetzung eines total reflektierten strahles bei ultraschall-wellen, *Acustica*, *2*(17).

Schoch, A. (1952b), Der schallbeugung durch platten, *Acustica*, *1*(2).

Schoenberg, M. (1997), Orthorhombic media: Modeling elastic wave behavior in a vertically fractured earth, *Geophysics*, *62*(6), 1954, doi:10.1190/1.1444297.

Shadlow, J. (2014), A description of seismic amplitude techniques, *Explor. Geophys.*, *45*(3), 154, doi:10.1071/EG13070.

Shen, F., J. Sierra, D. R. Burns, and M. N. Toksöz (2002), Azimuthal offset-dependent attributes applied to fracture detection in a carbonate reservoir, *GEOPHYSICS*, *67*(2), 355–364, doi:10.1190/1.1468596.

Shuey, R. T. (1985), A simplification of the Zoeppritz equations, *Geophysics*, *50*(4), 609, doi:10.1190/1.1441936.

Skopintseva, L., and T. Alkhalifah (2013), An analysis of AVO inversion for postcritical offsets in HTI media, *GEOPHYSICS*, *78*(3), N11–N20, doi:10.1190/geo2011-0288.1.

Stewart, R. R., N. Dyaur, B. Omoboya, J. J. S. de Figueiredo, M. Willis, and S. Sil (2013), Physical modeling of anisotropic domains: Ultrasonic imaging of laser-etched fractures in glass, *Geophysics*, *78*(1), D11–D19, doi:10.1190/geo2012-0075.1.

Swokowski, E. W. (1979), *Calculus with analytic geometry*, Prindle, Weber & Schmidt.

Tamir, T., and H. L. Bertoni (1971), Lateral Displacement of Optical Beams at Multilayered and Periodic Structures, *J. Opt. Soc. Am.*, *61*(10), 1397–1413, doi:10.1364/JOSA.61.001397.

Thomsen, L. (1986a), Weak elastic anisotropy, *Geophysics*, *51*(10), 1954, doi:10.1190/1.1442051.

Thomsen, L. (1986b), Weak elastic anisotropy, *Geophysics*, *51*(10), 1954, doi:10.1190/1.1442051.

Tsvankin, I. (1997), Anisotropic parameters and P-wave velocity for orthorhombic media, *Geophysics*, *62*(4), 1292, doi:10.1190/1.1444231.

Ursin, B., and G. Haugen (1996), Weak-contrast approximation of the elastic scattering matrix in

anisotropic media, *Pure Appl. Geophys.*, *148*(3–4), 685–714.

Vavrycuk, V. (1999), Weak-contrast reflection / transmission coefficients in weakly anisotropic elastic media : P -wave incidence, *Geophys. J. Int.*, *138*, 553–562, doi:10.1046/j.1365-246X.1999.00890.x.

Vavrycuk, V., and I. Pšenčík (1998), PP-reflection coefficients in weakly anisotropic elastic media, *Soc. Expl. Geophys*, *63*(6), 2129–2141.

Vestrum, R. W. (1994), Group and Phase-Velocity Inversions for the General Anisotropic Stiffness Tensor, October.

Vestrum, R. W., and R. J. Brown (1994), *From group or phase velocities stiffness tensor to the general anisotropic Robert W . Vestr um and R . Jame s B ro w n*.

Voigt, W. (1887), Theorie des Lichts für bewegte Medien, *Göttinger Nachrichten*, *7*, 41–51.

Walker, A. M., and J. Wookey (2012a), Computers & Geosciences MSAT — A new toolkit for the analysis of elastic and seismic anisotropy, *Comput. Geosci.*, *49*(October 2012), 81–90, doi:10.1016/j.cageo.2012.05.031.

Walker, A. M., and J. Wookey (2012b), MSAT-A new toolkit for the analysis of elastic and seismic anisotropy, *Comput. Geosci.*, *49*, 81–90, doi:10.1016/j.cageo.2012.05.031.

Wang, X., and I. Tsvankin (2013), Multiparameter TTI tomography of P-wave reflection and VSP data, *Geophysics*, *78*(5), WC51-WC63, doi:10.1190/geo2012-0394.1.

Wenk, H.-R. (1999), A voyage through the deformed Earth with the self-consistent model, *Model. Simul. Mater. Sci. Eng.*, *7*(5), 699–722, doi:10.1088/0965-0393/7/5/304.

Weyl, H. (1919), Ausbreitung elektromagnetischer Wellen über einem ebenen Leiter, *Ann. Phys.*, *365*(21), 481–500, doi:10.1002/andp.19193652104.

Wielandt, E. (1993), Propagation and structural interpretation of non-plane waves, *Geophys. J. Int.*, *113*(1), 45–53, doi:10.1111/j.1365-246X.1993.tb02527.x.

Young, G. B., and L. W. Braile (1976), A computer program for the application of Zoeppritz's amplitude equations and Knott's energy equations, *Bull. Seismol. Soc. Am.*, *66*(6), 1881–1885.

Yousef, B. M., and D. A. Angus (2016), *When do fractured media become seismically anisotropic? Some implications on quantifying fracture properties*.

Zheng, P., and B. Ding (2014), The Generalized Reflection and Transmission Matrix Method for Wave Propagation in Stratified Fluid-Saturated Porous Media, *Transp. Porous Media*, *102*(2), 185–206, doi:10.1007/s11242-014-0271-1.

Zheng, Y. (2006), Seismic azimuthal anisotropy and fracture analysis from PP reflection data, University of Calgary.

Zillmer, M., D. Gajewski, and B. M. Kashtan (1998), Anisotropic reflection coefficients for a weak-contrast interface, *Geophys. J. Int.*, *132*(1), 159–166.

Zoeppritz, K. (1919), Erdbebenwellen VII. VIIb. Über Reflexion und Durchgang seismischer Wellen durch Unstetigkeitsflächen. Nachrichten von der Königlichen Gesellschaft der Wissenschaften zu Göttingen, *Math. Klasse*, 66–84.